ELECTRIC STRESS AND INSULATION FAILURE MECHANISM OF MEDIUM VOLTAGE MEDIUM FREQUENCY TRANSFORMER

Zheng, Changjiang

DOI (link to publication from Publisher):
10.54337/aau561784653

Publication date:
2023

Document Version
Publisher's PDF, also known as Version of record

ELECTRIC STRESS AND INSULATION FAILURE MECHANISM OF MEDIUM VOLTAGE MEDIUM FREQUENCY TRANSFORMER

BY
CHANGJIANG. ZHENG

DISSERTATION SUBMITTED 2023

AALBORG UNIVERSITY
DENMARK

ELECTRIC STRESS AND INSULATION FAILURE MECHANISM OF MEDIUM VOLTAGE MEDIUM FREQUENCY TRANSFORMER

by

Changjiang. Zheng

AALBORG UNIVERSITY
DENMARK

Dissertation submitted

.

Dissertation submitted: May, 2023

PhD supervisor: Prof. Claus Leth Bak
Aalborg University

Assistant PhD supervisor: Associate Prof. Filipe Faria da Silva
Aalborg University

PhD committee: Associate Professor Peter Omand Rasmussen (chair)
Aalborg University, Denmark

Professor Gian Carlo Montanari
Florida State University, USA

Associate Professor Thomas Hammarström
Chalmers University of Technology, Sweden

PhD Series: Faculty of Engineering and Science, Aalborg University

Department: AAU Energy

ISSN (online): 2446-1636
ISBN (online): 978-87-7573-700-0

Published by:
Aalborg University Press
Kroghstræde 3
DK – 9220 Aalborg Ø
Phone: +45 99407140
aauf@forlag.aau.dk
forlag.aau.dk

Printed in Denmark by Stibo Complete, 2023

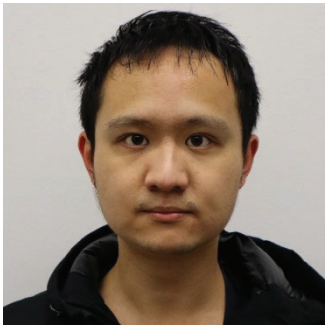

CV

Changjiang. Zheng was born in DeYang, Sichuan Province, P. R. China in December 12. He received his B. Sc degree in Automation from Northeastern University at QinHuangDao, Hebei China, in 2015. Receiving his M. Sc degree in Detecting technology and automatic equipment from Sichuan University, Sichuan, China, in 2018. He is currently pursuing a Ph.D. degree at the Department of Energy, Aalborg University, Aalborg, Denmark. His research interests include electric stress analysis on the winding of the medium voltage medium frequency transformer, PD inception and deterioration on the insulation of the transformer fed by pulse voltage.

ABSTRACT

Working under PWM voltage with fast rising/falling edges and a frequency much higher than the 50/60 Hz power frequency, medium frequency transformers may suffer from unusual electrical stress. Previous studies on other electrical devices show that fast rising/falling edge of PWM-like voltage can bring overvoltage inside the winding. This overvoltage can trigger partial discharge with a higher probability. Partial discharge (PD) is a phenomenon that can degrade the insulation material quickly and it is now considered as one of the main reasons for devices like inverter-fed motors to meet premature breakdown. Since transformers also have structures with windings and cores, with similar working voltage, this potential risk of electrical overstress should not be ignored.

In addition, environmental factors may also affect the medium frequency transformer's insulation reliability. Among them, temperature and pressure should be carefully considered. The rising of temperature can affect the dielectric properties of the insulation materials. Then, the material's ability against PD inception and deterioration can be different. Reducing of pressure can affect the breakdown strength of the air dielectrics, which can in turn affect the partial discharge inception voltage of the winding's insulation. These are practical problems faced by the medium frequency transformer: working under PWM voltage with frequency much higher than the power frequency, transformer would face increased copper and power loss that cause a temperature rise. another problem is that transformers would face low pressure condition if they are working in high altitude areas or in airplanes, per example.

To handle these above mentioned problems, this Ph. D. project proposes a study focusing on analyzing the electrical stress in medium frequency transformers, along with the PD inception and aging of the commonly used insulation material of the transformers.

Firstly, an equivalent circuit model of a specific medium frequency transformer's prototype is built through Finite Element Method (FEM) calculation. Based on this model, simulations on the inter-turn and inter-layer voltage drops are conducted. During the simulations, the changing of the parameters including pulse voltage rise time, permittivity of insulation material and structure of winding are taken into consideration. When the winding is added with pulse voltage with rise time from 100 ns to 1 μs overvoltage exists between adjacent turns and adjacent winding layers. The

results also show how the above mentioned parameters affect this overvoltage. Existence of overvoltage indicates that higher risk of PD inception would be faced by medium frequency transformers. Some suggestions about the regulating of voltage waveform, choosing of insulation material and winding's design can be given for mitigating this electrical stress. Meanwhile, the existence of overvoltage indicates the necessity to pay attention to the possible PD inception and deterioration in medium frequency transformers.

Secondly, a test system for the insulation is built. It consists of a pulse voltage generator, PD detection system along with the environment control equipment. With the ability of generating repetitive pulse voltage, detecting PD with high accuracy and breakdown protection, it can be used for partial discharge and endurance tests on insulation films. This system makes it possible to conduct the preceding studies.

By using the afore-mentioned test system, comparative Partial Discharge Inception Voltage (PDIV) and endurance tests are conducted on insulation materials commonly used for medium frequency transformers, namely Nomex paper, polyester film and polyimide film. Under pulse voltage, with temperature rise from room temperature to 110℃, Nomex paper shows an obvious decrease in PDIV. With the presence of continuous PDs generated in every pulse voltage cycle, Nomex paper would meet breakdown in a few minutes. Other two materials have relatively higher PDIV. Under low temperature condition, polyester shows highest PDIV value while under high temperature condition polyimide behaves better. Both of these materials endure much longer than the Nomex paper when stressed with continuous PDs, and polyimide lasts the longest. These results give some suggestions on selection of proper materials for the medium frequency transformer's design, which is one of the important steps for improving the transformer's insulation reliability.

Finally, PD and endurance tests are conducted on the polyimide film with different pressures from 1 Bar to 0.3 Bar. With pressure decreasing, PD can be triggered easier. In our experiments, PD intensity enhances when pressure goes lower except for the situation of lowest pressure (0.3 Bar). In high pressure range (from 1 Bar to 0.7 Bar), PD time lag goes shorter with pressure decreasing. While in low pressure range (from 0.6 Bar to 0.3 Bar) PD time lag presents an opposite trending. Endurance lifetime of the insulation film also decreases along with pressure except for 0.3 Bar. Under low pressure condition, PD eroded area of the aged materials becomes larger. These above results indicate that insulation of the medium frequency transformers may face

a reduction in insulation behavior when working in high altitude areas or airplanes, and also bring focus to the necessity of further studies on the complete transformer prototype and more transformer related insulation structures.

RESUMÉ

Ved at arbejde under PWM-spænding med hurtigt stigende/faldende flanker og en frekvens, der er meget højere end 50/60 Hz, kan mellemfrekvente transformatorer lide under usædvanlig elektrisk stress. Tidligere undersøgelser af andre elektriske enheder viser, at hurtigt stigende/faldende flanke af PWM-lignende spænding kan bringe overspænding inde i viklingen. Denne overspænding kan udløse partielle udladninger med større sandsynlighed. Partial discharge (partielle udladninger - PD) er et fænomen, der hurtigt kan nedbryde isoleringsmaterialet, og det anses nu for at være en af hovedårsagerne til, at enheder som f.eks. inverter-forsynede motorer møder for tidligt nedbrud. Da transformere også har strukturer med viklinger og kerner med lignende arbejdsspænding, bør denne potentielle risiko for elektrisk overbelastning ikke ignoreres.

Derudover kan miljøfaktorer også påvirke mellemfrekvenstransformatorens isoleringspålidelighed. Blandt dem skal temperatur og tryk nøje overvejes. Temperaturstigningen kan påvirke isoleringsmaterialernes dielektriske egenskaber. Så kan materialets evne mod PD startspænding og forringelse være anderledes. Reduktion af tryk kan påvirke nedbrydningsstyrken af luften, hvilket igen kan påvirke den partielle udladningers sstartspænding i viklingens isolering. Disse er praktiske problemer, som mellemfrekvenstransformeren står over for: arbejder under PWM-spænding med en frekvens, der er meget højere end 50 Hz, vil transformeren stå over for øget kobber- og strømtab, der forårsager en temperaturstigning. et andet problem er, at transformatorer vil blive udsat for lavtrykstilstand, hvis de arbejder i stor højde områder eller i fly.

For at håndtere disse ovennævnte problemer foreslår dette Ph.D.-projekt en undersøgelse, der fokuserer på at analysere den elektriske spænding i mellemfrekvente transformere, sammen med PD-startspænding og ældningen af transformatorernes almindeligt anvendte isoleringsmateriale.

For det første bygges en ækvivalent kredsløbsmodel af en specifik mellemfrekvenstransformers prototype ved hjælp af Finite Element Method (FEM) beregning. Baseret på denne model udføres simuleringer af inter-turn og inter-lag spændingsfald. Under simuleringerne tages der hensyn til ændringen af parametrene, herunder impulsspændingens stigetid, isoleringsmaterialets permittivitet og viklingens struktur. Når viklingen tilføjes pulsspænding med stigetid fra 100 ns til 1 μs, eksisterer der overspænding mellem tilstødende vindinger og tilstødende viklingslag.

Resultaterne viser også, hvordan de ovennævnte parametre påvirker denne overspænding. Eksistensen af overspænding indikerer, at mellemfrekvente transformatorer står over for en højere risiko for PD. Nogle forslag til regulering af spændingsbølgeform, valg af isoleringsmateriale og viklingens design kan gives for at afbøde denne elektriske belastning. I mellemtiden indikerer eksistensen af overspænding nødvendigheden af at være opmærksom på den mulige PD-start og forringelse i mellemfrekvenstransformere.

For det andet bygges et testsystem for isoleringen. Den består af en pulsspændingsgenerator, PD-detektionssystem sammen med tryk- og temperatur kammer. Med evnen til at generere gentagne pulsspændinger, detektere PD med høj nøjagtighed og nedbrudsbeskyttelse, kan den bruges til at måle partielle udladninger og udholdenhedstest på isoleringsfilm. Dette system gør det muligt at udføre de foregående undersøgelser.

Ved at bruge det førnævnte testsystem udføres sammenlignende partial discharge inception voltage (PDIV) og udholdenhedstest på isoleringsmaterialer, der almindeligvis anvendes til mellemfrekvenstransformatorer, nemlig Nomex-papir, polyesterfilm og polyimidfilm. Under pulsspænding, med temperaturstigning fra stuetemperatur til 110 ℃, viser Nomex-papir et tydeligt fald i PDIV. Med tilstedeværelsen af kontinuerlige PD'er genereret i hver pulsspændingscyklus, ville Nomex-papir møde nedbrud på få minutter. Andre to materialer har relativt højere PDIV. Under lave temperaturforhold viser polyester den højeste PDIV-værdi, mens polyimid under høje temperaturforhold opfører sig bedre. Begge disse materialer holder meget længere end Nomex-papiret, når de belastes med kontinuerlige PD'er, og polyimid holder længst. Disse resultater giver nogle forslag til valg af passende materialer til mellemfrekvenstransformatorens design, hvilket er et af de vigtige skridt til at forbedre transformatorens isoleringspålidelighed.

Til sidst udføres PD og udholdenhedstest på polyimidfilmen med forskellige tryk fra 1 Bar til 0,3 Bar. Med faldende tryk opstår PD lettere. I vores eksperimenter øges PD-intensiteten, når trykket bliver lavere, bortset fra situationen med laveste tryk (0,3 bar). I højtryksområdet (fra 1 bar til 0,7 bar) bliver PD-tidsforsinkelsen kortere med trykket faldende. Mens det er i lavtryksområdet (fra 0,6 bar til 0,3 bar), viser PD-tidsforsinkelse en modsat tendens. Holdbarheden af isoleringsfilmen falder også sammen med trykket bortset fra 0,3 bar. Under lavtrykstilstand bliver PD-eroderet område af de ældede materialer større. Disse ovenstående resultater indikerer, at isolering af mellemfrekvente transformatorer kan opleve en reduktion i isolationens

ydeevne, når der arbejdes i højhøjdeområder eller flyvemaskiner, og bringer også fokus på nødvendigheden af yderligere undersøgelser af den komplette transformerprototype og mere transformerrelaterede isoleringsstrukturer.

PREFACE

This Ph.D. thesis summarizes the outcomes from the Ph.D. project entitled "Electric stress and insulation failure mechanism of medium voltage medium frequency transformer", which is supported by AAU Energy, Aalborg University, Denmark. I'd like to express my acknowledgment to all the people who offer help for my Ph.D studies.

This Ph.D project was done under the supervision of Prof. Claus Leth Bak, Assoc. Prof. Filipe Miguel Faria da Silva, Assist. Prof. Qian Wang and Prof. Huai Wang. First, I would like to express my sincere gratitude to my supervisor Prof. Claus Leth Bak, for his guidance, encouragement, and valuable suggestions during my Ph.D. period. I would also like to sincerely thank my co-supervisors Filipe Miguel Faria da Silva and Qian Wang who give revisions patiently on my papers. Then I would like to thank my co-supervisor Huai Wang, who provide funding for the building of the test system, which is essential for all of my experiments. Then, I would like to thank Prof. Andrea Cavallini for providing me an opportunity of study abroad in the University of Bologna, Bologna, Italy, where I have broadened my knowledge related to my research filed.

Also I would like to thank all of my colleagues including Ph.D students, guests and staffs at AAU energy for their help and support. Firstly, I would like to give a special thank to Zhan Shen, who contributes most in the building of my test system. Then I would like to thank Mads Laud who provides lab for placing the test system, constructs safe-protecting switches and grants me the access for entering the lab to do the experiments. Then, I would like to thank Bo Yao, Huizhong Sun, Kaiqi Ma, Yaxun Guo, Wenbo Tian, Zhe Yang and Qi Zhang for acting as observers for safety during my high voltage experiments. Then, I would like to thank Henrik Nielsen who makes insulation structures and metal electrodes, which are necessary for me to fix the samples during the experiments.

At last, I would like to thank my parents because of their love and care. They encouraged me to apply for a Phd study abroad and provide the financial support to cover all of my life expense in Denmark. This is why I can start and finish my Ph. D study.

Changjiang. Zheng
Aalborg University, April 5, 2023

CONTENTS

PART. 1

REPORT

CHAPTER 1.

Introduction

In this chapter, the background of medium voltage medium frequency (MVMF) transformer and its potential insualtion problem are introduced in details. Then, previous studies on these transformers' electric stress and insulation failure mechanism are reviewed briefly. Based on these studies and the problems remaining, motivations along with research activities of this project are proposed. Afterwards, outline of this thesis and the published papers during this Ph. D project are given.

1.1 BACKGROUND

1.1.1 MEDIUM FREQUENCY TRANSFORMER

In power electronic systems such as DC-DC converter, transformers may be applied. They serve the functions of voltage level scaling up/down, electrical isolation and power transmission [1]. A typical topology of a power electronic system with a transformer is shown in Fig. 1.1. This topology is usually used in power distribution and transmission [2]. Power electronic switches are connected on both sides of the transformer. The prevailing working voltage of these power electronic devices lies in the range within 10 kV, which can be defined as medium voltage. While the working frequency lies from a few hundreds Hz to 100 kHz. Thus, the transformer in this system is a medium-voltage medium-frequency (MVMF) transformer.

Relationship between size of a transformer's core and its operating frequency can be described by equation (1) [3]:

$$A_C \cdot A_W \propto \frac{P}{K_f \cdot K_u \cdot f \cdot J \cdot B_{\max}} \tag{1.1}$$

In this equation, A_C is the magnetic core's cross-sectional area; A_w is the core's window area; P is the power; K_f and K_u are waveform-dependent constants and the conductor fill-factor respectively; f is the frequency of working voltage; J is the current density and B_{max} is the maximum flux density. With other conditions unchanged, the design of A_C and A_w can be smaller if higher working voltage frequency f can be reached, which means the size of the core of the transformer can be smaller. Then, the system in Fig. 1.1 can reach a smaller overall size compared with a single bulky conventional power frequency transformer, high power density can be achieved. Smaller size also means less material required and less weight, which reduces the manufacturing and transporting costs. Besides the merits brought from

smaller size, combined with power electronic switches, topologies in Fig. 1.1 or alike can realize control strategies including voltage sag compensation, power flow control and continuous on-load voltage regulation [4-6]. These control strategies are not possible for a single conventional transformer. Because of these advantages described above, converter systems consists of MVMF transformers are applied in many fields including railway traction and DC grids, etc [7-9].

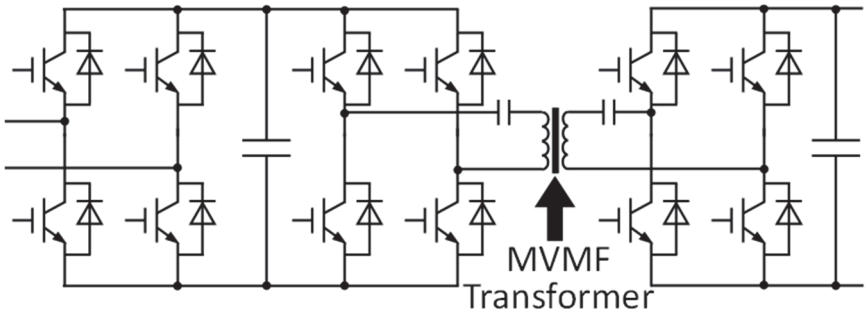

Fig. 1.1: MVMF transformer in power electronic system [2].

1.1.2 POSSIBLE INSULATION PROBLEM

Besides the advantages mentioned above, challenges certainly exist for the applying of MVMF transformers, such as increased leakage inductance [10] and the relatively low heat dissipation capability with a smaller size. Another critical problem maybe the the insulation [11]. Compared with tranditional sinusoidal voltage applied on conventional transformers, the PWM voltage that is applied on the MVMF transformer has much shorter rise time. Thus, MVMF transformer may confront electrical stress that is not the same as that faced by conventional transformer. Previous studies in the field of inverter-fed motors discovered that: for multi-turn winding, when fed by pulse voltage with very fast rising and falling edge, overvoltage like in Fig. 1.2 could be triggered between turns because of the stray parameters coming from the inductive and capacitive coupling [12-13]. Power electronic devices are developing with increasing switching speed to reduce switch loss [14], which means shorter rise/fall time, then the above-mentioned electrical stress in the winding could be even more severe.

The phenomena of overvoltage may lead to higher probability of partial discharge (in abbreviation PD). PD is a localized electrical discharge that only partially bridges the insulation between conductors and can or can not occur adjacent to a conductor [15]. With the presence of PD, insulation material can be degraded quickly [16]. Therefore, researchers regard PD as one of the main reasons that lead the electric devices working with PWM voltage such as inverter-fed motors to premature breakdown [17].

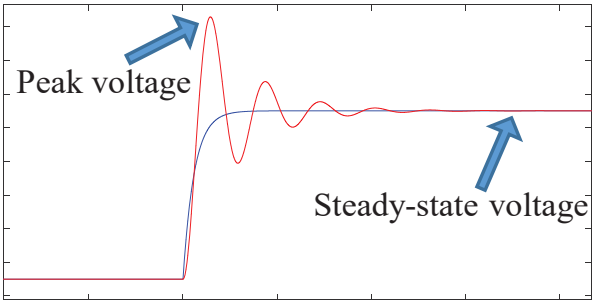

Fig. 1.2: Expected (blue line) and actual (red line) inter turn/layer voltage drop in the winding

Similar with the inverter-fed motors, medium frequency transformers also operate based on electromagnetic induction and have structures with winding and core. Different from conventional transformers, in which oil-paper insulation is usually applied, MVMF transformer usually use solid-type insulation. Air ducts may exist between adjacent turns or winding layers, or between primary and secondary windings. If the above-mentioned overvoltage is present in the transformer's winding, PD is also possible to be triggered. In addition, working under PWM voltage with frequency much higher than the 50/60 Hz power frequency, higher copper loss and core loss would be induced that can cause an obvious temperature rise [18-19]. This temperature rise can make the PD easier to be triggered and decrease the insulation endurance despite the temperature is not beyond the material's rated temperature [20]. On the other hand, with similar probability of PD inception, higher frequency can lead to more PDs during the same time interval, which can also degrade the insulation faster [21]. Combined with reducing size of medium frequency transformers, which means inevitable shorter insulation distance, and the power electronic switches' development of faster switching speed, the potential risk of PD inception and deterioration should not be ignored.

1.1.3 INFLUENCE OF ENVIRONMENTAL FACTORS

Some environmental factors can change the insulation's capability in resisting the PD inception (in other words, leading to higher or lower Partial discharge inception voltage value) and deterioration. Besides the temperature mentioned in the last section, one of the most critical factors may be the pressure. Seen from Fig. 1.3, in the Paschen Curve, with the air gap length d keeps unchanged, breakdown voltage of the gaseous dielectrics would be decreased when the pressure goes lower (before reaching the minimum value in the critical point) [22]. It is known that Paschen curve is derived with uniform distribution of electric field. Yet, even if the field is uneven, the similar trending of reducing breakdown voltage along with the reducing pressure can also be expected. For dry-type insulation, with the presence of air ducts, the reduction of air's breakdown voltage has a direct impact on its capability in resisting PD inception. The

mean free path of charge (or electron) can also be affected by reduced gas density. This factor can affect the intensity of partial discharge.

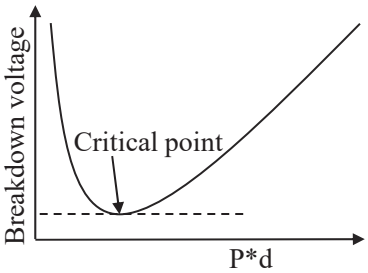

Fig. 1.3: Paschen Curve [22]

For MVMF transformers, the impact from low air pressure is a problem that cannot be ignored. Some of these transformers are applied in areas with high altitude. Recently, power electronic systems, in which the MVMF transformer is also one of the important components, are more adopted by aircrafts [23]. For the dry-type insulation structure of MVMF transformer, in the region between adjacent winding layers or adjacent windings where the potential difference can be very large, air ducts may exist as mentioned in section 1.1.2 and are likely to be the source of PD as seen in Fig. 1.4(a). In this sub-figure, conductors on the downside and upper side belong to adjacent layers of a winding or belong to different windings. Because of large potential difference and dielectric refraction, strong electric field can be created on the places pointed by red arrows, PD may be incepted in high probability and cause degradation on the insulation surface. In some of the MVMF transformers, additional inter-layer insulation may not be applied for the purpose of a compact design. As seen in Fig. 1.4(b), if enough distance between the conductors belong to different winding layers cannot be guaranteed, insulation film on the conductor may face greater threat of PD erosion directly. In these abovementioned air ducts, with pressure goes lower, the PD inception probability can even be further increased. Some other MVMF transformers may use an impregnated type of insulation structure. This can put the transformer into a free air access condition. Yet, after long period of thermal aging and mechanical oscillations in the operation, defects may be produced on the insulation surface or inside the insulation, which would distort the electric field and bring higher risk of PD inception. Seen in Fig. 1.5(a), if the cavity is contacted with the environment air, its PD inception would also be affected by the decreasing of pressure.

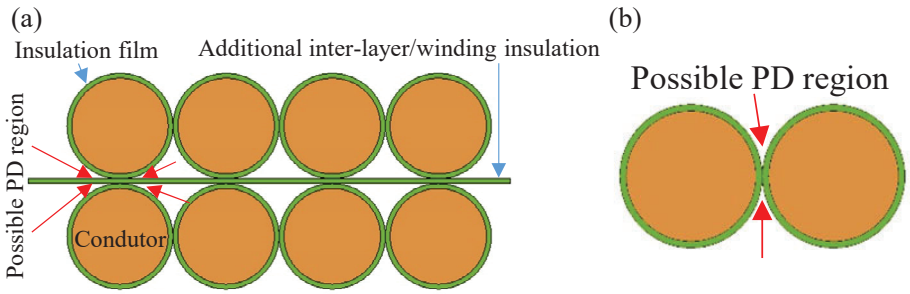

Fig. 1.4 Possible PD region in the winding of the transformer: (a) With additional inter layer/winding insulation. (b) Without additional inter layer insulation. [J2, 66]

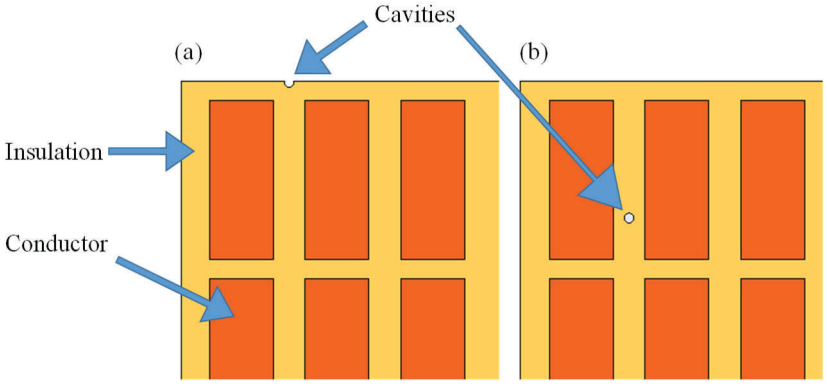

Fig. 1.5: Possible cavities in the insulation: (a) cavity on the insulation surface. (b) cavity inside the insulation

1.2 STATE OF ART

1.2.1 STUDIES ON THE ELECTRIC STRESS OF THE MEDIUM FREQUENCY TRANSFORMER

In recent years, some studies on the electrical stress suffered by MVMF transformers have been done. Authors in [24] find that for transformer with separated winding structure (HV winding and LV winding are not interleaved), the electric field concentrates around the region between the HV winding and LV winding, and the maximum electric field lies on one side of the HV winding that is facing the LV winding as shown in Fig. 1.6. Literature [25] investigates the electrical stress of medium frequency transformer used in a cascaded modular multi level power electronic transformer that works in SPWM model (power electronic switches are driven by combination of 50 Hz modulated wave and medium frequency carrier wave). In the top cell of the cascaded structure, the voltage waveform between the transformer's primary winding and ground contains a lot of high order harmonics and has larger magnitude than that between the winding terminals. In the harmonic

analysis of this winding-to-ground voltage waveform, besides the 50 Hz fundamental wave (comming from the 50 Hz modulated wave) and the 10 kHz harmonic (corresponds to the power electronic switching frequency), harmonics in 2.5 kHz and 15 kHz also have comparable magnitudes and can bring distortion to the electric field distribution in the insulation structure. In [26], for a specific transformer's winding, under DC field, electric field distribution is similar with the result presented in [24], the region between HV and LV winding shows strong field intensity. Whereas under AC field, the electric field hot spot lies between the two segments of the HV winding. Literature [27] analyzes electrical stress in frequency domain on a multi-cell solid-state transformer (SST) that is designed for a MV grid. The working voltage of the transformer is SPWM voltage with a series of multi-level medium frequency pulses that form a 50 Hz grid frequency siousoidal-like waveform. In this situation, 50 Hz component of this working voltage has largest magnitude. That's why in Fig. 1.7, the peak field intensity in medium frequency is lower than that of grid frequency. Also seen from Fig. 1.7, under 50 Hz, electric field concentrates between each turn of the MV winding and the core. While for medium frequency (sum of all the existing harmonics from 2 kHz to 96 kHz), the field mainly concentrates between the top turn of the MV winding and the core. With electric field in grid and medium frequencies added together (real situation), uneven field distribution exists and make the region around the top turn of MV winding suffer from stronger fields.

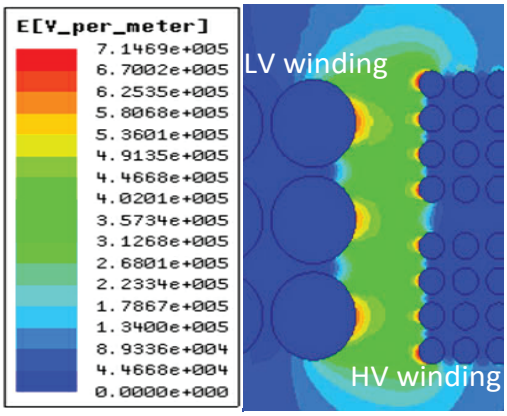

Fig. 1.6: Electric field distribution in the winding, mainly concentrates between HV and LV winding [24]

These above studies provide valuable information on how the electric field distributes inside the winding with different winding structures and variable electrical stress. Based on similar analysis, some strategies can be proposed for decreasing the field intensity in the hot spots including changing the conductor type [24], adding shields on the winding surface [25-28] or adding angle ring and electrostatic ring inside the winding structure [29]. Yet, when applying these strategies in the design of the transformer, their possible side effects on increasing the transformer's size or

weakening the transformer's heat dissipation capability should be carefully considered.

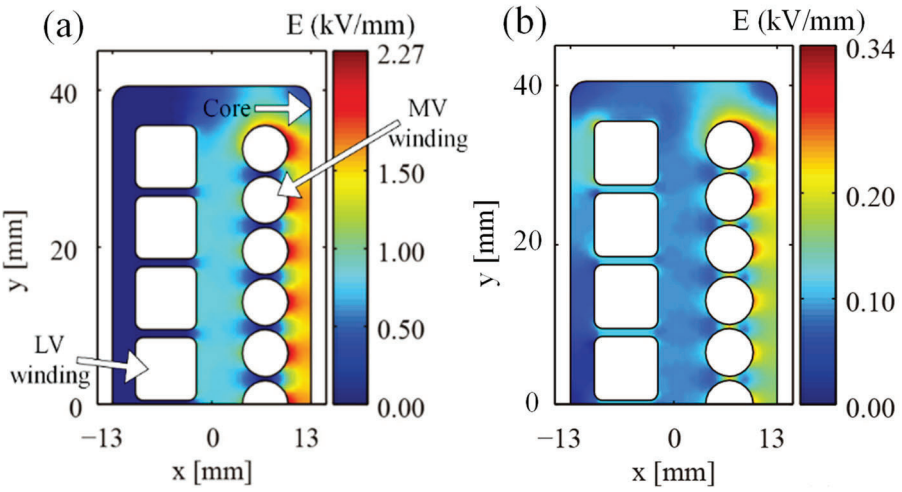

Fig. 1.7: The electric field under grid frequency (a) and medium frequency (b) [27]

1.2.2 STUDIES ON PD AND INSULATION ENDURANCE

Since similar problems were firstly discovered in the field of inverter-fed motors, a large amount of studies have been done with respect to PD detection, PD features under PWM-like voltage and the PD aging on the insulation material [30]. Medium frequency transformers also have winding-core structure and work under PWM voltage. The main study object of these above mentioned studies is polyimide, which is also one of the main insulation material applied in the medium frequency transformer [31]. Therefore, many of the conclusions of these studies can also be used for the field of medium frequency transformers directly. These conclusions including: 1) For the PD detection under PWM-like voltage, UHF antenna is the best method up to now [32-34]; 2) With the same peak magnitude, PD intensity under pulse voltage (simulate the PWM voltage) is much stronger than that under sinusoidal voltage [35]. Also pulse voltage with shorter rise time can make PD even stronger [36-38]. 3) Under continuous PDs, increasing of frequency, duty cycle and the shorter voltage rise time can make the insulation endurance lifetime shorter [39-41].

In the field of the medium frequency transformer, some related studies are also published. Most of them focus on the influence from the frequency. In [42], PD tests are conducted on the insulation paper used for on-board traction transformers. When tested under sinusoidal voltage superimposed with high frequency harmonics, PDIV would be lower than that under pure sinusoidal voltage. Literature [43] analyzes PDIV in the air gap between a MVMF transformer's two windings. Under pulse voltage,

with frequency increasing, PDIV decreases. Literature [44] investigates the PD situation in the PCB winding of a planar transformer prototype and twisted litz wires. With shorter pulse voltage rise time, repetitive PDs can be generated with relatively lower voltage magnitude. While the increasing of frequency can give rise to an opposite trending and makes the PD intensity weaker. Literature [45] conducts PD studies on the insulation cardboard used by a transformer under sinusoidal voltage. With increasing frequency, PDIV would be larger, which contradicts with the result in [43]. PD time lag (phase) would be longer, while the changing of PD number and intensity is not monotonous. Authors in [46] propose PD studies on the twisted pairs sample made by electromagnet wires from the transformer's winding. Under pulse voltage, PD would mainly be triggered on the voltage rising and falling edges. Both average and maximum PD magnitude decreases with increasing frequency, which is similar with that in [44]. When frequency is lower than 5 kHz, the number of PDs per cycle would increase when frequency goes higher while an opposite trending appears when frequency exceeds 5 kHz and keeps increasing.

1.2.3 CONSIDERATION OF THE ENVIRONMENT FACTORS

Among the afore mentioned environment factors that can cause influence on the PDIV and insulation endurance, some of the researchers in a related field (medium frequency transformer or inverted-fed motor) have taken temperature into consideration carefully. Some of the well-accepted knowledge has already been obtained including: 1) With temperature rise, the PDIV and endurance lifetime of the winding insulation decreases although the temperature is still within the insulation material's rated temperature [20, 47-50]. 2) Coupling effect exists between temperature and other parameters, with different electrical parameters (especially frequency), the effect from increasing temperature on the PD intensity, PD time lag and the PD induced aging speed would be different [20, 47-49].

On the impact from pressure, only a few of studies in the related field are presented. According to [50-51], relatively lower voltage magnitude would be enough to generate reptitive PDs with pressure decreasing. With this result, it maybe suitable to assume that PDIV would also be lower with pressure decreasing. In [52], under sinusoidal voltage, polyimide film shows increasing in lifetime along with pressure, and under higher pressure, PD energy shows a larger variation during the aging. In [53], when tested with sinusoidal voltage, the main energy of PD would shift to lower frequency range if pressure goes lower. While under pulse voltage, no such phenomenon exists. There are also some studies considering the pressure's effect in other fields focusing on objects including PCB board, silicone gel in the power electronic module package and aluminum bar [54-58]. The results of these papers indicate stronger PD intensity, higher PD repetition rate, and faster PD degradation when pressure decreases. Although the properties of their study objects are quite different from the insulation material and structure of transformer, they do indicate the necessity for the field of medium frequency transformer to conduct similar studies.

1.3 PROJECT MOTIVATIONS

In the previous studies about the medium frequency transformer, most of them conducted the analysis in steady state. They did not consider the possible overvoltage in the winding caused by the fast voltage rising edge. In the field of inverted-fed motors, some of the published studies have provide suitable methods for analyzing this overvoltage in transient time domain. That is, building a 3D or 2D winding model for the machine, and then, using the FEM calculation to get stray parameters of every turn in the winding. With these stray parameters, electric circuit model can be built in software for circuit analysis, which enables the simulation of the waveform for inter-turn voltage drop in time domain [12, 59-60]. For some of the HV motor, the dimension of the winding is large enough that a probe can be used for directly testing the inter-layer or inter-winding section voltage drop [61-62]. The results of these papers show that if pulse voltage is added to the winding, inter-turn overvoltage exists, and this overvoltage would be highest between turns closest to the winding terminals. Unlike the PD and endurance tests on the samples such as insulation film or electromagnet wires, the transformer's winding structure is not the same as that of the motor. Therefore, the conclusions from [12, 59-62] cannot be directly applied in the field of medium frequency transformer. Similar studies focusing on the electric stress suffered by MVMF transformer's winding in transient time domain is necessary.

The insulation material used by medium frequency transformer can be of different types [63]. If the possible overvoltage is confirmed by the studies mentioned in the last paragraph, based on the knowledge about how PD triggered by the pulse voltage degrades the insulation and leads to the breakdown rapidly, and how the rising of temperature affect these phenomena, it is necessary to conduct comparative studies on the different insulation materials to see their capability to withstand the PD inception and PD aging. This would help us decide which is the better insulation material for the application in MVMF transformer to face the potential electric-thermal combined stress, which is an important step in improving the medium frequency transformer's insulation reliability.

Considering the known detrimental effect from the low pressure on the insulation behavior of different kinds of electrical devices [52-58], is it reasonable to assume that similar effect also exists when the medium frequency transformer is applied in low pressure area. Therefore, a systematic investigation on the pressure's effect on the PD and insulation endurance lifetime under pulse voltage is needed. The results would help us confirm the assumption and get the idea about what to do next to help the medium frequency transformer working in the high altitude areas and aircraft (especially in more electric aircraft) cope with the effect from low pressure.

1.3.1 PROJECT QUESTIONS

- If the transformer's winding is added with PWM-like pulse voltage, would the inter-turn and inter-layer (if the winding has more than one layer) overvoltage exist? If the answer is true, how would the transformer's design affect this overvoltage?
- For the insulation materials usually applied in medium frequency transformers, which one would be better in resisting PD inception and deterioration under continuous PWM-like voltage along with temperature rise?
- Working under PWM-like voltage, how would the decreasing of pressure affect the MVMF transformer's insulation behavior in resisting PD inception and deterioration?

1.3.2 RESEARCH OBJECTS

With the above research questions, the objectives of this Ph.D project are summarized as follows:

- **Electric stress analysis on the medium frequency transformer's winding**
  Through FEM analysis, stray parameters of a transformer's HV winding are obtained. With these parameters, an equivalent circuit model is built. Transient inter-turn and inert-layer voltage drop waveform simulations are conducted on this circuit model. Simulation results show the existence of overvoltage when the winding is added with pulse voltage coming from power electronic switches, which indicates the necessity of evaluating of the insulation's capability against PD inception and PD deterioration in the field of transformers working in modern power electronic systems.

- **Building of the insulation test system**
  Repetitive pulse voltage generator is built in the laboratory. Combined with the proper PD detection device, control unit for the driving and breakdown protection, data collection unit and the oven for controlling the temperature, a test system is formed. This test system makes it possible for the conduction of the experiments in the following sections.

- **Comparative PDIV and endurance studies on different insulation materials**
  Different insulation material used by transformers, including polyimide, polyester and Nomex paper are selected as test objects. Using repetitive pulse voltage, comparative PDIV tests with rising temperature and endurance tests with higher temperatures in the oven are conducted. The results would indicate which material is a better choice for the construction of the MVMF transformer's insulation.

- **Studies on the effect of decreasing pressure on the PD and endurance**
  PDIV, PD feature and endurance tests on the polyimide insulation film are conducted under different pressures. The experiment results would answer that whether there is an increasing risk of PD inception and accelerated PD aging when pressure drops in the range from sea level to flight height around 9000 m. With this answer, some suggestions can be proposed for dealing with the low pressure's effect.

1.3.3 PROJECT LIMITATIONS

There are still several limitations in this Ph.D. project, as listed in the following:

- Different conductor types exist for medium frequency transformers including solid wire, litz wire and foil, which may lead to different electric stress in the winding. This aspect is worth investigation. Yet, in our analyze of the electric stress, we only focus on solid conductor with rectangle shape in cross section.

- The power electronic modules applied in our pulse generator is specially designed for the insulation samples like insulation film or electromagnet wires. It can not be connected with an inductive load. Therefore, we are not able to do experiments on the whole transformer prototype under pulse voltage to see the electric stress in a completely actual test device. Also, we are not able to conduct PD or aging tests on the whole transformer, which may be a better way to see how the electric overstress affect the transformer's reliability.

- For the analysis of PD and its induced aging process under different pressures, the pressure range from 1 Bar to 0.3 Bar is selected in the experiments. This pressure range corresponds to altitude from sea level to around 9000m, which covers all the high altitude areas in earth and the flight height of Short-haul flights. Yet, long-haul flights would reach higher altitude during the voyage. In addition, power electronic systems that contain transformers may also be applied in spacecrafts [64]. In these above mentioned situations, the pressure would go below 0.3 Bar and even be close to 0 Bar. This project have not taken this wider pressure range into consideration.

1.4 THESIS OUTLINE

This report contains 6 chapters to present the work done for the investigation of potential insulation problems faced by medium frequency transformers. A brief description of each chapter is given below:

- **Chapter 1 – Introduction**
  In this chapter, the background of the Ph. D project is presented. Then, state-of-art concerning the analysis on the MVMF transformer's electric stress, PD and

induced aging process on the transformer's insulation is introduced. Finally, project motivations, research questions, research objects and project limits are stated.

- **Chapter 2 – Electrical stress suffered by medium voltage medium frequency transformer**
  This chapter presents the analysis of electric stress in a transformer's winding. Stray parameters of each turn in a transformer's HV winding are obtained through FEM calculation and based on that, a circuit model of the HV winding is built. Using this model, simulations on the transient inter-turn and inter-layer voltage drops are conducted.

- **Chapter 3 – Building of the PD and endurance test system**
  For conducting the PD and endurance experiments, a test system is necessary. This system must have the ability to: 1) Output repetitive pulse voltage. 2) Detect PD signal in a high signal-to-noise ratio. 3) Switch off automatically when overcurrent happens. Chapter 3 introduce the building of this system.

- **Chapter 4 – Comparative PDIV and endurance studies on different insulating materials used for medium frequency transformers**
  In this chapter, for materials including polyimide, polyester and Nomex paper, their insulation behavior against PD inception with rising temperature and their endurance against continuous PDs under highest temperature (can be achieved by the oven we used) are compared.

- **Chapter 5 – Studies on the influence of pressure on the PD and induced aging behavior**
  Through using repetitive pulse voltage, PD and lifetime experiments with different air pressures are conducted on polyimide film. The impact from pressure on the PDIV, PD intensity, PD time lag, PD eroded area along with the insulation endurance lifetime is reported by this chapter.

- **Chapter 6 – Conclusions**
  In this last chapter, conclusions and contributions from all the studies conducted in this Ph.d project are summarized. Advices and future research perspectives for better improving the long term insulation reliability of medium frequency transformers are proposed.

1.5 LIST OF PUBLICATIONS

The research outcomes from the Ph.D. project have been disseminated in the form of publications, which include 2 journal papers and 3 conference papers [65-69]. Table 1.1 describes the corresponding relationship between papers and individual thesis chapters.

Journal papers:

J1 C. Zheng, Q. Wang, H. Wang, Z. Shen and Bak. C. L, “Electrical Stress on the Medium Voltage Medium Frequency Transformer,” Energies., Vol. 14, no. 16, 2021.

J2 C. Zheng, Q. Wang, Z. Shen, Bak. C. L, F. F. Silva and H. Wang, “Influence of pressure on the PD and induced aging behavior of polyimide insulation under repetitive pulse voltage,” IEEE Transactions on dielectric and electrical insulation. (Published online)

Conference papers:

C1 C. Zheng, Q. Wang, H. Wang, Z. Shen and Bak. C. L, “Electrical stress suffered by medium voltage medium frequency transformer,” IEEE Electrical insulation Conference, Denver, CO, USA, 29, November, 2021, pp. 116-119.

C2 C. Zheng, Q. Wang, H. Wang, Z. Shen, F. F. Silva and Bak. C. L, “Partial discharge inception and deterioration of Nomex paper under repetitive square wave voltage,” IEEE International Conference on High Voltage Engineering and Applications, Chongqing, China, December, 2022.

C3 C. Zheng, Q. Wang, H. Wang, Z. Shen, F. F. Silva and Bak. C. L, “Comparative PDIV and endurance studies on different insulating materials used for medium frequency transformers,” IEEE International Conference on High Voltage Engineering and Applications, Chongqing, China, December, 2022.

The publications finished during the Ph.D. period but not included in the Ph.D. thesis are listed below:

- C. Zheng. Q. Wang, H. Wang, Bak. C. L and Z. Shen, “Uneven Inter-turn Voltage Distribution among Windings of Medium-voltage Medium/High-frequency Transformers,” IEEE International Conference on High Voltage Engineering and Applications, Beijing, China, December, 2020.
- V. Jansen, C. Zheng, Bak. C. L, S. S. Vincenzo, R. Alberto and A. Cavallini, “Breakdown at medium frequencies of thermally-aged polyester films,” IEEE Electric insulation conference (accepted).

Table 1.1: Relationship between published papers and thesis chapters

Chapter	Associated publications
Chapter 1	
Chapter 2	J1, C1
Chapter 3	C1
Chapter 4	C2, C3
Chapter 5	J2
Chapter 6	

CHAPTER 2.

Electrical stress suffered by medium voltage medium frequency transformer

In this chapter, a 3D FEM model of a medium frequency transformer prototype is built. Afterwards an equivalent circuit model for this transformer's HV winding is established through FEM calculation. Afterwards, the mechanism of the possible overvoltage in the winding brought by PWM voltage is discussed in detail. Then, simulation on inter-turn and inter-layer voltage drop is conducted.

2.1 TRANSFORMER PROTOTYPE

A prototype of MVMF transformer proposed by literature [24, 70] is chosen as the case for the electrical stress analysis. This prototype's design and operating voltage are inherently different from a power transformer. Its rated working voltage is 1.5 kV while the working frequency is 1 kHz, which are within the range of the prevailling MVMF transformer's rated voltage and frequency. On the other hand, this transformer prototye is designed for a power electronic transformer system (PET), which can be applied in fields including high-speed railway systems, distribution system and smart grid [71-72]. Therefore, electric stress study based on this prototye has universality to some extent, which can be beneficial for electric stress analysis and insulation improvement in the design stage of other MVMF transformers in similar applications. In Table 2.1, its basic electric and design parameters are listed.

Fig. 2.1 shows the overall 3D outlook of the transformer and the partial cross-section (in 2D) of the transformer's winding. The core-type ferrite core has a dimension of 19 cm in width, 27 cm in height and 10 cm in thickness. The core's window area is 105 cm^2. The LV winding is made by copper foils with 0.4 mm in width and 110 mm in height. The HV winding, which is made by flat copper wires with 2 mm in width and 5 mm in height, has three layers. Both the HV and LV windings are distributed evenly around the core's two limbs as displayed in Fig. 2.1. This chapter aims at transient electrical stress in the winding rather than PD features or insulation aging. Therefore, we assume an ideal insulation condition for this transformer prototye, which means all of the gaps within the winding are completely filled by insulation (in Fig. 2.1, expressed by areas painted in yellow). In HV winding, inter-turn insulation distance is 0.6 mm, inter-layer insulation distance is 1 mm. With the mature transformer's design and manufacturing technology, compared with HV winding, the electric field intensity within LV winding is usually very low [28]. This

means that LV winding seldom faces the risk of electrical overstress. Therefore, we only focus on HV winding in the electric stress studies on this transformer prototype.

Table 2.1: Electric and design parameters of the selected transformer prototype [J1, 65]

Electrical Parameters	**Value**
Operation frequency	1 kHz
Rated power	35 kW
Turn ratio	120:32
HV winding rated voltage	1500 V
LV winding rated voltage	400 V
Design Parameters	**Type**
Core material	Ferrite (with permeability 1900)
Core size (width/height/thick)	19cm/27cm/10cm
Core structure	Core type
Window area	105 cm^2
Primary winding conductor	2 mm × 5 mm Flat copper wire
Secondary winding conductor	0.4 mm × 110 mm Copper foil
Insulation material	Polyimide
Inter turn insulation distance	0.6 mm (Primary)/ 0.3 mm (Secondary)
Inter winding insulation distance	1.5 mm

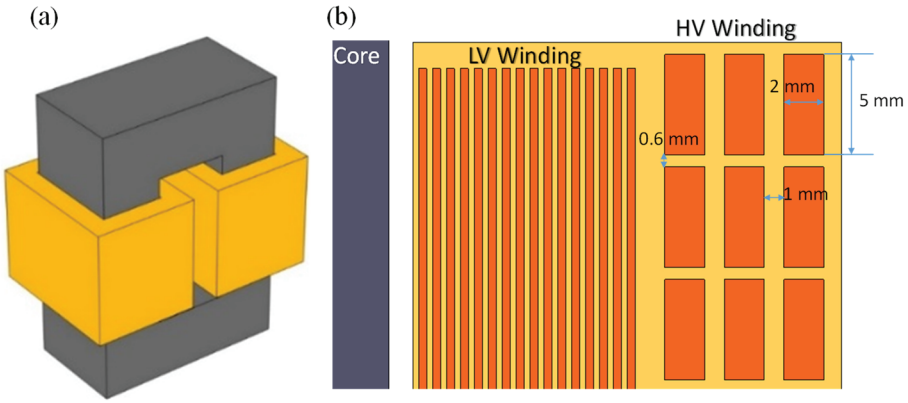

Fig. 2.1: Transformer prototype: (a) 3D overall outlook; (b) 2D cross-section of the winding. [J1, 65]

2.2 EQUIVALENT MODEL OF HV WINDING

An equivalent circuit model of the HV winding is necessary for conducting the transient voltage simulation. Stray parameters of each turn of the HV winding including resistance, capacitance and inductance are considered. Ansys Q3D - a FEM-based software, is chonsen for calulating these parameters. The 3D model used for FEM calculation is shown in Fig.2.1(a). The original insulation material is set as

polyimide with relative permittivity of 3.9 while the material of the winding conductor (turns) is set as copper (in section 2.4, the aforementioned stray parameters would be recalculated considering the changing of insulation material's permittivity and winding structure). Dirichlet boundary condition is applied as the electromagnet field boundary condition in the FEM calculation [60], the potential function is expressed by (2.1)

$$\emptyset|_{\Gamma} = g(\Gamma_1) = 0 \tag{2.1}$$

Where Γ_1 is the Dirichlet boundary, $g(\Gamma_1)$ is the ecumenical function of position. The element type is quadrilateral.

2.2.1 INDUCTANCE AND RESISTANCE

Square wave pulse voltage would be used for the simulation. This kind of waveform is a combination of a sinusoidal wave with fundamental frequency and odd harmonics [73]. The waveform would be more similar to an ideal square wave (in other words, the rise time would be shorter) if higher order of harmonics are accounted. Fig. 2.2 expresses the forming of square wave, of which the peak-to-peak value and fundamental frequency are the same as that listed in Table 2.1. Considering the harmonic decomposition, for a pulse voltage with rise time t, equivalent highest frequency f_u can be obtained by (2.2) approximately [74]:

$$f_u = \frac{1}{\pi t} \tag{2.2}$$

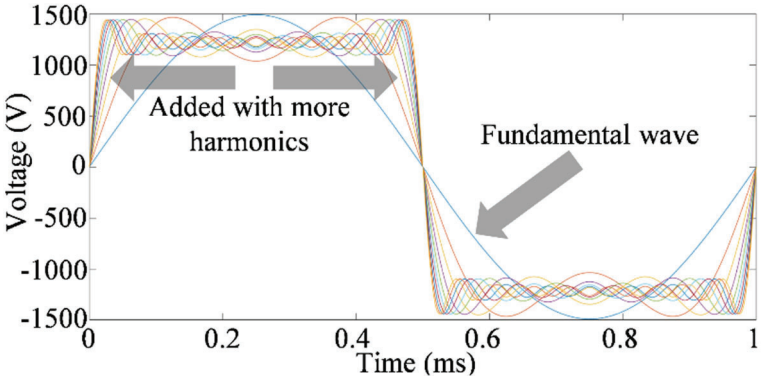

Fig. 2.2: Formation of the square wave. [J1, 65]

The rise time of PWM-like pulse voltage generated by power electronic switches is usually from hundreds of ns to several μs. So f_u is surely higher than 1 kHz. Frequency can affect the inductance [75]. Also, with frequency goes higher, resistance would be increased becuase of skin and proximity effects [76-77]. So these two parameters are calculated in frequency domain with the frequency of aforementioned

high order harmonics taken into consideration. Due to high relative permeability of the core's material, strong mutual inductive coupling exists among different turns in the winding even if they are non-adjacent. Therefore, to build the equivalent circuit model for the 120 turns HV winding in the selected transformer prototype, a 120x120 mutual inductance matrix obtained through FEM calculation is applied.

2.2.2 STRAY CAPACITANCE

According to results from FEM calculations, capacitances between non-adjacent turns (for example $C_{41\text{-}43}$) are much smaller than that between adjacent turns (for example $C_{41\text{-}42}$). Turn-to-core capacitances are much smaller than inter-turn capacitances because the distance between HV winding and core is very long (longer than 12 mm, while the distances between adjacent turns and adjacent layers are only 0.6 mm and 1 mm respectively). Therefore, in the building of the circuit model, inter-turn capacitances between non-adjacent turns and turn-to-core capacitances are not considered. On the other hand, this HV winding has three layers, capacitances between adjacent layers, like $C_{1\text{-}40}$ shown in Fig. 2.3 (Serial numbers of turns in the HV winding correspond to the numbers in this figure), should not be ignored since their values are comparable with the inter-turn capacitances like $C_{1\text{-}2}$.

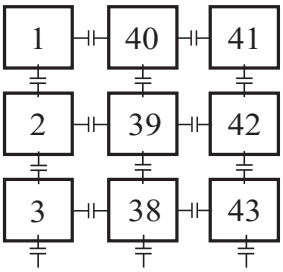

Fig. 2.3: Stray capacitance considered in the building of the circuit model [J1, 65]

Table. 2.2: Value ranges of stray parameters

Parameters	Range
Resistor (R_x)	0.03-0.06 Ω
Inductance (L_x)	50-70 nH
Capacitance ($C_{x\text{-}y}$)	50-80pF

2.3 ANALYSIS ON THE MECHANISM OF OVERVOLTAGE

Through FEM calculation described in section 2.2, stray parameters of the transformer's HV winding are acquired. These parameters include resistance R_x and self-inductance L_x of each turn (x varies from 1 to 120) along with mutual (inter-turn/layer) capacitances $C_{x\text{-}y}$ and mutual inductances $M_{x\text{-}y}$ between different turns (y

also varies from 1 to 120). Based on these parameters and the Matlab's module Simulink, an equivalent circuit model of the transformer's HV winding can be constructed, which is expressed by Fig. 2.4. Value ranges of the stray parameters R_x, L_x and C_{x-y} in Fig. 2.4 are listed in Table. 2.2. A pulse voltage source is connected between the terminals (between the 1st turn and the 120th turn) of the winding's circuit model. By using this model, an inter-turn voltage drop waveform simulation is conducted in advance. The pulse voltage's frequency and peak-to-peak value are set as 1 kHz and 1.5 kV respectively, while the rise time as 100 ns. Inter-turn voltage drops within the first 6 turns are recorded during the simulation (expressed by V_{n-n+1}). Fig. 2.5 shows typical waveforms of these inter-turn voltage drops within a half voltage cycle. Strong oscillation can be observed on the pulse voltage rising edge. This oscillation gives rise to a transient peak voltage value above 22 V, while the static voltage value is only around 4.7 V. Mechanism analysis is necessary for understanding why this overvoltage exists and what factors can affect it.

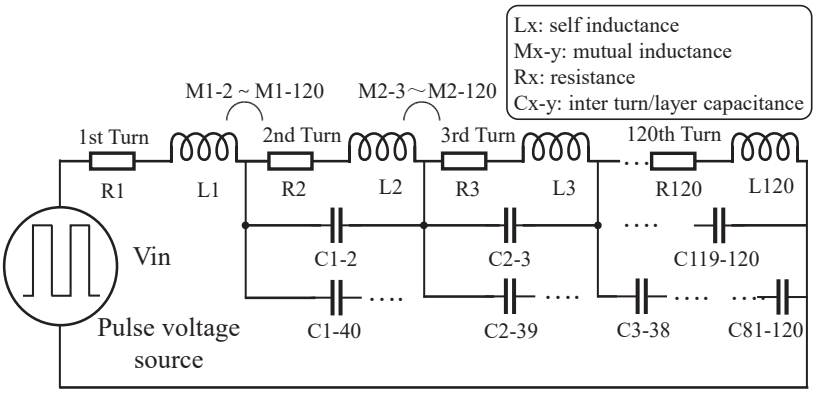

Fig. 2.4: Equivalent circuit model of the transformer's HV winding (values of L_x, Rx and C_{X-Y} lies in the range of R, L, C listed in Table 3) [J1, 65].

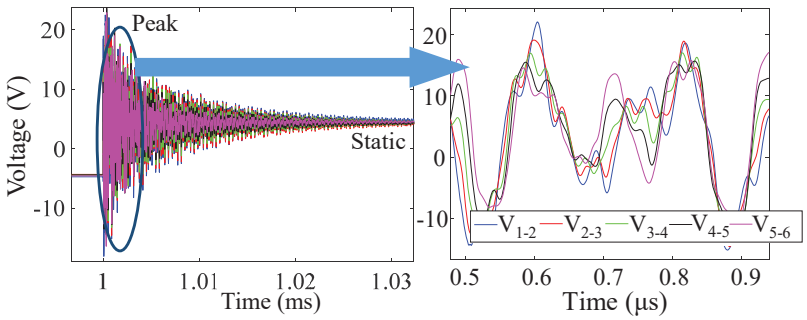

Fig. 2.5: Inter-turn voltage drop waveform [J1, 65].

Since the HV winding has 120 turns and 3 layers, the circuit model of the whole winding is very complex. Thus, it would be very complicated to analyze the mechanism of overvoltage by using this complete model. Yet, in the winding's design, inter-turn insulation distance (0.6 mm) is shorter than inter-layer insulation distance (1 mm). So inter-turn capacitance is larger than the inter-layer capacitance and would play a more important role in determining the transient inter-turn voltage. Therefore, for the sake of reducing the complexity of the overvoltage mechanism analysis, we ignore the inter-layer capacitance and simplify the three-layer winding into a winding with only one layer and n+1 turns. The simplified winding's circuit model is displayed by Fig. 2.6. All the turns are with the same R, L and C values. In the HV winding's circuit model, mutual inductance is always lower than the self-inductance and plays a less important role in determining the overvoltage. In the following analysis of this section, stray inductance would not be changed. Considering these two factors, to reduce the great complexity in the calculation of overvoltage, we ignored the mutual inductance although this may lead to a less accurate result. Equation (2.3), obtained through Laplace transformation, expresses the impedance $Z_{i+1,\ i+2}$ ($0<i\leq n$) between adjacent points (in Fig. 2.6, point 1 and 2, 2 and 3,…N+1 and N+2).

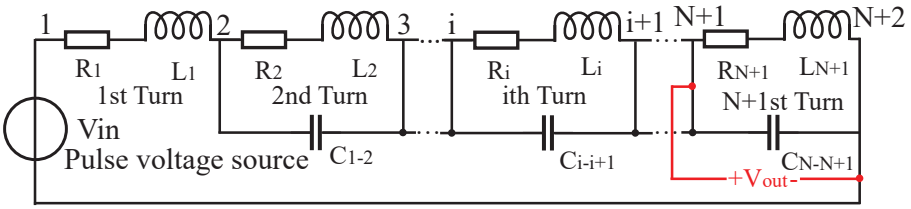

Fig. 2.6: Simplified circuit model [J1, 65].

$$Z_{12}(s) = R + Ls, Z_{i+1,i+2}(s) = \frac{R + Ls}{LCs^2 + RCs + 1} \tag{2.3}$$

Relationship between the output inter-turn voltage and input voltage is needed to understand why the voltage overshoot exists when pulse voltage is added on the circuit. V_{out} is used for expressing the voltage drop on the $(n+1)^{st}$ turn, then the transfer function between output voltage V_{out} and the source voltage V_{in} can be expressed by (2.4). Equation (2.4) can be simplified into (2.5) by factorization. Notice that the total number of turns equals to n+1.

$$\frac{V_{out}(s)}{V_{in}(s)} = \frac{Z_{n+1,n+2}(s)}{Z_{12}(s) + \sum_1^n Z_{i+1,i+2}(s)} = \frac{R + Ls}{L^2Cs^3 + (2RCL)s^2 + (R^2C + (n+1)L)s + (n+1)R} \tag{2.4}$$

$$\frac{V_{out}(s)}{V_{in}(s)} = \frac{R + Ls}{(R + Ls)(LCs^2 + CRs + n + 1)} = \frac{1}{LC}\left(\frac{1}{s^2 + \frac{R}{L}s + \frac{n+1}{LC}}\right) \quad (2.5)$$

With equation (2.5), relationship between V_{out} and V_{in} can be expressed through an open-loop system shown in Fig. 2.7. The pulse voltage we used for the simulation is different from a step signal, rise time exists (for the practical pulse voltage source, the situation is the same). Thus, according to the automatic control principle [78], a step function multiplied by a first-order inertia link (corresponds to Function 1 of Fig. 2.7) can be used to express the input voltage. In Function 1, T is the time constant and the input voltage rise time equals 2.2T. Function 2 is a typical 2 order system. Then, it is possible for us to analyze the mechanism of the overvoltage and factors that can influence it quantitatively based on these transfer functions and the theory of automatic control. Equation (2.6) can be used to express natural frequency ω_n and damping ratio ξ of Function 2. According to the value ranges of stray parameters in Table 2.2, poles of Function 2 are in the form of A±jB (both A, B <0), and the damping ratio is within the range 0<ξ<1. Therefore, Function 2 is a stable system and the output response waveform of V_{out} is a pulse voltage with damping oscillation on its rising edge as seen in Fig. 2.5. This phenomenon is similar with previous studies in the field of inverter-fed motors [59].

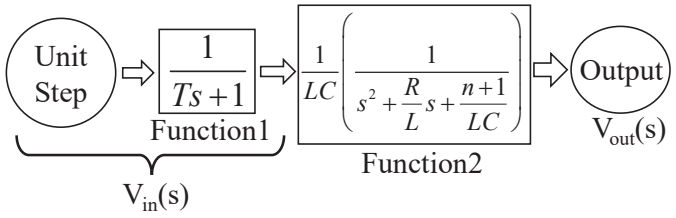

Fig. 2.7 Transfer function between V_{out} and V_{in} [J1, 65].

$$\omega_n = \sqrt{\frac{n+1}{LC}}, \xi = R\sqrt{\frac{C}{4L(n+1)}} \quad (2.6)$$

From (2.6), increasing the value of R or C can make damping ratio higher, then the oscillation should be weaker. To prove this deduction, we conduct simulation on the simplified circuit model in Fig. 2.6 to see the overshoot with different R and C values. Before the simulation, n in (2.5) is set as 1 for decreasing the simulation time. As a result, the model in Fig. 2.6 changes into a simplest winding with only two turns. The input pulse voltage has 1 V peak value and 20 ns rise time. Table 2.3 lists the parameters of the simulation and the output voltage overshot. Overshot σ is calculated by through (2.7).

Table 2.3 Simulation results on the simplified circuit model

Group	L (nH)	R (Ω)	C (pF)	σ (%)
A	50	0.04	50	10.7
B	50	0.4	50	8.46
C	50	0.04	500	32.24

$$\sigma = \frac{V_{peak} - V_{static}}{V_{static}} \tag{2.7}$$

Where V_{peak} and V_{static} represent the transient peak value and static value of the output voltage respectively. Values of L, R and C in Group A are in accordance with the value ranges listed in Table 2.2. Group B and Group C in Table 2.3 are added for comparing the overshoot with higher R and C values. Comparing the result of Group A with Group B, we can see increased R makes the overshot lower because of higher ξ. On the contrary, by comparing the results between Group A and Group C, we can see larger stray capacitance makes overshot higher although ξ is also increased. This result can be explained by the decreased ω_n in (2.6) because of larger C value.

The natural frequency ω_n of Function 2 refers to the resonant frequency of the simplified circuit model. As mentioned in Section 2.2.1, pulse voltage has a large content of high frequency components, of which the highest frequency f_u is calculated approximately by (2.2). If the circuit model is fed by pulse voltage, resonance can be triggered on the output inter-turn voltage by the above-mentioned high frequency components. This is one of the important factors that causes overvoltage on the rising edge. Considering the rise time t_r and the values of C and L in Group A of Table. 2.3, f_u is much smaller (approximately 15.9 MHz) than ω_n (approximately 894 MHz). If the C value is fixed, according to (2.2), shorter rise time leads to higher f_u. Then f_u gets closer to ω_n and stronger resonance can be achieved. Correspondingly, with the rise time kept unchanged, according to (2.6), increasing of C can reduce the ω_n and makes it closer to f_u. Both of these two changes can give rise to a higher output voltage overshoot. Keeping values of L and R the same as that of Group A in Table 2.3, simulation is repeated with the capacitance value increases from 10 pF to 1000000 pF continuously. The change trending of overshoot with increasing C is plotted in Fig. 2.8. The overshoot curve can be separated into two regions. In region 1, the decreasing of ω_n with increasing C plays a dominant role in determining the resonant oscillation intensity, which leads to higher overshoot. In the meantime, ξ is also growing. Its effect in decreasing the oscillation intensity becomes more obvious when C is larger than 10000 pF, which makes the growing speed of overshoot slower. The curve meets a saturation when C reaches a value around 80000 pF. In region 2, with C larger than 80000 pF, increasing of ξ due to larger C plays a dominant role in affecting the oscillation and leads to lower overshoot. The inter-turn capacitance in a practical transformer can never be as large as 80000 pF. Therefore, we draw the conclusion: when inter-turn capacitance increases, higher inter-turn voltage overshoot can be expected.

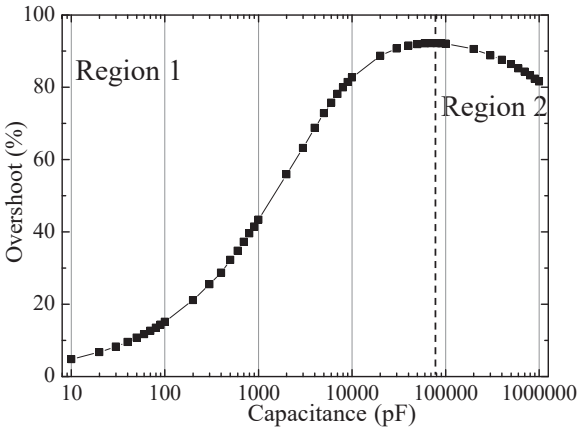

Fig. 2.8: Overshoot with different capacitances [J1, 65].

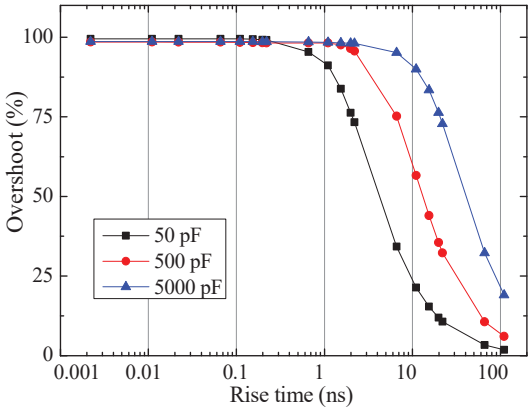

Fig. 2.9: Overshoot with different rise times and capacitances [J1, 65].

We also conduct the simulation with C equals to 50 pF, 500 pF and 5000 pF under decreasing voltage rise time (R is kept as 0.04 Ω and L as 50 nH, same as that of group A in Table 2.3). Output voltage overshot is plotted in Fig. 2.9. With input voltage rise time goes shorter, overshoot grows higher obviously from the beginning and then reaches a stable value. When the rise time is short enough, f_u exceeds ω_n, which means the resonance frequency of the circuit model is covered by the frequency of the pulse voltage's high order harmonics. Then, strongest resonance on output voltage is already triggered. Therefore, no much difference can be expected with further decreasing of voltage rise time. In each curve of Fig. 2.9, there is a rise time value with which the overshoot no longer increases obviously with further rise time reduction. We define this value as critical rise time. Then we can also see from Fig. 2.9 that with larger capacitance, critical rise time would be longer. The reason is that larger capacitance leads to lower ω_n. Then, with the same rise time, f_u gets closer to ω_n, strong resonance is easier to be triggered. Correspondingly, with decreasing of rise

time (from 100 ns), if C value is larger, f_u can exceed ω_n with relatively longer rise time. This means longer rise time can already give rise to strongest resonance. The explanation on the mechanism of how do rise time and stray capacitance affect the overshoot on the inter-turn voltage drop is confirmed by these results in Fig. 2.8 and Fig. 2.9.

The study object for analyzing the mechanism of inter-turn overvoltage and the impact from rise time and stray capacitance in this section is a most simplified model with one layer and two turns. Whether the similar situation of electrical stress exists in the complicated 3 layers 120 turns model built for the selected practical transformer's HV winding with the existence of mutual inductance between turns and inter-layer capacitance in Fig. 2.4 needs to be verified. This will be discussed in the following section.

2.4 SIMULATION ON THE COMPLETE MODEL

For the transformer applied in power electronic systems, working voltage rise time can be variable becuase of the difference in switching speed among different semiconductor switches. In the transformer's design, with the insulation distance kept constant, applying different insulation materials can also affect the winding's inter-turn and inter-layer capacitance because of different relative permittivity. Previous study on the electrical stress of the transformer's winding show that changing the winding structure can be helpful in reducing the static inter-layer voltage drop [79]. Whether this method can also help relieve the transient inter-turn and inter-layer overvoltage cuased by fast rising edge of PWM-like voltage is worth study. Therefore, simulation on the whole module in Fig. 2.4 is necessary for proving the accuracy of the mechanism analysis in section 2.3 and for investigating the aforementioned factors' impact on the electrical stress.

2.4.1 TESTING OF INTER-TURN AND INTER-LAYER VOLTAGE

In the first layer of the HV winding, inter-turn voltage drops from 1st and 6th turns would be measured. Correspondingly, inter-turn voltage drops from 21st to 26th turns, which refer to the first 6 turns in the second layer, along with inter-turn voltage drops from 41st to 46th turns, which refer to the first 6 turns in the third layer, would also be measured. $V_{n-(n+1)}$ is used to express these inter-turn voltage drops (for example $V_{1\text{-}2}$ expresses voltage drop between the 1st and 2nd turns). As mentioned in Section 1.1.3, if the winding has more than one layer, electric stress brought by fast rising edge of pulse voltage can also threaten the inter-layer insulation. So the simulation on inter-layer voltage drop is also necessary. Test points seen in Fig. 2.10 are used for the measaurement of inter-layer voltage waveform. V1-V3 are used to measure the voltage drop between the first layer and the second layer while V4-V6 used for that between the second layer and the third layer.

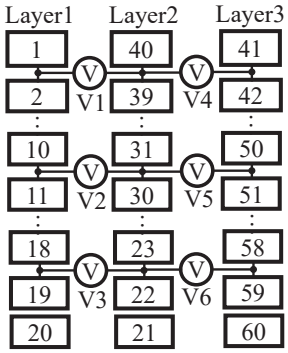

Fig. 2.10: Test points for measuring inter-layer voltage drop in C-type winding [J1, 65].

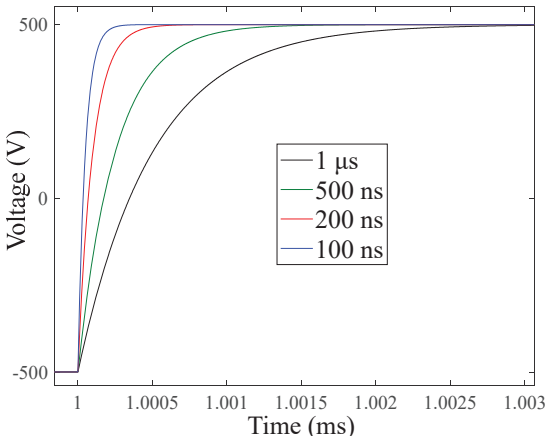

Fig. 2.11: Pulse voltage with different rise times for simulation.

2.4.2 OVERVOLTAGE UNDER DIFFERENT RISE TIMES

For the sake of reducing switching loss, power electronic switches are developing to have faster switching speed. Recently, some of the SiC-based switches can reach voltage rise/fall time shorter than 100 ns [80]. This factor may give rise to stronger electric stress on the medium voltage electrical devices working in power electronic systems. For proving the impact from rise time on the electric stress faced by the winding of MVMF transformer, rise times including 100 ns, 200 ns, 500 ns and 1 μs are selected, shown in Fig. 2.11. The parameters of the simulation in this section are listed in Table. 2.4. Notice that the winding structure is C-type, its winding layout is seen in Fig. 2.10.

During the simulation, typical inter-turn voltage waveforms are similar with that shown in Fig. 2.5. Taking Group 1 in Table 2.4 as an example, peak voltage values

V_{peak} between different adjacent turns during the pulse voltage rising flank are plotted in Fig. 2.12. Unlike the results from inter-turn voltage simulation on motor's winding [60], which shows voltage between the first two turns has highest V_{peak}, peak voltage value between different adjacent turns of this selected transformer's HV winding does not decrease monotonously. The reason is that MVMF transformer's winding and core have different structures compared with HV form-winding motor [81]. In this case study, inter-layer capacitance and mutual inductance (between non-adjacent turns) exist in the three layer HV winding of the selected transformer prototype. Thus, the capacitive and inductive coupling within this transformer's winding is very different from the motor's winding, which give rise to a different voltage distribution.

Table. 2.4: Simulation on the whole model under different rise times

Group	t_r (ns)	ε_r	Winding Structure
1	100	3.9	C-type
2	200		
3	500		
4	1000		

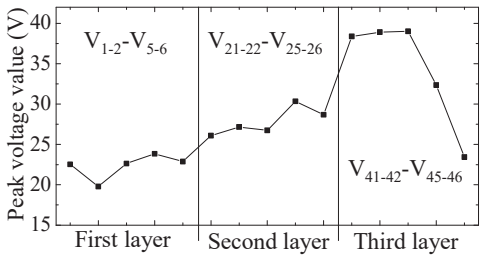

Fig. 2.12: Inter-turn peak voltage value [J1, 65].

Nevertheless, peak values of inter-turn voltage V_{peak} are obviously higher than the static voltage values (V_{static}), which can also threaten the transformer's inter-turn insulation. The overvoltage ratio, expressed by $R_{ov}=V_{peak}/V_{static}$, is used for the description of the extent of overvoltage. The R_{ov} values with different rise times are shown in Fig. 2.13. Notice that, in the HV winding, the length of each turn is not completely the same, the turns in inner layer are shorter than that in outer layer. Also, for turns in different position, the proximity effect may also be different. These factors leads to different resistance for different turns and cause different V_{static}. This is why the shape of line of R_{ov} in Fig. 2.13 is different from that of V_{i-i+1} in Fig. 2.12.

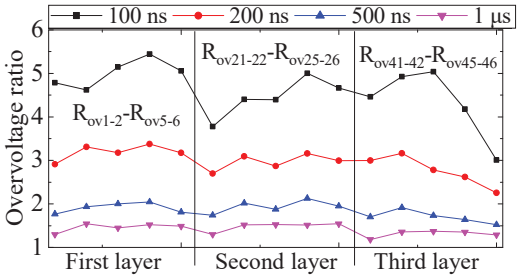

Fig. 2.13: Inter-turn overvoltage ratio with different rise times (C-type winding, ε_r=3.9) [J1, 65].

For inter-layer voltage drops, typical waveform is plotted in Fig. 2.14 (parameters same as that of Group 1 in Table 2.4). Static inter-layer voltage value measured by different test points is of a great variety. This situation is normal for a winding with three layers and C-type structure because V1 measures voltage drop between the 1st turn and 40th turn (39 turns in between), while V3 measures voltage drop between 18th turn and 23rd turn (only 5 turns in between). Therefore, although R_{ov} of V1 in Fig. 2.14 maybe lower than that of V3, the peak voltage value in V1 is still much higher than that in V3. In this situation, R_{ov} is no longer suitable for comparing the extent of inter-layer overvoltage in different test points with different simulation parameters. In comparison, peak voltage value is more suitable because it at least shows transient maximum inter-layer potential difference, which can reflect the inter-layer electrical stress. Fig. 2.15 shows peak inter-layer voltage values with different voltage rise times.

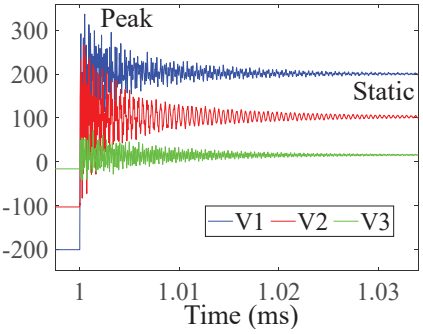

Fig. 2.14: Inter-layer voltage waveform (C-type winding) [J1, 65].

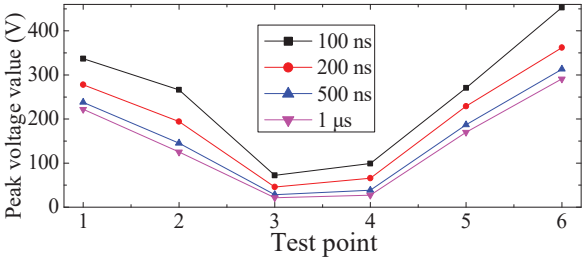

Fig. 2.15: Peak inter-layer voltage under different rise times (C-type winding, ε_r=3.9) [J1, 65].

It is clear that shorter rise time gives rise to stronger transient electric stress on the transformer's winding. Especially for the inter-layer voltage drop. Under shortest rise time 100 ns, in the test point V6, the peak voltage value can reach around 450 V, which is nearly 190 V higher than the static voltage value. For a transformer, in real situation, unlike the ideal insulation condition we assumed in section 2.1, air ducts may be left in regions between adjacent turns or winding layers unintentionally. If that happens, electric field intensity in the air duct may exceed the air's ionization strength. Then partial discharge may be triggered with high probability. Therefore, methods for prolonging the working PWM voltage rise time is recommended for releasing this possible electric overstress [82-83].

2.4.3 OVERVOLTAGE UNDER DIFFERENT PERMITTIVITY

According to different working conditions, different materials may be used for constructing the insulation of transformers [84]. These materials include polyester, polyimide, DMD paper and Nomex paper etc. Among them, besides the difference in dielectric strength, relative permittivity is another variable and important property that can leads to different insualtion behavior. The value of capacitance is proportional to relative permittivity ε_r. Therefore, in transformer's winding, variable ε_r leads to different inter-turn and inter layer capacitances. As analyzed in Section 2.3, this factor may in turn affect the winding's inter-turn overvoltage. In this section, simualtions on the complete winding's circuit model would be conducted under different ε_r of insulation for verifying the impact from stray capacitance on the overvoltage and investigating the impact from different insulation materials on the electric stress suffered by MVMF transformer. Among the materials usually used for medium frequency transformer's insulation, ε_r of Polyimide can be as high as 3.9, ε_r of polyester lies in the range from 2.9 to 3.4, ε_r of DMD is usually lower than 3.0 while that of Nomex can be as low as 1.6 [84]. Considering the above-mentioned range of ε_r, three different ε_r values including 3.9, 2.7 and 1.6 are chosen for representing these aforementioned materials in the comparative simulation. Table. 2.5 lists the parameters of the simulation in this section.

Table 2.4 Simulation under different permittivity

Group	t_r (ns)	ε_r	Winding Structure
1	100	3.9	C-type
2		2.7	
3		1.6	
4	200	3.9	C-type
5		2.7	
6		1.6	
7	500	3.9	C-type
8		2.7	
9		1.6	

With rise time 200 ns, simulation results of inter-turn and inter-layer voltage under different ε_r are plotted in Fig. 2.16 and Fig. 2.17 respectively. Lower ε_r (means lower inter-turn capacitance) can decrease the overvoltage a bit. To see the comprehensive effect of relative permittivity and rise time, the inter-turn overvoltage ratio within the first layer (from 1st to 6th turns) and inter-layer peak voltage value with different relative permittivity and rise times are plotted in Fig. 2.18 and Fig. 2.19 respectively. Reduction of ε_r can cause greater decreasing in overvoltage if rise time is shorter. Taking the inter-turn voltage as an example, under 100 ns, R_{ov} of $V_{1\text{-}2}$ drops by 27.08% when ε_r changes from 3.9 to 1.6, while with rise time 500 ns, R_{ov} decreases by only 16.07% with the same reduction of ε_r. Simulation results in section 2.4.2 and 2.4.3 are similar with that of the simulation and mechanism analysis based on the most simplified one-layer two-turns model in section 2.3. Table 2.5 shows detailed similarities between simulation results in section 2.3 and this section. Similar results can also be found in experiments proposed by literature [85], which show that shorter rise time causes higher voltage drop across each turn of transformer's winding and the voltage value does not show a monotonous decreasing trending from the first turn to the last turn.

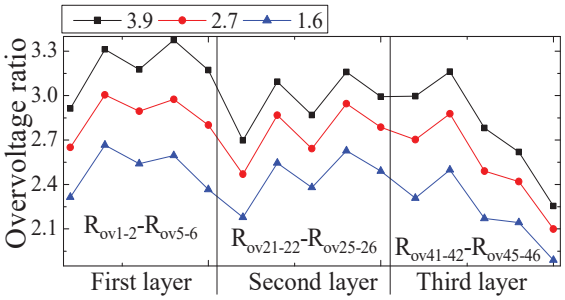

Fig.2.16: Inter-turn overvoltage ratio with different relative permittivity (C-type winding, 200 ns rise time) [J1, 65].

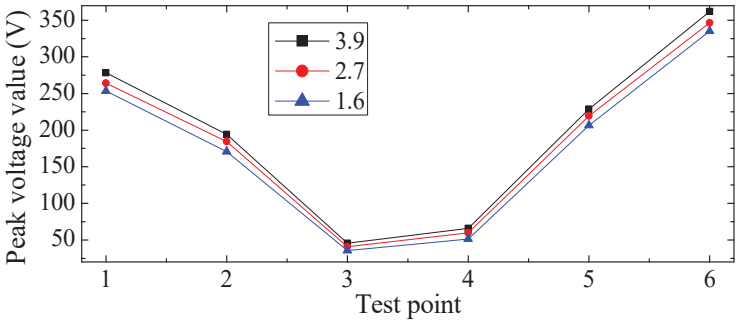

Fig. 2.17 Peak inter-layer voltage with different relative permittivity (200 ns rise time, C-type) [J1, 65].

Table 2.5: Similarities between simulation results in simplified model and complete model.

Simulation Results	Simplified Model	Complete Model
Overshoot on voltage rising edge exists?	Yes	Yes
Peak voltage value with shorter rise time	Higher	Higher
Peak voltage value with larger stray capacitance	Higher	Higher

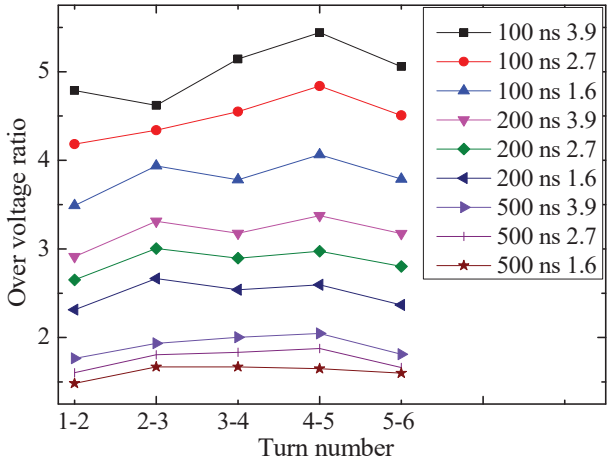

Fig. 2.18: Inter-turn overvoltage ratio under different rise times and relative permittivity [J1, 65].

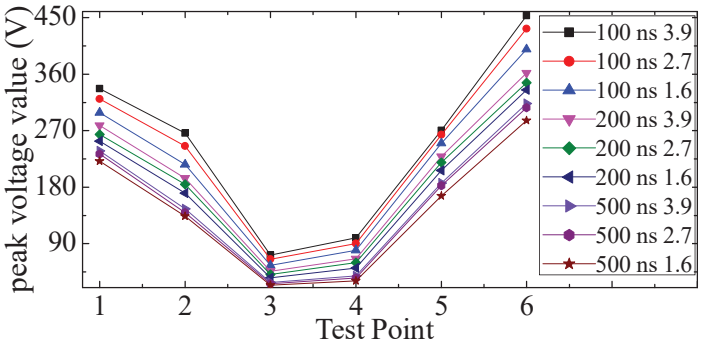

Fig. 2.19: Inter-layer peak voltage under different rise times relative permittivity [C1, 65].

2.4.4 OVERVOLTAGE UNDER DIFFERENT WINDING STRUCTURES

For the transformer's winding with more than one layers, C-type structure is the easiest to be constructed. However, with this structure, insulation between adjacent layers may suffer from a high static voltage drop. With Z-type structure, this inter-turn voltage drop can be effectively reduced [79]. Suppose that a winding has 2 layers,

and each layer with 2n turns. When fed by voltage with magnitude U, static inter-layer voltage drop under the above-mentioned two winding structures can be displayed by Fig. 2.20. With C-type winding, the highest inter-layer voltage drop is U, while with Z-type winding, the inter-layer voltage drop is constant as U/2. This conclusion is certainly useful for the design of transformer working under conventional power frequency sinusoidal voltage. Nevertheless, how would this changing of winding structure affect the transient electric stress brought from PWM-like voltage worth further investigation.

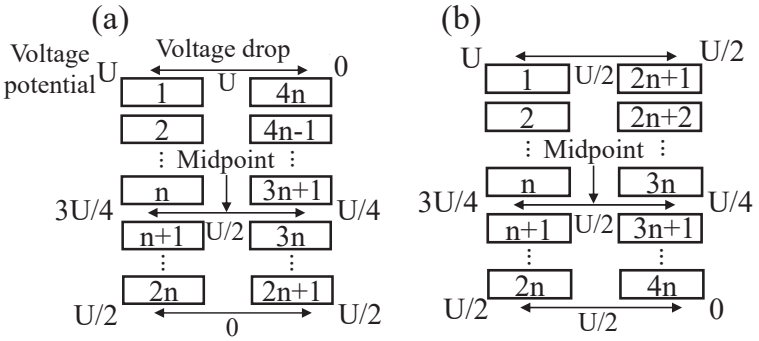

Fig. 2.20: Inter-layer voltage drop: (a) C-type winding; (b) Z-type winding [J1, 65].

The winding layout and the measurement of inter-layer voltage drop of the Z-type winding are shown Fig. 2.21. The position of V1-V6 are the same as that in Fig. 2.10, while the serial number of the turns is not the same because of a different structure. Parameters of the simulation under different winding structures are listed in Table. 2.6.

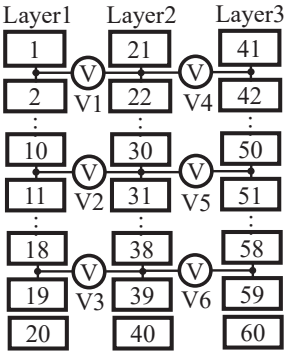

Fig. 2.21: Test points of the interlayer voltage drop in Z-type winding [J1, 65].

Table. 2.6: Parameters of simulation under different winding structures

Group	t_r (ns)	ε_r	Winding Structure
1	200	3.9	C-type
2			Z-type

Results of inter-turn and inter-layer voltage drop simulation are plotted by Fig. 2.22 and Fig. 2.23 respectively. Except R_{ov} between the 45th and the 46th turns in the third layer, most of the inter-turn overvoltage ratio decrease when the winding changes from C-type to Z-type. For the inter-layer voltage drop, from V1 to V6, the peak voltage values in Z-type winding are very different from C-type winding. The reason can be found by comparing Fig. 2. 10 and Fig. 2.21. As described before, under C-type winding, inter-layer voltage drop measured by V1, V2, V3 equals to the voltage difference between the 1st turn and the 40th turn, between the 10th turn and the 31st turn, between the 18th turn and the 23rd turn respectively. Number of turns between terminals of the test point is various. For test points V4, V5 and V6, the situation is similar. While under Z-type winding, the distances with respect to electrical connection between two terminals of the test points are always the same (For example, V2 between the 10st turn and the 30st turn, V3 between the 18th turn and the 38th turn, always 20 turns in between). Therefore, among different test points in Z-type winding, the changing of peak voltage value is less compared with C-type winding. Because of this even distribution of inter-layer voltage, except for V3 and V4, inter-layer peak voltage values in others test points are obviously decreased with winding changes into Z-type.

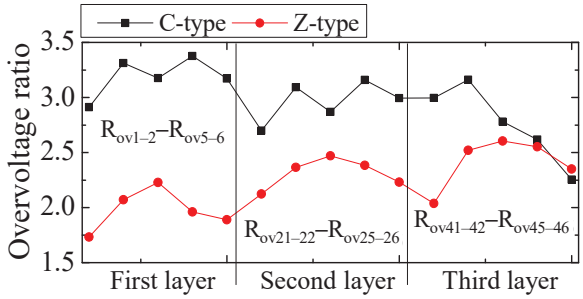

Fig. 2.22: Interturn overvoltage ratio under different winding structures (rise time 200 ns, ε_r = 3.9) [J1, 65].

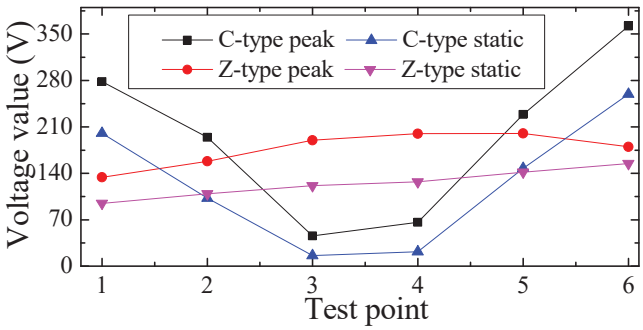

Fig. 2.23: Peak and static inter-layer voltage value with different winding structures (rise time 200 ns, $\varepsilon_r = 3.9$) [J1, 65].

In Fig. 2.23, static voltage values detected by all the test points are also added for displaying the difference between transient inter-layer voltage simulation in this section and static inter-layer voltage analysis proposed by the previous literature [79]. Because of the proximity effect, the resistance of turns in the HV winding are not the same. This is why static voltage value from test points V1 to V6 is not constant under Z-type winding even though numbers of turns in between the two terminals of these test points are the same. For the curve of voltage value vs. test points, although the trending of peak voltage value is almost the same as that of static voltage value, a difference exists in test points V2 and V5. Similar with that in Fig. 2.20, these two points are also mid-points between adjacent layers. Thus, in V2 or V5, static voltage drops under C-type and Z-type windings are almost the same as seen in Fig. 2.23. However, with the presence of pulse voltage induced overshoot, transient peak voltage values measured by V2 and V5 with Z-type winding are lower than that under C-type winding.

From the above results, compared with C-type winding, using Z-type winding can help MVMF transformer relieve the electric stress bought by the PWM working voltage. Therefore, for the design of MVMF transformer, this winding structure is more recommended.

2.5 SUMMARY

In this chapter, a circuit model of a MVMF transformer prototype is built. Based on that, transient voltage waveform simulations are conducted. The results show that inter-turn and inter-layer overvoltage would be triggered when the winding is fed by pulse voltage. This overvoltage would be more severe if the applied pulse voltage has shorter rise time. Reduction of insulation relative permittivity and changing the transformer's winding from C-type to Z-type can reduce the overvoltage. According to these results, some suggestions including regulating the output voltage rise time of semiconductor switches or applying better winding structure and insulation material in the transformer's design phase can be given to limit the voltage overshoot.

On the other hand, the presence of the overvoltage in the winding indicates that potential risk of PD inception also exist in the transformers applied in power electronic systems. This points out the necesity of studies in the following sections concerning the PD and its induced aging behavior on MVMF transformer's insulation.

CHAPTER 3.

Building of the test system for PD and endurance studies

For conducting the PD and endurance studies, a test system with the ability to produce repetitive pulse voltage is necessary. This system should also be able to detect PD signals with high accuracy and protect itself from overcurrent (usually occurs when the samples under test meet breakdown). The chapter introduces the building of this system in details.

3.1 PULSE VOLTAGE GENERATOR

A half bridge SiC power electronic switch module is selected as the core component of the pulse voltage generator. Its brief structure can be expressed by Fig. 3.1. Switch unit in the module is formed by several SiC MOSFETs connected in series. By doing so, it can reach a voltage rating higher than 5 kV. LV control unit is integrated into the module. It receives enable signal and driving signal. With this module, a pulse voltage generator in Fig. 3.2 is constructed. A high voltage DC source is applied for giving the input voltage. Capacitor is used for stabilizing this input DC voltage. With the 25 V low voltage input, the control unit of the module is powered. LV pulse acts as driving signal for controlling the on-off of the inner switch unit. Resistor connected with the output terminal is used for restricting the current magnitude when the insualtion sample under test meets breakdown. If the sample between output terminals is insulation film or insulated electromagnet wires, the output voltage rise time can be adjusted by changing this resistor's resistance value [86]. This pulse generator is able to output repetitive unipolar pulse voltage seen in Fig. 3.3.

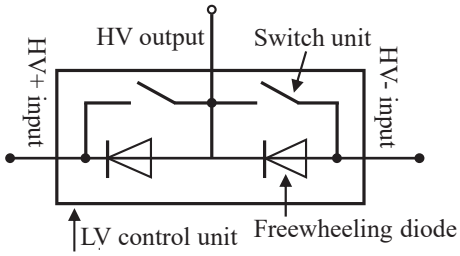

Fig. 3.1: Brief structure of the half bridge power electronic module

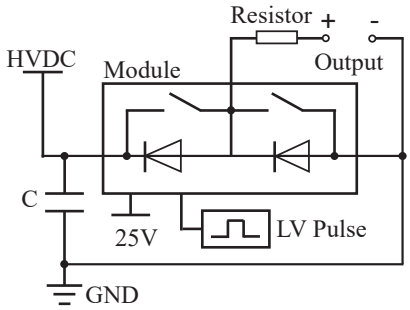

Fig. 3.2: HV pulse voltage generator [C2, 68].

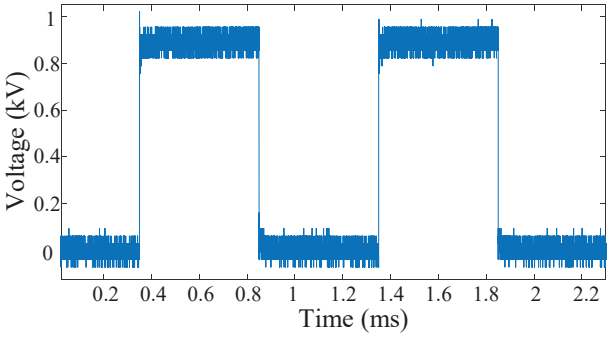

Fig. 3.3: Output pulse voltage waveform [C2, 68].

3.2 PD DETECTION

3.2.1 CHALLENGES IN PD DETECTION UNDER PULSE VOLTAGE

For PD tests, PD signal sould be detected with high accuracy. Due to the on-off of the power electronic switches, a strong interferece is generated [87], which brings the traditional PD detection devices like current sensor or high frequency current transducer (HFCT) difficulties in figuring out the PD signal. With reduction of the voltage rise time (faster switching speed), this interference would be even stronger [88]. In recent years, some studies have been proposed in finding suitable way for improving the signal-to-noise ration in PD tests under pulse voltage [89]. Some methods for signal processing such as wavelet analysis can extract the PD signal from the interference [90-91], but a higher signal-to-noise ratio is still very difficult to be achieved with no advance on the detecting devices. Since emission of photons is one of the important characteristics of external PD, some researchers use photo multiplier tube (PMT) for PD detection [92-93]. This detecting method can completely avoid interference from power electronic switches. However, it can only be available in a dark room, as any visible light can strongly decrease the accuracy of the PD detection.

3.2.2 ADVANTAGE OF UHF ANTENNA

In the analyzes of the interference and PD signal, it is found that in frequency domain, main energy of interference caused by power electronic switches distributes within 400 MHz. While the energy of PD under pulse voltage concentrates on frequency range higher than 500 MHz and can even spread to higher than 1.5 GHz [94]. Therefore, UHF antenna would be a suitable device for PD detection since it usually has high gain in frequency domains higher than 500 MHz. Another advantage is that UHF antenna is used to catch the electromagnet wave radiated by PD. Therefore, it would not be electrically connected with the main circuit. Electromagnet waves can break through the glass wall, so UHF antenna is also able to detect PD inside the oven or climate chamber with glass wall. The UHF antenna applied in this study and its gain in frequency domain are shown in Fig. 3.4. The antenna's gain can reach more than 2 dB in frequency from 500 MHz to 1.5 GHz, which would be suitable for catching PD signal under pulse voltage according to its energy distribution. The output interface of antenna would be connected to a 400 MHz-3 GHz band-pass filter for further suppressing the interference.

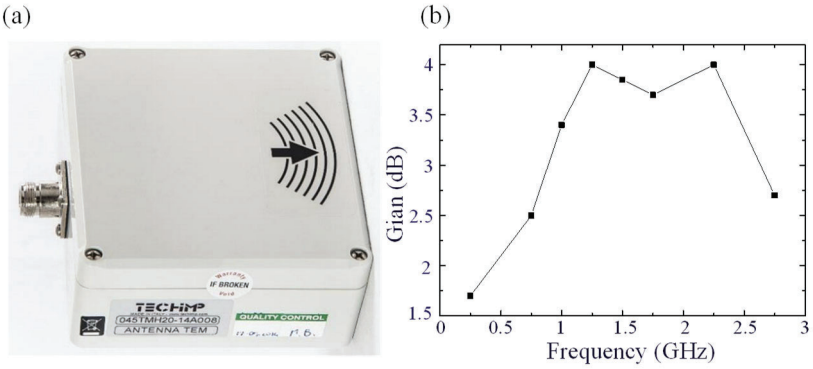

Fig. 3.4: UHF antenna: (a) Antenna's outlook; (b) Gain in frequency domain [C2, 68].

3.3 REMOTE CONTROL

For the purpose of generating the repetitive pulse voltage effectively along with the breakdown protection, a control system in Fig. 3.5 is applied. With the Ethernet formed by router, signal communication can be realized between computer and HVDC source and RTbox Controller. Two routers are applied for avoiding address conflict. Then, output voltage magnitude of the HVDC source can be controlled by the Labview program in computer. While the Controller is used to give enable and trigger signals that are provided by the computer to the power electronic module. The PLECS program for controlling the module is seen in Fig. 3.6. Digital pulse signal with variable frequency would be sent to channel 3 of the controller, the controller

would convert it into analog pulse signal to trigger the module. During the operation of the module, current sensor would monitor the output current and send the current value to the controller (Analog in) in real time. The PLECS program would receive this value and compared it with Max allowed current. If the sample under tests fails electrically, the current value would exceed the Max allowed value, switch enable signal would be changed into low level, the module would be blocked. This can protect the module from the damage caused by overcurrent.

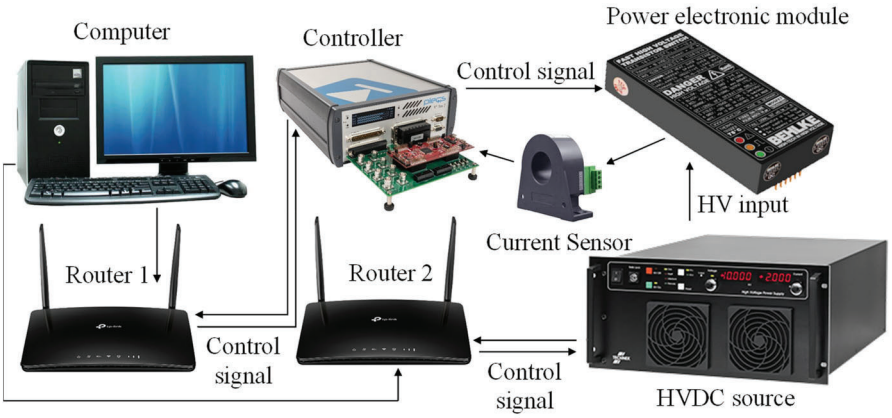

Fig. 3.5: Remote control for the pulse voltage generator

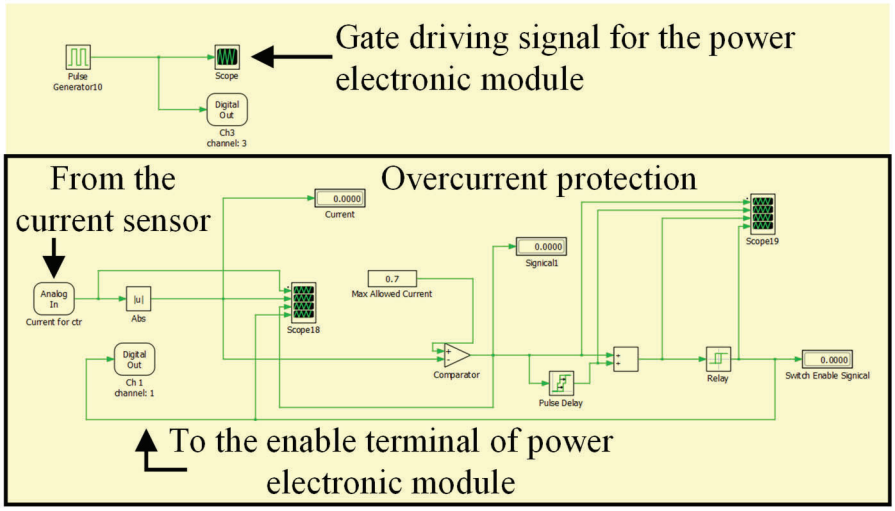

Fig. 3.6: Program for controlling the power electronic module

3.4 EXPERIMENTS

To approve the effectiveness of this test system, some experiments should be conducted. These experiments can help us investigate PD inception and deterioration on the insulation of medium voltage medium frequency transformers.

3.4.1 EXPERIMENT SETUP

The insulation sample used in this experiment is the Nomex paper that is usually applied in the insulation of transformer, seen in Fig. 3.7. The thickness of the sample is 0.05 mm. The sample is fixed by a sphere-plate electrode seen in Fig. 3.8. The sphere electrode (with diameter 25 mm) is connected with the output terminal of the pulse generator in Fig. 3.2, while the plate electrode is connected to ground. In this electrode setup, when added with overvoltage, main type of PDs would be the corona discharge that bridges the air duct between the insulation sample and the sphere electrode. This kind of PD can erode the insulation film's upper surface directly. According to section 1.1, Fig. 1.4 and Fig. 1.5, possible PD faced by transformer would also be the corona discharge that bridges the air duct and damage the insulation surface. Therefore, although the test sample is just a simple insulation film, studies on its PD inception and erosion can reflect the insulation failure mechanism faced by the medium voltage medium frequency transformer to some extent. The sample under tests would be put into an oven for controlling the environment temperature. Seen in Fig. 3.9, this oven can reach a maximum temperature 110 ℃, which can be used to simulate the temperature rise of the MVMF transformer in operation. Since the UHF antenna and its signal line cannot withstand a high temperature, it would be placed outside the oven and facing the oven door's glass part and direct to the sample inside the oven as seen in Fig. 3.9(b).

Fig. 3.7: Nomex paper

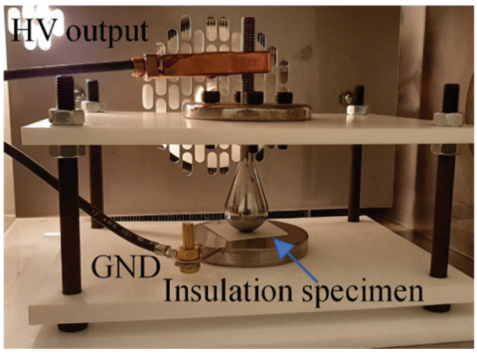

Fig. 3.8: Sphere-plate electrode [C3, 69].

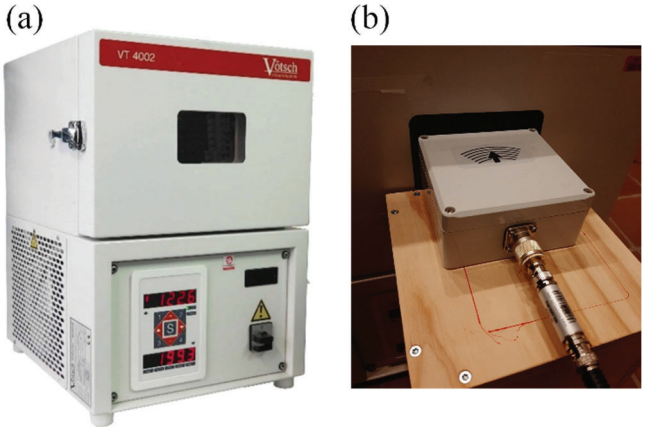

Fig. 3.9: Placement of UHF antenna for PDIV tests in the oven (a) outlook of the oven (b) position of the antenna.

Both PDIV and lifetime experiments are conducted to validate the system's ability in PD detection and breakdown protection. Table. 3.1 lists the parameters of the PDIV experiment. In each group, 5 samples are used for the tests. During the tests, voltage would be raised slowly with 10 V/s until the first PD can be detected by the antenna. PDIV value would be defined as the peak voltage value when the first PD is detected. The average PDIV value obtained under highest temperature in the PDIV tests would be recorded as $PDIV_m$. And this value would be applied in the following lifetime tests, of which the parameters are listed in Table. 3.2. Notice that to trigger repetitive PDs, voltage magnitude equals to PDIV is not enough [95-97]. According to previous literature [21, 40], usually pulse voltage with magnitude higher than 1.2 times PDIV or even higher than 1.4 times PDIV would be used for analyzing the PD feature or insulation endurance. That's why in Table 3.2, the peak voltage value is chosen from $1.3 \times PDIV_m$ to $1.5 \times PDIV_m$.

Table. 3.1: Parameters of the PDIV experiments

Group	Volage rise time	Frequency	Temperature
1	40 ns	1 kHz	20 ℃
2			50 ℃
3			80 ℃
4			110 ℃

Table. 3.2: Parameters of the PDIV experiments

Group	Peak voltage value	Frequency	Temperature
1	1.5×$PDIV_m$	1 kHz	20 ℃
2	1.5×$PDIV_m$		50 ℃
3	1.5×$PDIV_m$		80 ℃
4	1.5×$PDIV_m$		110 ℃
5	1.4×$PDIV_m$		110 ℃
6	1.3×$PDIV_m$		110 ℃

3.4.2 EXPERIMENT RESULTS

During the PDIV tests, the pulse voltage waveform detected by the HV probe along with the output signal of the UHF antenna with and without PD are plotted in Fig. 3.10. The interference brought by the module's switching is suppressed and the PD signal can be detected effectively. PDIV values with increasing temperature are plotted in Fig. 3.11. The $PDIV_m$ is 840V.

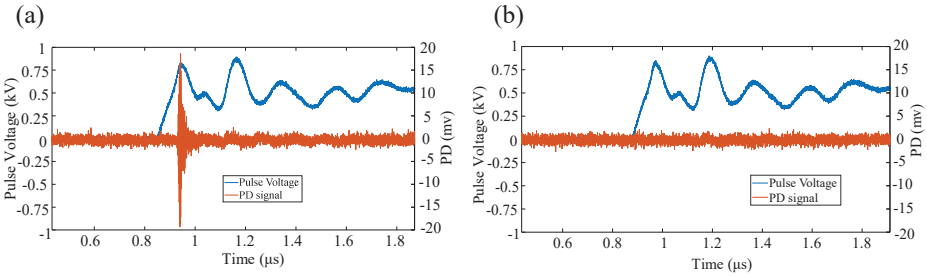

Fig. 3.10: Waveforms with and without PD: (1) With PD, (2) Without PD [C3, 69].

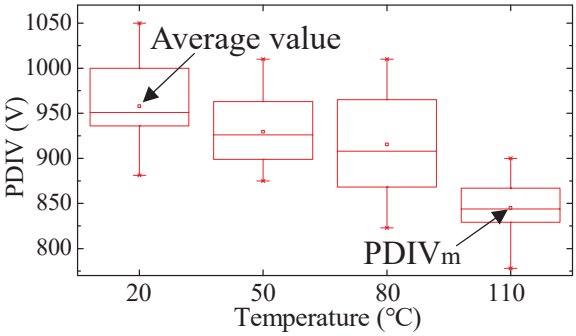

Fig. 3.11: PDIV under different temperatures [C2, 68].

In the endurance tests, when breakdown happens, the module would be blocked immediately and the current value in Analog In of Fig. 3.6 drops to 0, which proves the effectiveness of the breakdown protection described in Section 3.3. Also 5 samples are used in each group of Table 3.2. Results of endurance lifetime under different temperatures and different peak voltage values are shown in Fig. 3.12 and Fig. 3.13 respectively. With the electric overstress, the threshold temperature beyond which thermal aging can be induced is lower [98]. This is why temperature rise can make the electrical-thermal aging faster if continuous PD exists, even though the temperature does not exceed the rated temperature of Nomex paper (220 °C).

No breakdown happens on insulation samples in group 6 of Table 3.2 after 6 hours of electrical aging. In this group, with peak voltage value equals to $1.3\times PDIV_m$ (1.092 kV), PD can only be triggered with a very low probability (less than 1 PD per 5000 voltage cycles). While for other groups with peak voltage $1.4\times PDIV_m$ (1.176 kV) or $1.5\times PDIV_m$ (1.26 kV), continuous PDs can be triggered in each voltage cycle.

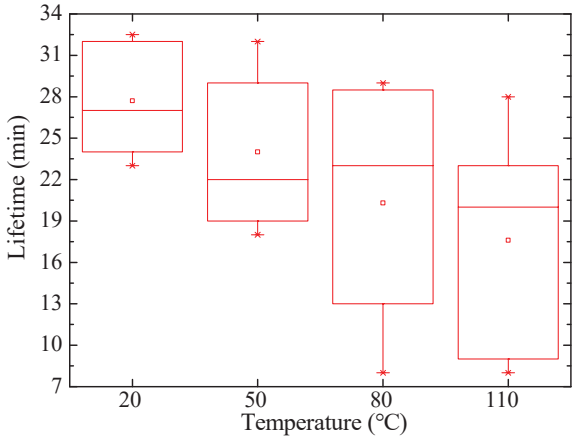

Fig. 3.12: Endurance lifetime with different temperatures [C2, 68].

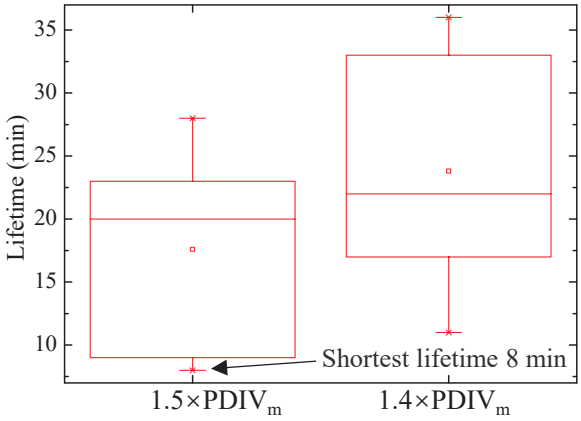

Fig. 3.13: Endurance lifetime under different peak voltage values [C2, 68].

It is obvious that pulse voltage induced partial discharge is extremely detrimental to Nomex paper's endurance. In the worst case, around 500000 pulse voltage cycles (8 min seen in Fig. 3.13) can already lead the insulation paper into final breakdown even though the material's breakdown strength is 440 V higher than the applied voltage magnitude (The dielectric strength of Nomex paper is 34 kV/mm, with 0.05 mm thickness, its intrinsic short time breakdown voltage is 1700 V). Lower voltage magnitude would surely decrease the PD intensity. Yet, with the existence of continuous PDs, this reduction in voltage magnitude can only prolong endurance lifetime by a few minutes. Only when the applied voltage is not enough to trigger repetitive PDs in each voltage cycle can the insulation material withstand the electric stress for a much longer time. Different from the oil-paper insulation usually applied by conventional transformer, for the dry type insulation usually applied by MVMF transformers, air ducts may exist between adjacent winding layers or adjacent windings where the potential difference is very large as described in Section 1.1.3. With the presence of overvoltage discussed in Section 2, the above-mentioned voltage drop can be even higher. Although impregnation on the Nomex paper surface can be applied when constructing the transformer's insulation, long period of thermal aging and mechanical fatigue (especially in railway and aircrafts) can still cause a partial low impregnation quality, making the fiber structure of Nomex paper directly face the PD inception and aging. Electric overstress combined with temperature rise caused by increased core loss and copper loss due to higher working frequency leads to a high PD inception probability. Besides the effect of higher temperature, higher voltage frequency can also give rise to more PD events per seconds. Therefore, the insulation aging speed would be further accelerated. Because of these factors, greater risk of insulation premature failure would be faced by MFMF transformer. Designers should consider better insulation materials or higher margin in insulation distance for providing long-term insulation reliability to these transformers.

3.5 SUMMARY

A test system is constructed for the investigation of PD inception and PD induced insulation aging. In this system, the most important part is a pulse voltage generator. It can generate repetitive pulse voltage to simulate the medium frequency and fast rising edge of PWM voltage, which is MVMF transformer's working voltage. UHF antenna combined with band-pass filter is chosen for the PD detection. Remote control based on Ethernet and current sensor is applied for a stable voltage output and breakdown protection. The system's effectiveness in PD detection and breakdown protection is proved by PDIV and endurance experiments.

The experiment results also indicate that MVMF transformer faces the risk of PD induced accelerated insulation aging since overvoltage and overtemperature, which can give rise to a high PD inception probability, have been proved exist via the last chapter and previous studies. For the design of MVMF transformer, to reach an expected insulation reliability, better insulation material or higher margin in insulation distance should be applied.

CHAPTER 4.

Comparative PDIV and endurance studies on different insulating materials used for medium frequency transformers

Finding better materials for the medium frequency transformer's insulation is an important step in improving its long term insulation reliability. In this chapther, based on the test system presented in the last chapter, comparative PDIV studies with rising temperature and endurance lifetime studies are conducted on different insulation materials typically used in MVMF transformer.

4.1 EXPERIMENT SETUP

Test system built in chapter 3 is utilized for the following experiments. Its overall diagram can be shown in Fig. 4.1. Its ability in PD detection and breakdown protection was proved in Section 3.4. During the experiments, the oscilloscope would display the applied pulse voltage waveform and output signal of antenna synchronously.

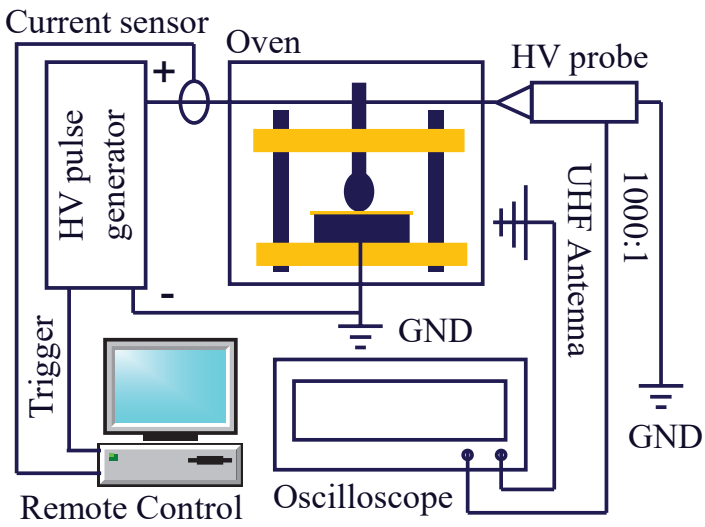

Fig. 4.1: Test system [C3, 69].

Three different insulation materials that are usually applied in the transformers are used for comparative studies: polyimide, polyester and Nomex paper [84] seen in Fig. 4.2. These materials are with the same thickness 0.05 mm and are cut into the same square shape with side length 2.5 cm. All of the insulation samples are cleaned by alcohol and then dried in the oven with 50 ℃ for 24 hours before the experiments.

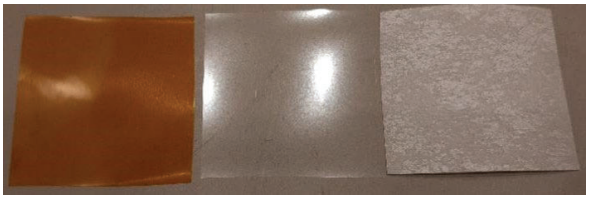

Fig .4.2 Polyimide (left), Polyester (middle) and Nomex paper (right) [C3, 69].

In the comparative PDIV tests, pulse voltage frequency (expressed by f) would be kept as 1 kHz, which is the working frequency of some MVMF transformers' applications [70]. While the rise time would be kept as 40 ns. For the MVMF transformers in operation, with working frequency much higher than the 50/60 Hz power frequency, higher copper loss and core loss can give rise to an obvious temperature rise. In some cases, the whole transformer's temperature can be raised to more than 100℃ [99]. Considering this factor, 4 temperature values from room temperature (20℃) to 110℃ are chosen. Table 4.1 shows detailed parameters of the comparative PDIV tests. During the tests, 5 samples would be used in each group and the average PDIV values would be recorded. After the tests, the PDIV average value under highest temperature obtained for polyimide, polyester and Nomex paper would be recorded as $PDIV_1$, $PDIV_2$ and $PDIV_3$ respectively. These values are used for the following endurance lifetime tests.

Table. 4.1: Parameters of PDIV tests [C3, 69]

Group	Material	Rise Time	Frequency	Temperature
1	Polyimide	40 ns	1 kHz	20 ℃
2				50 ℃
3				80 ℃
4				110 ℃
5	Polyester	40 ns	1 kHz	20 ℃
6				50 ℃
7				80 ℃
8				110 ℃
9	Nomex paper	40 ns	1 kHz	20 ℃
10				50 ℃
11				80 ℃
12				110 ℃

In the comparative endurance tests, for each kind of the materials, voltage peak magnitude is raised to 1.5 times the average PDIV values obtained under highest temperature during the PDIV tests (110℃). Temperature and voltage frequency are fixed at 110℃ and 1 kHz respectively. Detailed parameters are listed in Table. 4.2. Usually, Nomex paper is used along with impregnation to achieve better insulation capability, while other two materials do not need to be impregnated. As described in the last chapter, considering the solid-type insulation (the solid insulation paper would not be completely submerged into insulation oil) used by the MVMF transformer and the possible mechanical stress [100] and thermal stress, the insulation may not be in a good impregnation condition. Therefore, in this chapter, we also assume a worst condition that some part of the insulation paper would directly face the electric overstress. Then, comparative studies would be conducted using pure materials.

Table. 4.2 Parameters of endurance lifetime tests

Group	Material	Peak voltage	Frequency	Temperature
1	Polyimide	$1.5\times PDIV_1$	1 kHz	
2	Polyester	$1.5\times PDIV_2$		110 ℃
3	Nomex paper	$1.5\times PDIV_3$		

4.2 RESULTS OF COMPARATIVE PDIV TESTS

During the PDIV experiments, the trigger mode of oscilloscope is set as single-step. Voltage magnitude would be raised with 5V/s until the first PD happens. For each group in Table. 4.1, 5 samples are used for the tests. Average PDIV value with different materials and temperatures are shown in Fig. 4.3.

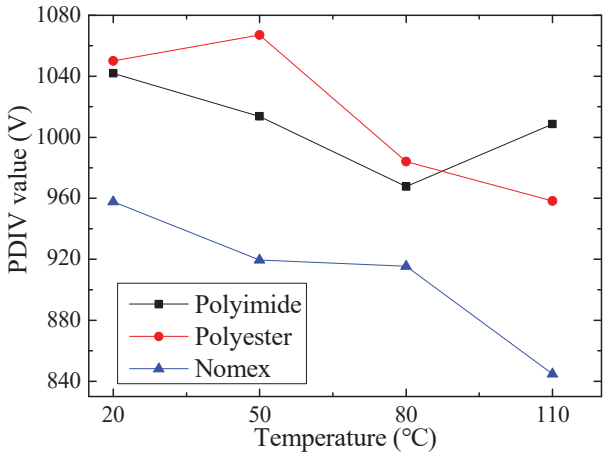

Fig. 4.3: PDIV values under different temperatures [C3, 69].

It is clear that, compared with Nomex paper, Polyimide and Polyester can better resist PD inception. With temperature rise from 20 ℃ to 110 ℃, PDIV of Nomex paper decreases by 12.2%, which is a most obvious reduction. When temperature is within 80℃, PDIV of polyester is highest while under 110 ℃, polyimide has relatively higher PDIV. In this experiment, voltage is added between two dielectrics, air and insulation film. In a parallel-plate capacitor like Fig. 4.4, suppose the electric field strength in air and insulation as E_{air} and E_d respectively, then relation between E_{air} and E_d can be expressed through (4.1) [22].

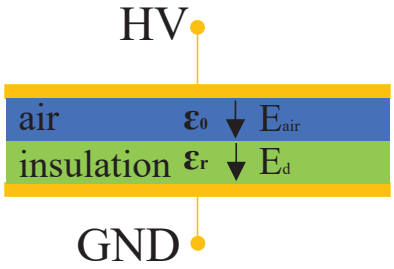

Fig. 4.4: Electric field in the parallel-plate capacitor with two dielectrics

$$\frac{E_{air}}{E_d} = \frac{\varepsilon_r}{\varepsilon_0} \tag{4.1}$$

Where ε_r is the insulation material's relative permittivity. ε_0 is the permittivity of the air. For a solid insulation material, its ε_r is usually much higher than ε_0. So electric field would concentrate in the air duct and becomes even stronger if ε_r increases. The electrodes used in this experiment are not a parallel-plate, as seen in Fig. 4.5(a). The air duct shape is completely different from that in Fig. 4.4 and the air duct length is not constant. Dielectric refraction exists and the distribution of electric field is uneven. Thus, it becomes more difficult to express the relationship between E_{air} and E_d quantitatively. Yet, similar situation like the parallel-plate can also be expected. Setting the voltage value of the sphere electrode as 1 kV and the Plate electrode as 0V (connected to ground), electric field distribution through FEM simulation is plotted in Fig. 4.5(b). In this simulation, ε_0=1, while ε_r=4. Strongest electric field lies in the air duct that is close to the contact point. Combined with the knowledge that dielectric strength of the air is usually lower than the solid insulation material, the main type of PD in this experiment should be the corona discharge that breaks through the air and strike the insulation surface. By repeating the simulation with ε_r equals to 3.5 and 3, simulation results are plotted in Fig. 4.6. With decreasing of ε_r, strongest electric field intensity in the hot spot is reduced. Therefore, permittivity of the insulation film is one of the important factors in determining the PDIV.

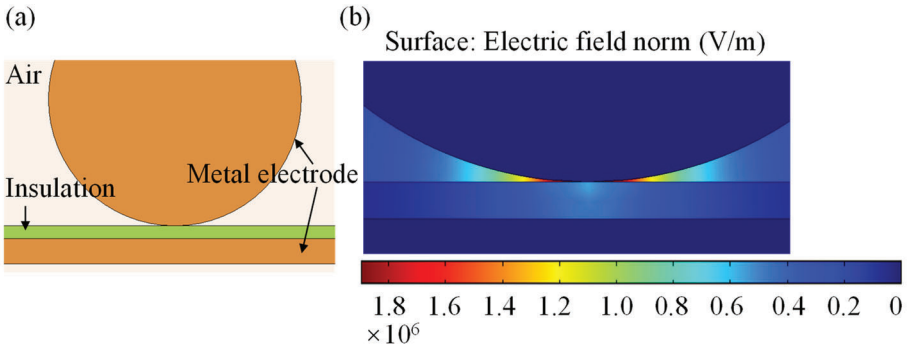

Fig. 4.5: Sphere-plate electrodes: (a) 2D Cross-section outlook, (b) Electric filed distribution

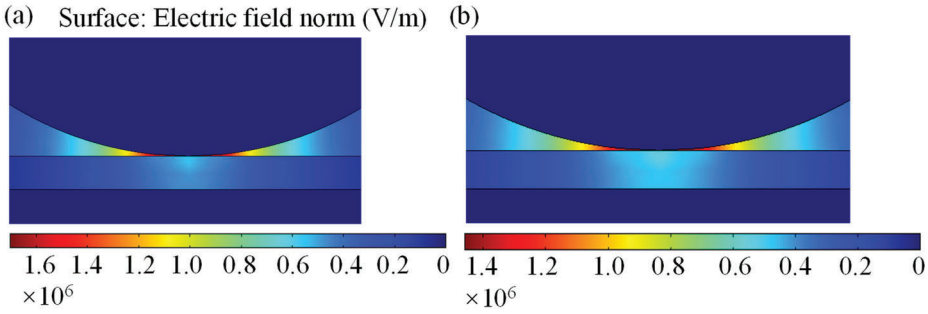

Fig. 4.6: Electric field distribution with lower ε_r: (a) ε_r=3.5, (b) ε_r=3

Although previous literature sources suggest the value range of ε_r of different materials used in this section [84], measuring the exact ε_r of these materials is necessary for better investigating the mechanism that leads to different PDIV among them. Dielectric analyzer seen in Fig. 4.7(a) [101] is used to measure the ε_r. The test setup is plotted in Fig. 4.7(b). Sample would be placed in a chamber (temperature inside can be controlled) and fixed in a modular test electrode, which integrates voltage input and signal communication. For each material, tests are conducted with frequency gradually increases from 0.1 Hz to 1 MHz. With different temperatures, permittivity of polyimide and polyester are plotted in Fig. 4.8. Since frequency of pulse voltage used in this PDIV study is 1 kHz, due to its fast rise time, high order harmonics exists as described in (2.2), we focus on frequency range from 1 kHz to 1 MHz for comparing the ε_r. Under room temperature (20°C), ε_r of polyimide in the above frequency range lies between 3.45 and 3.55, while polyester lies between 3.2 and 3.43. That's why in room temperature condition PDIV of polyester is higher than that of polyimide. With increasing temperature, the air molecule density would be reduced, lower breakdown strength of air duct can be expected [102]. This factor makes PDIV decrease with temperature goes higher in most of the cases. Yet, for the film insulation material, higher temperature can increase the material's surface conductivity [11]. With higher surface conductivity, surface charge, which is one of

the main sources of the initial electron to form the PD [103], would be dissipated faster. Then, PD inception requires higher voltage magnitude. On the other hand, in our experiment setup, humidity is not controllable. Yet, it is known that with temperature rise, humidity in the test environment would be decreased [104]. Releasing of initial electron may be more difficult due to decreased moisture absorption [105]. This is why in some situations (for polyester from 80 ℃ to 110℃, for polyimide from 20℃ to 50℃), PDIV value becomes higher when temperature rises.

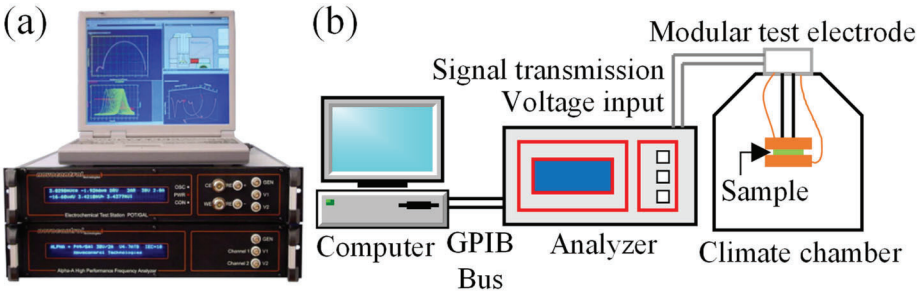

Fig. 4.7: Permittivity measurement: (a) Outlook of the dielectric analyzer, (b) Measurement setup

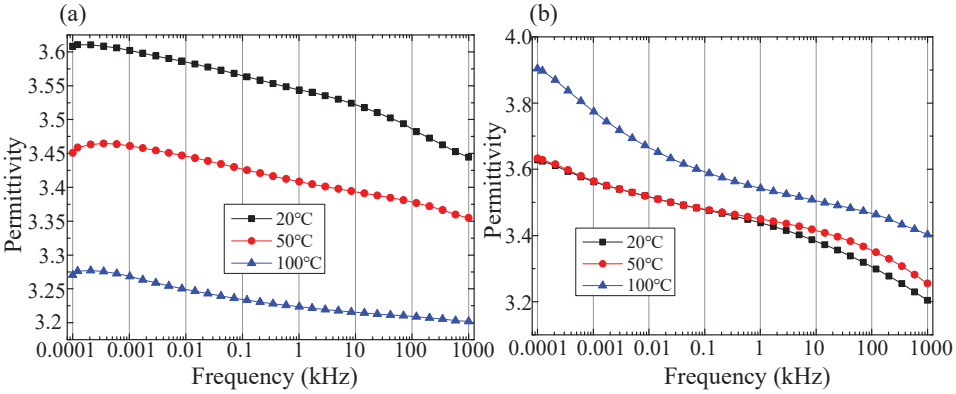

Fig. 4.8: Permittivity of polyimide and polyester: (a) Polyimide, (b) Polyester

From the above-mentioned factors and the difference in physical and chemical properties between polyimide and polyester, it may be difficult to analyze theoretically the different change trendings of PDIV values among these two materials. Nevertheless, from the Fig. 4.8, we can see that, with temperature rising, polyimide shows decreasing of ε_r while polyester has an obvious increase of ε_r from 50℃ to 100℃. This maybe the main reason why in relatively high temperature condition (more than 100℃), polyimide has higher PDIV than the polyester.

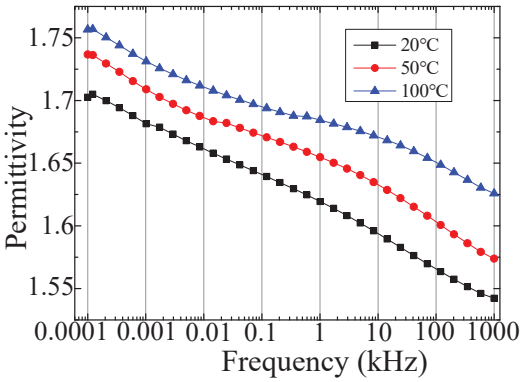

Fig. 4.9: Permittivity of Nomex paper

Permittivity of the Nomex paper is shown in Fig. 4.9. It is certainly that Nomex paper has obviously lower ε_r compared with other two materials. However, unlike the film insulation, surface of the paper insulation has a much higher porosity, which can give rise to strong electric field distortion and leads to lower PDIV. The aforementioned decreasing air density and the obvious increase of ε_r with temperature also contribute to its decreasing PDIV in Fig. 4.3.

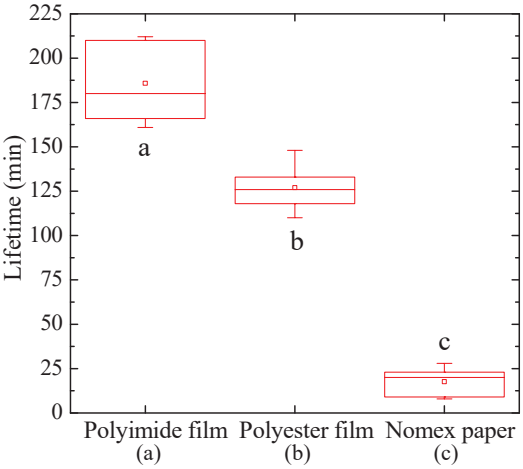

Fig. 4.10: Lifetime of different insulation materials [C3, 69].

4.3 RESULTS OF COMPARATIVE ENDURANCE TESTS

Similar with section 3.4.2, 5 specimens are used in each group of Table. 4.2 during the tests, all the samples are aged under continuous PDs until the final breakdown. Lifetime of different materials are plotted in Fig. 4.10. With continuous PDs, Nomex paper breaks down much faster than other materials while polyimide shows longest

endurance. Compared with dense film material, PD is more detrimental to porous fiber structure of the Nomex paper. Cracks due to PD erosion can easier be formed and grow faster through the whole paper and leads to final breakdown.

According to these above results, if Nomex is chosen for the MVMF transformer's insulation, higher quality of impregnation should be applied to better prevent the paper insulation from directly facing the electric stress bought by PWM-like voltage. Considering the cost of Nomex paper and impregnation, other two materials are more recommended for constructing the transformer's insulation. For different applications of medium frequency transformer, if the cooling system is powerful enough to keep the whole transformer in temperature lower than 80°C, polyester may be a suitable choice since it has better ability in resisting PD inception under relative low temperature condition. Otherwise, concerning the MVMF transformer's temperature rise, polyimide would be the best choice since it has higher PDIV in relative higher temperature condition. In addition, due to its longer endurance lifetime in resisting PD degradation, it is possible that with a very low probability of PD inception, the transformer can avoid premature insulation breakdown within its rated lifetime.

4.4 SUMMARY

Using repetitive pulse voltage, comparative PDIV and endurance tests are conducted on materials that are typically used for transformer's insulation: polyimide film, polyester film and Nomex paper. According to the results, Nomex paper has lowest PDIV and most obvious PDIV reduction with increasing temperature. In relatively low temperature condition, polyester has highest PDIV, whereas polyimide has best reliability in resisting PD inception under relatively high temperature condition. Without impregnation, under continuous PD aging, endurance lifetime of Nomex paper is much shorter than the other two materials, while polyimide has the longest lifetime.

Therefore, when using Nomex paper as the main insulation material of medium frequency transformer, higher quality of impregnation is needed to achieve an expected insulation reliability. In contrast, the other two materials are more recommended because of their better insulation behavior. Considering the possible temperature rise faced by medium frequency transformer and the longest PD endurance, polyimide may be the best choice.

CHAPTER 5.

Studies on the Influence of pressure on the PD and induced aging behavior

Since reducing air pressure can directly decrease the air's breakdown strength, it may also affect the capability of solid-type insulation of MVMF transformer in resisting PD inception and PD aging. In this section, PD and endurance tests are conducted on polyimide insulation film with different pressures. Pressure's impact on the PD magnitude, PD time lag and the PD aging are discussed in detail.

5.1 EXPERIMENT SETUP

To create lower pressure condition, a pressure tank is added into the test system. Seen from Fig. 5.1. By connecting the outlet valve with air extractor, pressure inside can be changed from 1 Bar to 0.3 Bar, which corresponds to the altitude from sea level to around 9000 m. This range covers all the high-altitude areas on earth and the flight height of short-haul flights. The insulation film would be fixed by the sphere-plate electrodes inside. The sphere electrode has 20 mm in diameter, smaller than the electrode in Fig. 3.8.

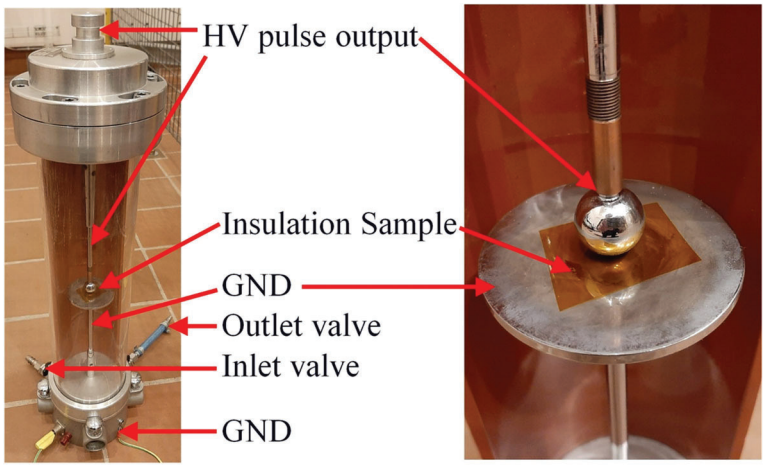

Fig. 5.1: Pressure tank [J2, 66].

With this tank, the test system's diagram in Fig. 4.1 is changed into Fig. 5.2. Since UHF antenna is designed for detecting electromagnetic wave radiated by the PD, the distance between the antenna and the pressure tank is kept at around 8 cm for the sake of reducing attenuation when PD signal travels through the air, seen in Fig. 5.3. The

sample for the experiments is polyimide film with 0.05 mm thickness, same as that in Fig. 4.2. The shape of the specimen is also square with 2.5 cm side length.

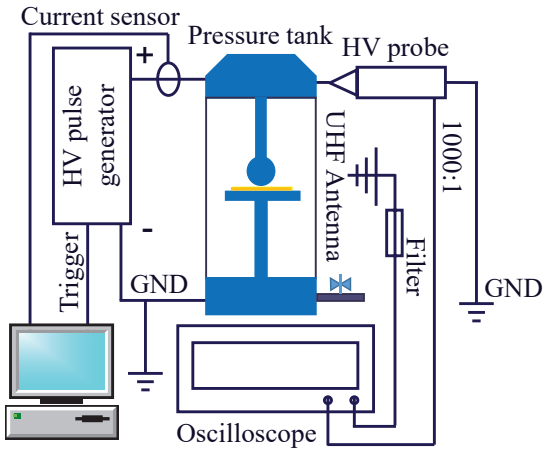

Fig. 5.2: Test system [J2, 66].

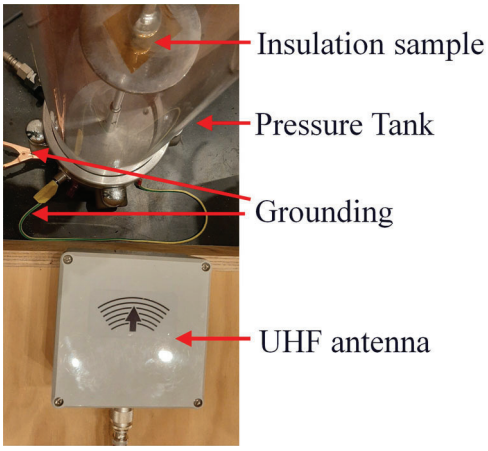

Fig. 5.3 Placing of UHF antenna [J2, 66].

5.2 PDIV EXPERIMENTS

Since the dimension of the sphere-electrode is different from that in Fig. 3.8, the electric field distribution is also different. This means that even under same pressure and room temperature as the Group 1 of Table. 4.1 (all the experiments in the last chapter are conducted under sea level pressure), PDIV may be different. Therefore, through this modified test system, a single PDIV test is conducted in advance under 1 Bar pressure. The result is 1350 V, which is obviously higher than the average PDIV

value in Fig. 4.3. Because of this, PDIV tests should be reconducted at sea level pressure. In addition, considering that in the following PD feature and endurance tests, higher voltage peak value is needed. For restricting the current when breakdown happens (including expected breakdown in endurance tests and unexpected breakdown during the PD tests), higher resistance value for the Resistor in Fig. 3.2 is necessary. With a 1 kΩ resistor applied, the pulse voltage rise time is 250 ns. Table. 5.1 lists the parameters of PDIV tests.

Table. 5.1: Parameters of PDIV tests under different pressures

Group	Rise time	Frequency	Pressure
1	250 ns	1 kHz	1 Bar
2			0.9 Bar
3			0.8 Bar
4			0.7 Bar
5			0.6 Bar
6			0.5 Bar
7			0.4 Bar
8			0.3 Bar

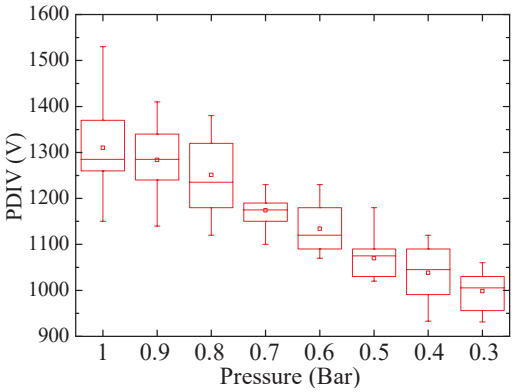

Fig. 5.4: PDIV with decreasing pressure [J2, 66].

The process of PDIV tests is the same as that described in section 4.2. Experiment results are shown in Fig. 5.4. With pressure decreasing, statistic PDIV value of the insulation film decreases monotonously. Although the electric field in the air duct between insulation film and sphere electrode is not uniform as expressed in Fig. 4.5 (with different sphere electrode diameter, the strongest filed intensity would not be the same, but the same overall field distribution can be expected), similar results are obtained compared to the Paschen's Curve measured with uniform electric field distribution.

5.3 PD FEATURE EXPERIMENTS

5.3.1 EXPERIMENT PARAMETERS

For analyzing statistical PD features, continuous PDs should be generated. Considering that in this chapter, only one kind of insulation specimen is selected for the study (no difference in the dielectric strength), PD feature experiments would be conducted using a same peak-voltage value 1.96 kV, which equals to 1.5 times the average PDIV value measured with 1 Bar. Table. 5.2 lists detailed parameters of the PD feature experiments.

Table. 5.2: Parameters of PD tests under different pressures

Group	Rise time	Peak voltage value	Frequency	Pressure
1	250 ns	1.96 kV	1 kHz	1 Bar
2				0.9 Bar
3				0.8 Bar
4				0.7 Bar
5				0.6 Bar
6				0.5 Bar
7				0.4 Bar
8				0.3 Bar

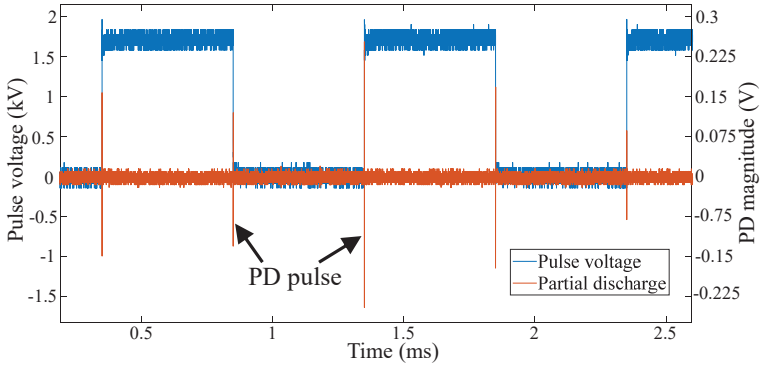

Fig. 5.5: PD generated by pulse voltage [J2, 66].

5.3.2 EXPERIMENT RESULTS

In the experiments, voltage magnitude is raised to the set value quickly. PD waveform displayed on the oscilloscope can be seen in Fig. 5.5. PDs are mainly triggered on the voltage rising and falling edges, or at least very close to the pulse edges (in low pressure condition, seen in Fig. 5.6). On the rest of the pulse voltage plateau regions, no obvious PD happens. The mechanism of this phenomenon would be discussed in section 5.3.3.

If the pulse voltage has symmetric waveform with 50% duty cycle and rise time equals to fall time, PDs on rising edge would have similar statistical features with that on falling edge [106-107]. Therefore, for analyzing the PD feature under symmetric pulse voltage and decreasing pressure, we mainly aim at the PDs happen around the rising edge. In each group of Table. 5.2, for acquiring statistical PD features, 300 cycles of data are collected by the oscilloscope. Fig. 5.6 shows time resolved PD patterns.

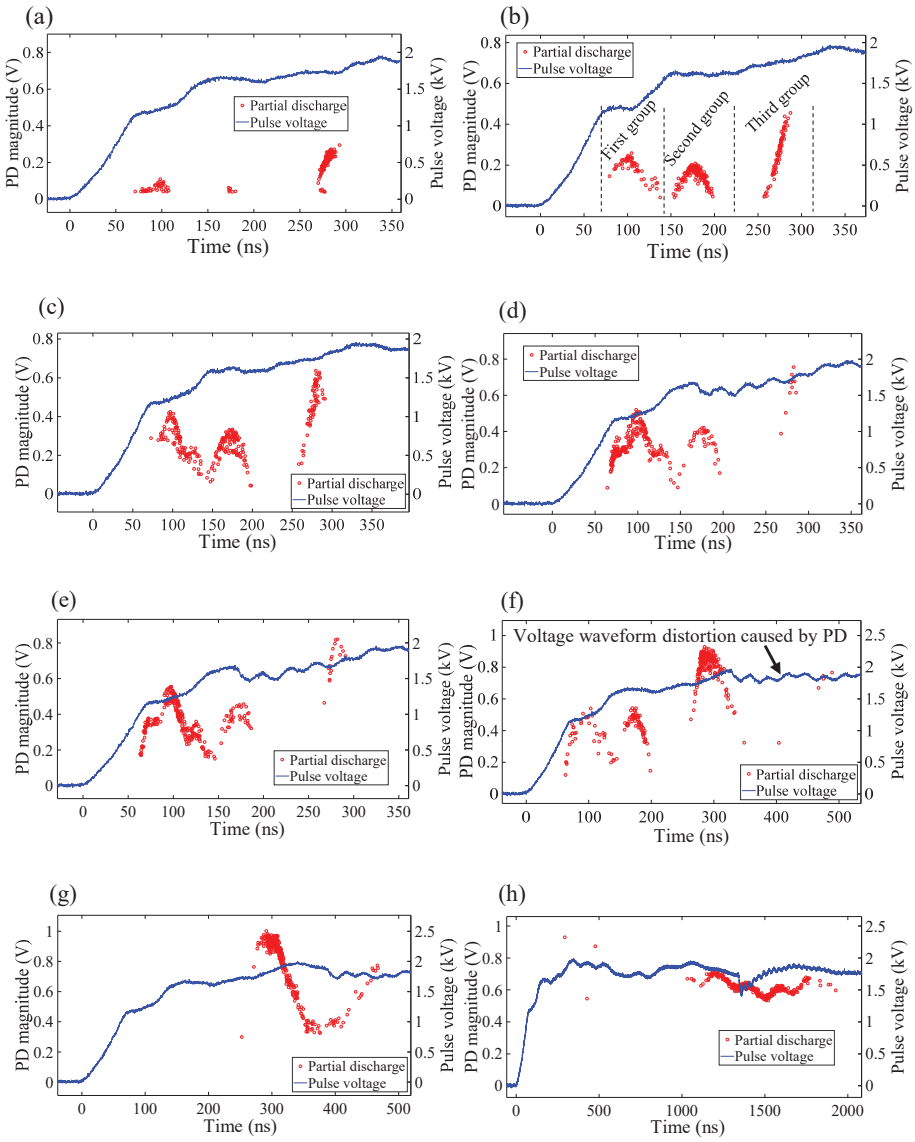

Fig. 5.6: PD patterns with different pressures: (a) 1 Bar, (b) 0.9 Bar, (c) 0.8 Bar, (d) 0.7 Bar, (e) 0.6 Bar, (f) 0.5 Bar, (g) 0.4 Bar, (h) 0.3 Bar [J2, 66].

With pressure from 1 Bar to 0.5 Bar, PDs distribute in three clusters. As shown in Fig. 5.6(b), these PDs can be divided into three groups according to which cluster they belong to. The beginning of the voltage rising edge (voltage value still equals to 0) is defined as zero point, where time=0 ns. Then the first group of PDs happen at around 100 ns. In the second group, PDs happen at around 170 ns while the third group of PDs at around 270 ns. PD firing voltage is defined as the instantaneous voltage value when PD happens [38]. Then it is clear that for the second group of PDs, the PD firing voltage is higher than that of the first group. However, despite randomness exists in the recorded PD magnitude, under the same pressure and voltage condition, the first group of PDs have stronger statistic intensity than the second group in most of the situations (from 1 Bar to 0.6 Bar). With pressure further decreases into 0.4 Bar and 0.3 Bar, the PD distribution becomes completely different with only one cluster.

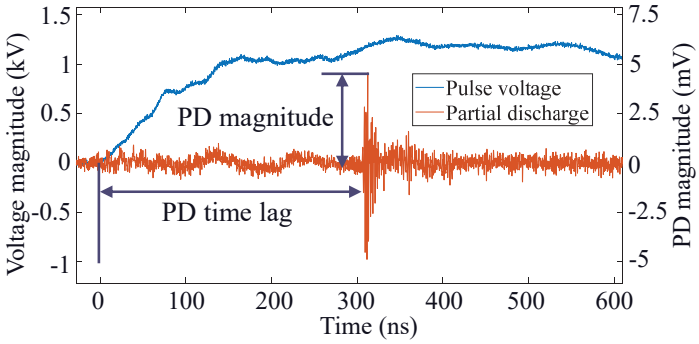

Fig. 5.7: Definition of PD magnitude and PD time lag [J2, 66].

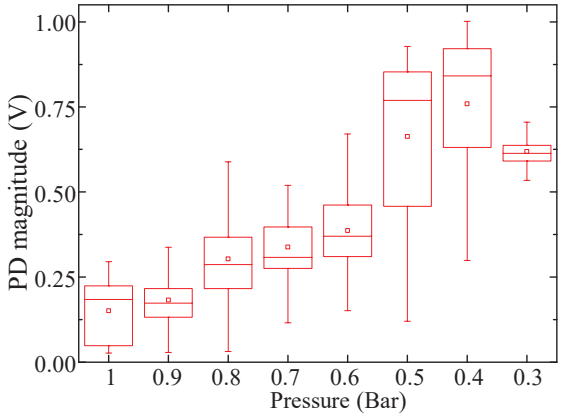

Fig. 5.8: PD magnitude with different pressures [J2, 66].

To display the effect from pressure on PD feature, statistical PD magnitude and PD time lag with different pressures should be compared. Fig. 5.7 shows the definitions of magnitude and time lag of PD. Notice that this waveform is obtained in PDIV tests, so the pulse voltage magnitude is different from that in PD feature experiments seen from Fig. 5.6. PD magnitude and PD time lag are plotted in box-chart by Fig. 5.8 and Fig. 5.9 respectively. From 1 Bar to 0.4 Bar, PD intensity becomes stronger when the pressure decreases. With pressure decreases from 0.4 Bar to 0.3 Bar, the PD magnitude reduces. In relatively high-pressure range (higher than 0.7 Bar), PD time lag becomes shorter with pressure goes lower. When the pressure is below 0.7 Bar, with further dropping of pressure, PD time lag increases and there is a tremendous time lag increase with pressure changes from 0.4 Bar to 0.3 Bar.

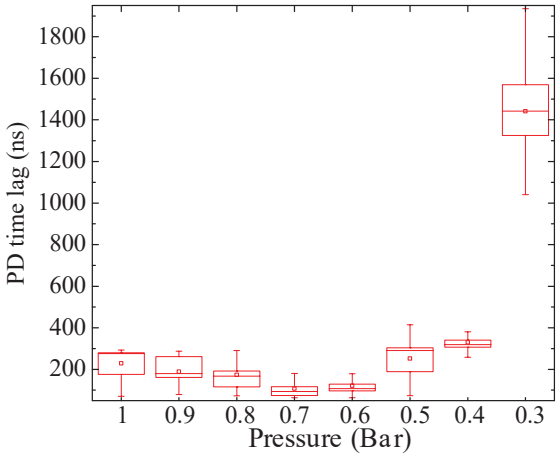

Fig. 5.9: PD time lag under different pressures [J2, 66].

5.3.3 DISCUSSION

In the determination of the PD intensity, apparent discharge q is an important factor [103, 108]. The main type of partial discharge in this experiment is the corona discharge that bridges the air duct between the insulation surface and sphere electrode. For analyzing the intensity of this kind of discharge, air duct can be defined as a capacitor C, then q can be estimated by (5.1).

$$q = V_c \cdot C = C \cdot h \cdot f \cdot E_i \tag{5.1}$$

Where V_c is the PD firing voltage, h is the air duct length (height), and f is the field enhancement factor coming from the difference in permittivity between the air and the polyimide [22]. E_i is the total electric field that equals to E_a-E_q. E_a is the applied electric field, E_q is the electric field formed by surface charge, of which the polarity is usually opposite to E_a. From the contact point to the outer area, h is not constant but increasing. On the other hand, the bottom side of the air dielectric is not in contact

with the metal electrode, but with the insulation surface. These two factors make h and C values very difficult to be determined. Thus, the equation (5.1) is only suitable for a rough estimation. Beginning from the contact point, with longer distance, h is also longer. Under voltage magnitude U, the electric field intensity would be lowered due to the well-known relationship E=U/h. Then higher voltage magnitude is needed for longer air duct to reach breakdown threshold. Because of this fact, we can simply divide the air duct into three regions for analyzing the PD situation approximately, seen in Fig. 5.10. In this figure, the density of the red line represents the electric field intensity.

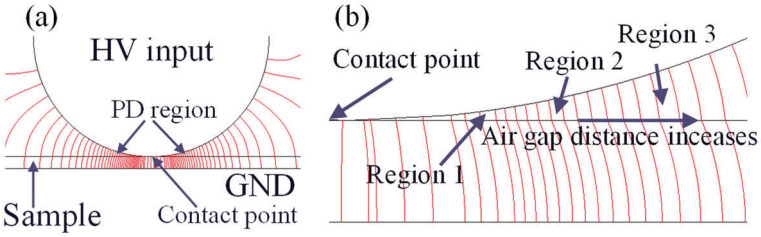

Fig. 5.10: Three regions of the air duct: (a) Overall cross section of the electrodes, (b) zoom in of the air duct close to the contact point [J2, 66].

This division is based on the air duct breakdown voltage V_b, which corresponds to partial discharge inception field E_{pdiv} multiplied by air duct height h. In region 1, V_b is below 1.58 kV. In region 2, V_b is above 1.58 kV and below 1.7 kV. In region 3, the V_b is beyond 1.7 kV. These value ranges of V_b cover the PD firing voltages of the three groups like Fig. 5.6(b). Notice that, before PD happens, there exists a time delay Δt for the presence of initial electron (pressure has no obvious impact on this process) and the formation of electron avalanche (pressure can affect this process, the mechanism is discussed in detail afterwards) after the electric field strength exceeds E_{pdiv} [108]. Because of this Δt, instantaneous value of E_i when PD happens (corresponds to PD firing voltage) may not be the same as E_{pdiv}. Yet, when the pressure is beyond 0.4 Bar, the total Δt is not very long. Therefore, for these three air duct regions in Fig. 5.10(b), the practical breakdown voltage lies within the above-mentioned V_b value ranges.

For the pulse voltage used in this study, Fig. 5.11 shows the zoom-in of its rising edge. During the rising edge, E_i in region 1 exceeds the E_{pdiv} at first, which mainly forms the first group of PDs. Afterwards, at 150 ns after the pulse voltage zero point, E_i in region 2 would exceed E_{pdiv} and mainly give rise to the second group of PD. Because of the stray parameters of the power electronic module and the resistor, the rising edge is not a smooth curve. As seen in Fig. 5.11, when the first group of PD is triggered, voltage still keeps rising. Then a higher E_i in region 1 when PD happens can be expected after Δt. While during the time when the PD of the second group is about to happen, the voltage stops rising and even decreases a little bit. This factor

can cause lower E_i when PD happens in region 2. Because of this, PD in the first group usually has larger magnitude than the second group. After E_i reaches E_{pdiv} of the region 3, the applied voltage also keeps rising. In addition, the length of air duct in region 3 is relatively longer, which leads to longer Δt necessary for the formation of the electron avalanche. Both of these two factors give rise to highest E_i for PDs in the third group, then strongest PD intensity is formed.

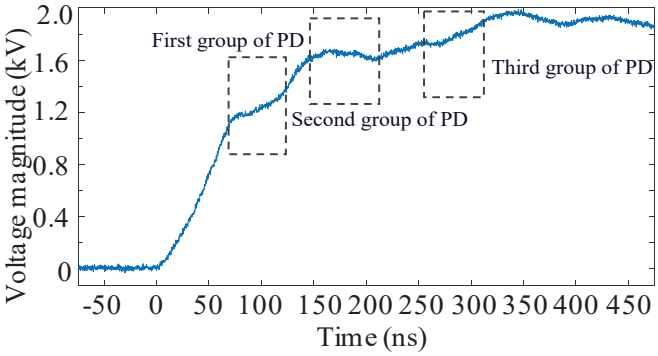

Fig. 5.11: Rising edge of the pulse voltage [J2, 66].

Notice that although PD patterns from 0.9 Bar to 0.5 Bar plotted in Fig. 5.6 are mainly contributed by situations of PDs in the three regions seen in Fig. 10(b) as discussed before, it doesn't mean that the three PD groups in Fig. 5.11 completely correspond to PDs in these three regions. Fig. 5.6(a) shows an exception. PDIV obtained under 1 Bar has largest statistical value, while PD tests in every group of Table. 5.2 are conducted using the same peak-to-peak voltage value 1.96 kV. Thus, the overvoltage related to PDIV is lowest with 1 Bar. As a result, in the first group, less PDs can be triggered even in region 1 because the instantaneous voltage value is not large enough. While more PDs would be triggered in the third group. Therefore, in Fig. 5.6(a), the third group of PDs are contributed not only by PDs happen in region 3, but also by PDs in region 1 and region 2.

Choosing one of the air duct regions as an example, the change of E_i can be plotted approximately in Fig. 5.12 [109]. At first, on the rising edge, E_i increases along with E_a. When E_i goes beyond E_{pdiv} and the initial electron is present, PD happens. PD brings a large amount of surface charge that deposits on the surface of polyimide film. The surface charge forms electric field E_q with polarity opposite to the E_a (without PD, the amount of surface charge is rare, E_q would be very low). Then E_i drops into $E_{res}=E_a-E_q$, which is well below the E_{pdiv}. Afterwards, the square wave voltage (corresponds to E_a) reaches the plateau region and stops rising. E_q may decrease because of the dissipation of surface charge. However, before meeting the pulse voltage falling edge, this charge dissipation would not be enough for E_i to exceed E_{pdiv} again. When the falling edge comes, E_a drops quickly, $E_i=E_a-E_q$ exceeds E_{pdiv} in an opposite polarity. The PD happens again and E_i drops into E_{res2}. The above-mentioned

process repeats when the next cycle of pulse voltage comes. This is the reason why obvious PDs can only be discovered around the rising/falling edge.

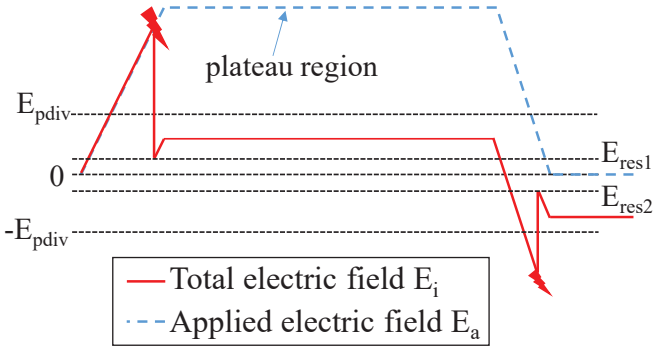

Fig. 5.12: Electric filed during the pulse voltage application [J2, 66].

As mentioned before, for triggering PD, E_i in the air duct must be higher than the E_{pdiv} and the initial electron should be present. Then, seen from Fig. 5.13, the total PD time lag can be divided into two parts. At first, a t_l is needed for the E_i to exceed E_{pdiv} and then, Δt should be waited for the generation of initial electron and the formation of electron avalanche. When pressure becomes lower, E_{pdiv} decreases. This means t_l would be shorter since E_i can exceed E_{pdiv} earlier. This is why PD time lag becomes shorter with reducing of pressure from 1 Bar to 0.7 Bar. On the other hand, gas density N would be lower because of the reducing pressure, which leads to reduced gas molecules that can be ionized. This also means prolonged distance between these gas molecules and prolonged mean free path of the electron. Thus, the time for the formation of electron avalanche becomes longer, which in turn makes Δt longer. With pressure lower than 0.7 Bar, this increasing of time spent for electron avalanche plays a more important role in affecting the total PD time lag. Therefore, with further reducing of pressure (from 0.7 Bar to 0.4 Bar), PD time lag increases. With pressure 0.4 Bar, the time for the formation of electron avalanche becomes so long that PD cannot be triggered before 200 ns in Fig. 5.11. Thus, the first and second group of PDs disappear, which gives rise to a completely different PD pattern in 0.4 Bar compared with higher pressures. Breakdown voltage is affected by air duct length d (same as air duct height in (5.1)) times pressure p as seen in x-axis of Paschen's curve (Fig. 1.3). When d is very short and p is already very low, if p further decreases, the breakdown voltage would increase from the minimum value (in critical point). For the air duct in this study seen in Fig. 5.10(b), with pressure changes from 0.4 Bar to 0.3 Bar, a part of region 1 closest to the contact point meets an increase in breakdown voltage (corresponds to E_{pdiv} multiplied by d). In other words, in this part of region 1, p*d moves to the left side of the critical point of Pachen's curve. Then, in this place, PD inception probability would be lower. However, for other parts in the air duct, p*d is still on the critical point's right side, which can give rise to lower PDIV if pressure decreases. Seen in Fig. 5.14, compared with the part closest to the contact point, the

distance of PD (related to the air duct height) in other regions is longer. Both the decreasing number of air molecules and prolonging of PD distance increase the time needed to form the electron avalanche to a large extent, which contribute to a much longer statistical PD time lag in 0.3 Bar compared with that of 0.4 Bar and higher pressures.

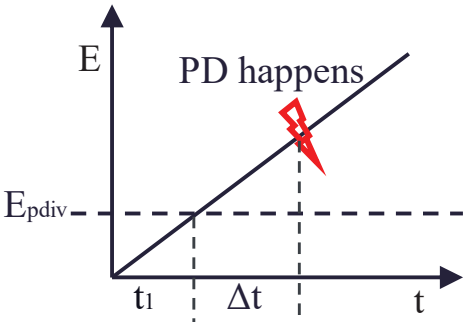

Fig. 5.13: PD time lag [J2, 66].

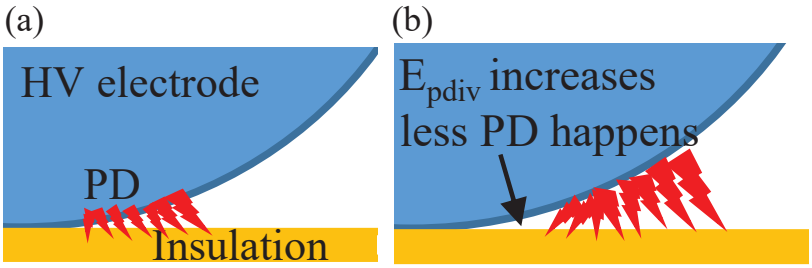

Fig. 5.14: PD distance: (a) Under higher pressures, (b) Under 0.3 Bar [J2, 66].

If electric field intensity E is not changed, decreasing of the air density N makes E/N higher. Electron energy can be represented by this E/N [58]. If the PD time lag is similar, PD intensity can be stronger due to the increased electron energy. On the other hand, as mentioned in the last paragraph, with relatively low-pressure range (lower than 0.7 Bar), further reducing of pressure can give rise to longer PD time lag. During the voltage rising edge, seen in Fig. 5.11, although there is a segment (the PD in the second group happens in this segment) where voltage instantaneous value reduces a bit and makes E_i lower for PD happens in region 2 (shown in Fig. 5.10), prolonged PD time lag still gives rise to higher PD firing voltage and higher E_i in the rest parts of rising edge. With pressure higher than 0.7 Bar, increasing of electron energy and decreasing of PD time lag have opposite effects in affecting PD intensity when pressure decreases. While the former factor plays a dominant role. With pressure below 0.7 Bar and further decreases, both the increased electron energy and time lag intensify the PD activity.

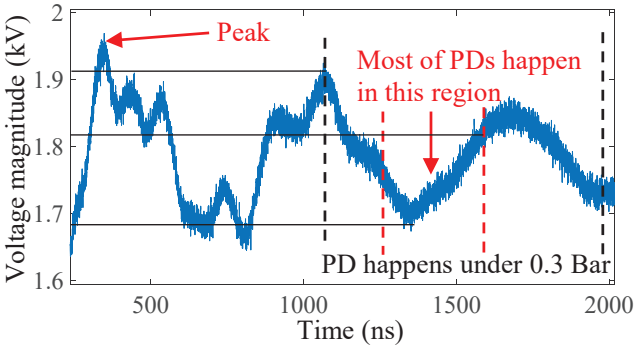

Fig. 5.15: PD region under 0.3 Bar [J2, 66].

With 0.3 Bar, seen from Fig. 5.9, most of the PDs have time lag from 1300 ns to 1600 ns. This time range lies behind the voltage rising edge seen in Fig. 5.15. The instantaneous voltage value in this time range is from 1.68 kV to 1.82 kV, while the pulse voltage peak value is obvious larger with 1.96 kV. Thus, compared with the third group of PDs under 0.5 Bar and most of the PDs under 0.4 Bar, of which the PD firing voltage is usually higher than 1.9 kV (these PDs are mainly triggered around the pulse voltage peak point), the E_i of the PDs under 0.3 Bar is lower. This factor makes statistical PD magnitude with 0.3 Bar smaller.

5.4 ENDURANCE LIFETIME EXPERIMENTS

5.4.1 EXPERIMENT PARAMETERS

Detailed parameters of the endurance lifetime tests are listed in Table. 5.3. For accelerating the aging speed, the frequency is increased to 2 kHz while other parameters are kept the same. Similar with the comparative endurance tests in section 4, 5 specimens are used for each group in Table. 5.3 to get statistical lifetime results.

Table. 5.3 Parameters of endurance lifetime tests

Group	Rise time	Peak voltage value	Frequency	Pressure
1	250 ns	1.96 kV	2 kHz	1 Bar
2				0.9 Bar
3				0.8 Bar
4				0.7 Bar
5				0.6 Bar
6				0.5 Bar
7				0.4 Bar
8				0.3 Bar

5.4.2 EXPERIMENT RESULTS

Box-chart of endurance lifetime is shown in Fig. 5.16. In most of the situations, the lifetime of the polyimide film decreases along with the pressure. This change trending is in accordance with the PD feature experiment results, which shows that stronger PD intensity leads to faster insulation aging speed. While an obvious increase in lifetime can be discovered when pressure changes from 0.4 Bar to 0.3 Bar. With 0.3 Bar, the average lifetime is even longer than that under 0.7 Bar. For the aged insulation specimen, PD eroded areas are shown in Fig. 5.17. Other parts of these aged insulation films are cut off for the sake of observing and comparing the eroded areas with the same lens.

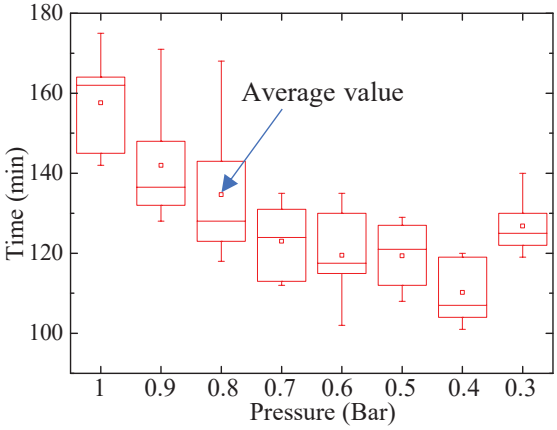

Fig. 5.16: Lifetime under different pressures [J2, 66].

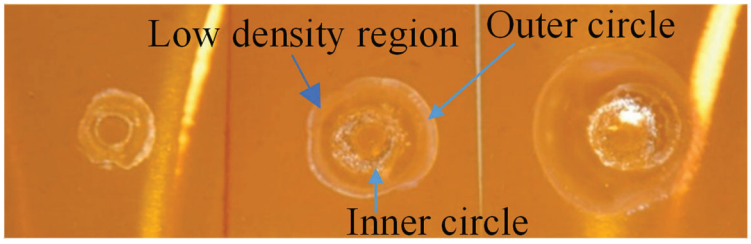

Fig. 5.17: Eroded area aged under 1 Bar (left), 0.4 Bar (middle) and 0.3 Bar (right) [J2, 66].

Continuous PDs can degrade the molecules matrix of the polyimide gradually. In the early stage, some chemical bonds, such as C-H bond in aromatic ring and C-N-C bond in imide ring, would be destroyed. Then, other relatively stronger bonds would also be involved in this destructive process [110]. An unsmooth low-density region of byproducts seen in Fig. 5.17 would be formed by the above-mentioned aging process. In the PD eroded area, cavities may exist. Due to the byproducts like nitric acid and

amic acid that are produced by the PD erosion, surface conductivity of the PD eroded (before breakdown) polyimide film would be higher. Surface charge would be dissipated faster by this increased surface conductivity. Since surface charge is one of the main sources of initial electron, PD activity may be suppressed during the early stage of PD aging [111]. However, with further development of PD degradation, roughness of the eroded area would be more serious. Electric field distribution would be distorted by grown cavities and cracks with other shapes. This factor can give rise to higher probability of PD inception and stronger PD intensity. It can also be seen from Fig. 5.17 that decreasing of pressure can enlarge the PD eroded area. For the specimen aged under 1 Bar, around the contact point, only a small circle of eroded area is formed. In comparison, eroded areas under 0.4 Bar and 0.3 Bar are obviously larger. These areas can be separated into outer circle and inner circle. Compared with 0.4 Bar, larger outer circle in the specimen under 0.3 Bar can be discovered. This phenomenon indicates that PD under 0.3 Bar expands to larger area although a decreasing in PD magnitude is detected. Because of more serious PD erosion, rougher inner circles of specimens under low pressure conditions can be observed compared with those aged with 1 Bar.

5.4.3 DISCUSSIONS

PD aging of the insulation is a complicated process. For organic insulation material, its molecule chain can be broken progressively by PD induced temperature rise and chemical reactions. Among the chemical reactions, intense oxidation plays an important role in destroying the organic molecules [110]. Discharge can change O_2 into O_3 [112], which is more destructive to the insulation material because of stronger oxidability. These abovementioned aging factors would surely be enhanced by PDs with larger magnitude. However, lower pressure reduces the amount of O_2 and other compositions of air that can be involved in the insulation aging process. Thus, the chemical reactions can be slowed when the pressure is very low. Combined with decreasing PD magnitude seen in Fig. 5.8, a prolonged endurance lifetime with 0.3 Bar can be expected.

For a certain kind of gas dielectric (including air), a constant $(E/p)_C$ can be used to define its breakdown threshold. In the sphere-insulation film-plate structure used in the experiment (similar with that in Fig. 4.5), if the applied E/p (electric field intensity divided by pressure) goes beyond $(E/p)_C$, partial discharge can be incepted in the air duct. As mentioned before, with constant applied voltage magnitude, electric field in the air duct reduces from the contact point to the outer area because of increasing air duct length. With all these above mentioned factors, Fig. 5.18 can help describing the changing of PD eroded area with pressure decreasing [113]. This figure briefly displays a half of cross section of the insulation film and electrodes. C_0 refers to air's $(E/p)_C$. Under pressure p_1, the function between E/p_1 and the distance from the contact point L, which is written as $E/p_1=f(L)$, can be shown by the black curve in Fig. 5.18. This curve intersects with the y-axis at point A. If the distance is shorter than L_1, E/p_1

value would be larger than C_0, which means PD can be triggered within a circle with the contact point as center and L_1 as radius. If the pressure reduces into p_2, with the voltage magnitude unchanged, function $E/p_2=f(L)$ can be expressed by the red curve, which intersects with the y-axis at a higher point B. Then PD can be incepted within a larger circle with the same center and a longer radius L_2. Therefore, through PD aging under lower pressure, PD eroded area would be larger.

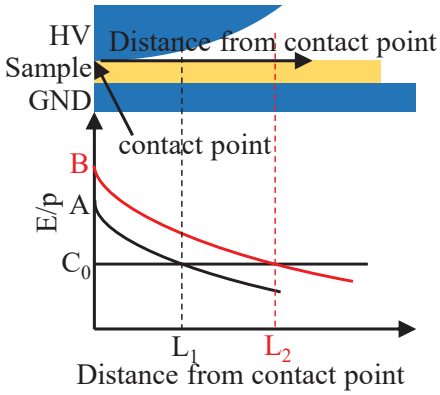

Fig. 5. 18: PD area with different pressures [J2, 66].

From these above studies we can see polyimide insulation film would confront greater risk of PD inception and faster PD deterioration. Extremely low pressure (for example, lower than 0.3 Bar/30 kPa used in this study, which corresponds to altitude higher than 9000 m) may reduce the PD aging speed due to the decreasing number of gas molecules. However, with much higher probability of PD inception in low pressure conditions, the insulation's endurance may still be much lower than that at sea level. Polyimide is one of the main insulation materials utilized in the transformer [31]. According to section 1.1.3, possible type of PD in medium frequency transformer would be the corona discharge that bridges the air duct and touch the insulation surface, which is similar with the PD generated in this chapter's experiments. With these two factors and the experiment results, it can be expected that transformers working in the power electronic systems in high altitude area or more electric aircraft (MEA) would confront greater risk of PD inception and more severe PD deterioration. For the same working voltage and frequency rating, higher insulation margin should be considered if the MVMF transformer is going to be used under low pressure condition. In addition, according to the experience from the field of inverter-fed motor, some methods are worth considering. One of them is conducting PDIV tests on the transformer before it is put into application. According to the PDIV value, strategies such as modifying the insulation design can be taken to guarantee that the transformer can avoid any PD inception during its expected lifetime. Another available method would be lifetime tests on the whole transformer or its insulation structure to determine whether a specific transformer's design can

meet the requirement of lifetime if PD is inevitable. According to experiment results in this chapter, these tests should be conducted under the pressure same as the places where the transformer would be applied if possible. If the low-pressure condition cannot be realized by the manufacturers or users, PDIV or lifetime tests under sea level pressure are still feasible with precisely predicted PDIV or lifetime reduction with decreasing pressure. To obtain the precise PDIV and lifetime reductions, further studies on the PDIV and lifetime under different pressures should be conducted with wider pressure range and more insulation specimens to get more statistical results. Previous studies have proven the correctness of using mathematical model for the prediction of insulation lifetime considering the voltage magnitude, frequency and temperature [48]. With the above-mentioned statistical relationship between PDIV/lifetime and pressure, a similar mathematical model can be built to predict the reduction of PDIV/lifetime with decreasing pressure precisely. Besides the insulation tests before the transformer is put into application, online monitoring is also important. The data about whether the PD is generated or the total number of PDs during the operation is important for maintenance staff to predict the rest of insulation lifetime and to decide whether they should apply another transformer with higher insulation capability. Good news is that PD detection may be easier under the low-pressure condition since PD would be triggered with larger magnitude and longer time lag. The interference brought from PWM voltage concentrates in the time range that meets the voltage rising edge [33]. If PD happens behind the rising edge, it would not be submerged by the interference signal.

5.5 SUMMARY

Using repetitive pulse voltage, comparative PDIV tests, PD feature tests and endurance tests are conducted on polyimide film with different pressures from 1 Bar to 0.3 Bar. Results show that:

Under pulse voltage and uneven field distribution caused by the sphere electrode, PDIV decreases along with pressure. This phenomenon is similar with the trending of Paschen Curve obtained using sinusoidal voltage and even field distribution. Because of this PDIV reduction, in the PD feature tests, shorter time is needed for electric field in the air duct to reach the PD inception field. Thus, in relatively high-pressure ranges, PD time lag becomes shorter when pressure decreases. However, with pressure going lower, air molecules that can be ionized reduces, and longer time delay would be necessary to form electron avalanche. That's why in relatively low-pressure range PD time lag increases with pressure decreasing.

When pressure goes lower, electron energy would be higher, and increased PD time lag (under relatively low-pressure range) can lead to higher PD firing voltage. These two factors can make PD intensity stronger. However, under very low-pressure conditions, PD would be triggered behind the rising edge, which makes PD firing voltage lower and reduces PD intensity.

The aging process, including partial temperature rise and chemical reactions, can be intensified by PDs with larger magnitude. This factor can shorten the insulation endurance lifetime. Yet, with further decreasing of pressure, the numbers of oxygen and other gas molecules in the air that can be involved in the chemical reaction would be obviously reduced. Then, the aging process is suppressed and endurance lifetime is longer. Reducing the pressure can also enlarge the PD eroded area on the insulation surface.

These results show that medium frequency transformers would confront greater risk of PD inception and more severe PD erosion when working under lower pressure. Therefore, to guarantee these transformers' insulation reliability, higher insulation margin should be considered for the transformer's design. Also, PDIV or lifetime tests are needed before the transformers are put into application. These tests should be conducted under the same pressure under which these transformers would be applied, or at sea level pressure with a precisely predicted PDIV/lifetime reduction with decreasing pressure. Further studies on the PDIV/lifetime with wider pressure range and more samples are needed to get this precisely predicted PDIV/lifetime reduction.

CHAPTER 6.

Conclusions

This chapter summarize the outcomes of Ph. D project – Electric stress and insulation failure mechanism of medium voltage medium frequency transformer. The main contributions are pointed out. Research perspectives are discussed.

6.1 SUMMARY

In chapter 1, the study background of this Ph. D project was introduced in several aspects: 1) The definition of medium voltage medium frequency transformer along with its application and development. 2) The possible insulation problem faced by the medium frequency transformers. 3) The influence from environment factors. Afterwards, a state-of-the-art of the related studies was prepared, which included electric stress analysis, PD and endurance studies with or without considering the changing of temperature and pressure. Based on the contributions of these studies and the problems remained, research objectives are proposed, listed below:

(1) Transient electric stress analysis on MVMF transformer's winding considering the fast rising front of the PWM working voltage.

(2) Building of the PD and endurance test system.

(3) Comparative PDIV and endurance studies on different insulation materials considering the effect of rising temperature.

(4) Studies on the impact from pressure on the PDIV, PD features and PD induced insulation aging process.

In Chapter 2, a transformer prototype in previous literature was chosen as the study object. FEM calculation is used to obtain the stray parameters of each turn of the transformer's HV winding. Based on these parameters, an equivalent circuit model for the winding was constructed. Inter-turn and inter-layer voltage drop simulations were conducted under different pulse voltage rise times, relative permittivity and winding structures. The results show that overvoltage exists in the winding when added with pulse voltage. Shorter voltage rise time and higher relative permittivity of insulation can cause higher overvoltage. With winding structure changes from C-type to Z-type, the transient overvoltage is reduced.

In Chapter 3, a PD and endurance test system was built. In this system, with a pulse voltage generator based on power electronic module, pulse voltage with

adjustable rise time and frequency can be generated. This generator can be controlled remotely with overcurrent protection unit. An UHF antenna combined with band-pass filter is chosen as PD detection method. PDIV and endurance experiments on the Nomex paper prove the effectiveness of this test system in detecting PD with high signal-to-noise ratio and timely breakdown protection.

In Chapter 4, comparative PDIV tests with rising temperature and endurance lifetime tests were conducted on materials including polyimide film, polyester film and Nomex paper. Polyester and polyimide have higher PDIV than Nomex paper. With temperature rise, Nomex paper shows a most obvious reduction in PDIV. In low temperature conditions, polyester has highest PDIV, while with relatively high temperature condition, polyimide has higher PDIV. Facing with pulse voltage induced PD aging, lifetime of Nomex paper is much lower than other materials while polyimide shows longest endurance.

In Chapter 5, PDIV, PD feature and endurance lifetime tests were conducted on polyimide film with different pressures. PDIV decreases when pressure goes lower. From pressure 1 Bar to 0.7 Bar, PD time lag decreases with pressure decreasing. While from 0.7 Bar to 0.3 Bar, PD time lag increases with further decreasing of pressure. In most of the situations, PD magnitude becomes larger with pressure decreasing, while from 0.4 Bar to 0.3 Bar, PD magnitude shows a reduction. Usually, endurance lifetime decreases along with pressure due to stronger PD activity. Yet, in very low-pressure condition, PD aging speed would be slowed due to reduced gas molecules that can be involved in the aging process and gives rise to longer lifetime.

In summary, the studies in Ph. D research prove the possible electric overstress suffered by the transformer working in power electronic systems and discovered the factors that can make them more critical. Among the three kinds of materials that are usually used for the insulation of transformer, difference in their capabilities in withstanding the PD inception and PD deterioration are revealed. The pressure's effect on the PD activity and the PD induced insulation aging behavior are also investigated and analyzed in detail.

6.2 MAIN CONTRIBUTIONS

Based on the research outcome of this Ph. D project, the main contributions are summarized as follows:

A. Transient electric stress analyses are conducted on medium voltage medium frequency transformer's winding

- By using the equivalent circuit model of the transformer's winding, transient inter-turn and inter-layer voltage drop simulations using pulse voltage can be conducted. This transient voltage analysis compensates the limitations of

previous FEM electric field analysis in steady-state, which cannot take the transient effect of the short voltage rise time into consideration adequately.

- From the simulation results, overvoltage in the winding caused by pulse voltage indicates that potential risk of accelerated insulation aging due to higher PD inception probability exists in the transformer working in power electronic systems, which is similar with the situation of inverter-fed motors. This brings focus to the need of PD and endurance tests on the insulation material, insulation structure of the medium voltage medium frequency transformer or on the whole transformer prototype.

B. Advices are given to improve the medium voltage medium frequency transformer's insulation reliability

- From the transient electric stress analysis, strategies can be recommended for reducing the inter-turn and inter-layer overvoltage, such as prolong the output voltage rise time of the power electronic switches (within the accepted switching loss range).
- Compared with C-type winding, Z-type winding not only reduces static inter-layer voltage drop, but also reduces transient inter-layer overvoltage caused by pulse voltage steep rising edge. Therefore, this winding structure is more recommended for the design of MVMF transformer.
- Applying insulation material with lower relative permittivity can also reduce the overvoltage. However, for different insulation materials, not only relative permittivity, but other properties including the surface roughness and chemical bond strength would also be much different. In the choosing of proper insulation material for reducing the transformer's electric stress, all these properties that can affect the insulation reliability should be considered comprehensively.
- From the comparative PDIV and endurance studies, among the materials polyimide film, polyester film, and Nomex paper, if the cooling system is good enough to keep the whole transformer in temperature no higher than 80 ℃, polyester may be the best choice , because it behaves best in resisting PD inception in low temperature condition. Otherwise, polyimide film would be better for it behaves best in resisting PD inception and PD aging in relatively higher temperature condition.

C. Pressure's effect on pulse voltage induced PD features and PD aging speed are analyzed

- From the studies in Chapter 5, in most of the situations, low pressure condition can make the pulse voltage induced PD intensity stronger and give rise to faster insulation aging speed. This indicate that medium voltage medium frequency transformer would face greater challenge in insulation reliability when working in high altitude areas or in electric aircrafts.
- To cope with this greater risk in insulation reliability, some advice can be given including higher insulation margin in the design and on-line PD

monitoring. Among them, PD monitoring under low pressure condition may be relatively easier because PD is less likely to be submerged in the pulse voltage switching interference.

In general, this project reveals electric overstress faced by MVMF transformer and raises the necessity of subsequent insulation failure mechanism investigations including PD and endurance studies. Electric stress analysis combined with comparative PD and endurance studies on different materials give suggestions in the selection of proper insulation materials and winding structures for the design of the transformer. Investigations on the pressure's impact offer advice for improving the MVMF transformer's insulation reliability to cope with the low pressure condition including higher insulation margin and PD monitoring.

6.3 RESEARCH PERSPECTIVES

The entire Ph.D. work analyzed electric stress on the winding of MVMF transformer, built the insulation test system, conducted PD and endurance studies on different insulation materials and different pressures. For further analyzing the electric stress and better improving the MVMF transformer's insulation reliability, some extended work based on the present thesis is worth to be carried out in the future for the following aspects:

- In Chapter 2, for analysis of electric stress under different winding structures, we only considered Z-type and C-type structures. Actually, other structures like segmented type may also be used for medium voltage medium frequency transformers. On the other hand, for the conductor of the winding, we only considered the solid wire with rectangle shape in cross section. Other conductor types like solid wire with round shape in cross section, Liz wire, and foil conductor can give rise to different stray parameters, which can in turn affect the transient electric stress. Therefore, further analysis on the transient electric stress with different winding structures and winding conductor types would help improving the transformer's insulation reliability in the design stage.
- Because of lacking a transformer prototype and the limitation of our devices (especially for the power electronic module in our test system, the rated current is very low), we were not able to conduct experiments on the transformer to see the inter-turn and inter-layer overvoltage in completely real situation. If the transformer prototype and better experiment devices can be acquired, experiments would make the electric stress analysis more convincible.
- In our PD and endurance lifetime studies, only insulation materials with square shape are selected as the test objects. Although the type of PDs during the experiments is the same as that is possible to be triggered in the transformer's insulation when working under PWM voltage, same

experiments on the complete transformer or the insulation structures more related to the transformer's winding would give rise to more convincible and more accurate results.

- For power electronic systems working in long-haul flight and spacecrafts, the pressure of the working condition would go below 0.3 Bar, which is the lowest pressure chosen in our studies. On the other hand, besides polyimide, effects of pressure on the behavior of other insulation materials used in the transformer also worth investigation. Further studies on the insulation behavior with lower pressure range and more materials would help us see how the insulation reliability of medium voltage medium frequency transformer would be affected by these extremely environments.

Bibliography

Reference

[1] M Mogorovic, “Modeling and Design Optimization of Medium Frequency Transformers for Medium-Voltage High-Power Converters,” Phd dissertation, Power Electronics Laboratory., Swiss federal Institute of Technology in Lausanne, Lausanne, 2019

[2] L. Heinemann, “An actively cooled high power high frequency transformer with high insulation capability,” in *Proc IEEE Appl. Pow. Electr. Conf. Expo (APEC)*, Dallas, TX, USA, August. 2002, vol. 1, pp. 352-357, DOI: 10.1109/APEC.2002.989270.

[3] Q. Chen, R. Raju, D. Dong, and M. Agamy, “High Frequency Transformer Insulation in Medium Voltage SiC enabled Air-cooled Solid-State Transformers,” *IEEE Energy Conversion Congress and Exposition (ECCE)*, Portland, OR, USA, September. 2018, pp. 1-10, DOI: 10.1109/ECCE.2018.8557849.

[4] X. She, R. Burgos, G. Y. Wang, F. Wang, and A. Q. Huang, “Review of solid state transformer in the distribution system: From components to field application,” in *Proc IEEE Energy Convers. Congr. Expo. (ECCE)*, Raleigh, NC, USA, September. 2012, pp. 4077–4084, DOI: 10.1109/ECCE.2012.6342269

[5] J. W. Yang, C. X, Mao, D. Wang, J. M. Lu, X. Q. Fu, and X. Chen, “Fast and continuous on-load voltage regulator based on electronic power transformer,” IET Electr. Power Appl., Vol. 7, no. 6, pp. 499–508, July. 2013.

[6] P. Shuai and J. Biela, “Design and optimization of medium frequency medium voltage transformers,” in Proc Eur. Conf. Power Electron. Appl. (EPE), Lille, France, September. 2013, pp. 1-10, DOI: 10.1109/EPE.2013.6634423

[7] V. Hamidi and K. S. Smith, “Smart grid technologies for connection of offshore wind farms,” in Proc IET Conference on Renewable Power Generation, Edinburgh, UK, September, 2011, DOI: 10.1049/cp.2011.0150

[8] N. Kimura, T. Morizane, I. Iyoda, K. Nakao, and T. Yokoyama, “Solid State Transformer Investigation for HVDC Transmission from Offshore Windfarm,” in Proc International Conference on Renewable Energy Research and Applications (ICRERA), San Diego, CA, USA, December. 2017, DOI: 10.1109/ICRERA.2017.8191126

[9] J. H. Feng, W. Q. Chu, Z. X. Zhang, and Z. Q. Zhu, “Power electronic transformer-based railway traction systems: Challenges and opportunities,” IEEE J. Emerg. Sel. Topics Power Electron., vol. 5, no. 3, pp. 1237-1253, 2017

[10] S. Baek, Y. Du, G. Y. Wang, and S. Bhattacharya, “Design considerations of high voltage and high frequency transformer for solid state transformer application,” in Proc IEEE Annu. Conf. Ind. Electron, Glendale, AZ, USA, November. 2010, pp. 421-426, DOI: 10.1109/IECON.2010.5674991

[11] T. Liu, Q. M. Li, X. W. Huang, Y. F. Lu, M. Asif, and Z. D. Wang, “Partial discharge behavior and ground insulation life expectancy under different voltage frequencies,” IEEE Trans. Dielectr. Electr. Insul., vol. 25, no. 2, pp. 603-613, April. 2018.

[12] J. Wan, Z. Lin, and H. Yu, “Research of PWM pulse voltage distribution in motor winding,” in Proc International Conference on Electrical Machines and Systems, Shenyang. China, August. 2001, pp. 43-46, DOI: 10.1109/ICEMS.2001.970605

[13] M. Melfi, A. M. J. Sung, S. Bell, and G. L. Skibinski, “Effect of surge voltage risetime on the insulation of low-voltage machines fed by PWM converters,” IEEE Trans. Ind. Appl., vol. 34, no. 4, pp. 766-775, July. 1998.

[14] J. Sakata, M. Taguchi, S. Sasaki, T. Kuroda, and K. Toda, “An EMI-Less Full-Bridge Inverter for High Speed SiC Switching Devices,” in Proc IEEE Applied Power Electronics Conference and Exposition, San Antonio, TX, USA, March. 2018, pp. 2570-2576, DOI: 10.1109/APEC.2018.8341379

[15] High-Voltage Test Techniques-Partial Discharge Measurements, Standard IEC 60270, 2000

[16] D. Fabiani, G. C. Montanari, and A. Contin, “Aging Acceleration of Insulating Materials for Electrical Machine Windings Supplied by PWM in the Presence and in the Absence of Partial Discharges,” in Proc IEEE International Conference on Solid Dielectrics, Eindhoven, Netherlands, June. 2001, pp. 283-286, DOI: 10.1109/ICSD.2001.955625

[17] M. Kaufhold, G. Borner, M. Eberhardt, and J. Speck, “Failure mechanism of the interturn insulation of low voltage electric machines fed by pulse controlled inverters,” IEEE Elect. Insul. Mag., vol. 12, pp. 9-16, September. 1996

[18] O. M. O. Gatous and J. Pissolato, “Frequency-dependent skin-effect formulation for resistance and internal inductance of a solid cylindrical conductor,” in Proc Microwaves Antennas Propagation, Sao Paulo, Brazil, November. 2004, vol. 151, pp. 212–216, DOI: DOI: 10.1109/TDC.2004.1432505.

[19] P. Meyer and Y. Perriard, “Skin and proximity effects for coreless transformers,” in Proc IEEE International Conference on Electrical Machines and Systems, Beijing, China, August. 2011, pp. 1-5, DOI: 10.1109/ICEMS.2011.6073351.

[20] P. Wang, H. Y. Xu, J. Wang, A. Cavallini, and G. C. Montanari, “Temperature Effects on PD Statistics and Endurance of Inverter-fed Motor Insulation under Repetitive Square Wave Voltages,” in Proc IEEE Electrical Insulation Conference, Montreal, QC, Canada, June. 2016, pp. 202-205, DOI: 10.1109/EIC.2016.7548695

[21] P. Wang, G. C. Montanari, and A. Cavallini, “Partial discharge phenomenology and induced aging behavior in rotating machines controlled by power electronics,” IEEE Trans. Ind. Electron., vol. 61, no. 12, pp. 7105-7112, April. 2014

[22] High voltage engineering, Butterworth-Heinemann, 2nd ed., Oxford, UK, 2000

[23] S. Jean, B. Reda, M. Xavier, M. Philippe, M. Arnaud, G. Stephane, B. Taoufik, “Planar Magnetic Components in More Electric Aircraft: Review of Technology and Key Parameters for DC–DC Power Electronic Converter,” IEEE Transactions on Transportation Electrification., Vol. 3, no. 4, pp. 831-842

[24] P. Huang, C. X. Mao, and D. Wang, “Electric Field Simulations and Analysis for High Voltage High Power Medium Frequency Transformer,” Energies., Vol. 10, no.3, March. 2017

[25] W. W. Wang, J. F. He, X. Wang, Y. Liu, S. T. Li, “Analysis of Electric Field Stress and Dielectric Loss in Insulation of Magnetic Component for Cascaded Power Electronic Transformer,” IEEE International Conference on HVDC (HVDC), Xi’ an, Shanxi, China, November, 2020, pp. 1078-1083. DOI: 10.1109/HVDC50696.2020.9292863

[26] T. Guillod, F. Krismer, and J. W. Kolar, “Electrical shielding of MV/MF transformers subjected to high dv/dt PWM voltages,” in Proc IEEE Appl. Power Electron. Conf. Expo, Tampa, FL, USA, March. 2017, pp. 2502-2510, DOI: 10.1109/APEC.2017.7931050

[27] T. Guillod, J. E. Huber, G. Ortiz, A. De, C. M. Franck, and J. W. Kolar, “Characterization of the voltage and electric field stresses in multi-cell solid-state transformers,” in Proc IEEE Energy Convers. Congr. Expo. (ECCE), Pittsburgh, PA, USA, September. 2014, pp. 4726-4734, DOI: 10.1109/ECCE.2014.6954048

[28] T. Guillod, “Modeling and Design of Medium-Frequency Transformers for Future Medium-Voltage Power Electronics Interfaces,” Phd dissertation, Power

Electronics Laboratory., Swiss federal Institute of Technology in Lausanne., Lausanne, Switzerland, 2018.

[29] F. C. Lü, D. R. Li, Y. X. Guo, C. Fu, and H. Wang, “Optimal Design of Compact Main Insulation Structure of PETT,” in Proc International Conference on Electrical Machines and Systems Conf. (ICEMS), Pattaya, Thailand, October. 2015, pp. 303-306, DOI: 10.1109/ICEMS.2015.7385047

[30] A. Cavallini, “Reliability of Low Voltage Inverter-fed Motors, What have we learned, perspectives, open points,” IEEE International Symposium on Electrical Insulating Materials, Toyohashi, Japan, September, 2017, pp. 13-22.

[31] Y. K. Zhao, G. Q. Zhang, Z. H. Liao, L. J. Wan, Y. F. Li, and F. Y. Yang, “Optimal Design of Insulation Structure of HV-HF Transformer Based on High-Frequency Insulation Properties of Gas-Solid System,” in Proc IEEE Electrical Insulation Conference, Knoxville, TN, USA, July. 2020, pp. 482-485, DOI: 10.1109/EIC47619.2020.9158702.

[32] D. Fabiani, A. Cavallini, and G. C. Montanari, “A UHF technique for advaced PD measurements on inverted-fed motors,” IEEE Trans. Power. Electr, vol. 23, no.5, pp. 2546-2556, September. 2008

[33] W. Y. Zhou, P. Wang, Z. J. Zhao, Q. Wu, and A. Cavallini, “Design of an Archimedes spiral antenna for PD tests under repetitive impulsive voltages with fast rise times,” IEEE Trans. Dielectr. Electr. Insul., Vol. 26, no. 2, pp. 423–430, March. 2019

[34] J. P. Uwiringiyimana, U. Khayam, Suwarno, G. C. Montanari, “Comparative Analysis of Partial Discharge Detection Features Using a UHF Antenna and Conventional HFCT Sensor,” IEEE Access., Vol. 10, pp. 107214-107226, 2022.

[35] P. Wang, J. Wang, H. Y. Xu, K. Zhou, Y. Lei, and Q. Zhou, “Comparative Study of PD Characteristics for Inverter-fed Motor Insulation under Sinusoidal and Repetitive Square Wave Voltage conditions,” in Proc IEEE International Conference on High Voltage Engineering and Application, Chengdu, China, December. 2016, DOI: 10.1109/ICHVE.2016.7800806

[36] T. Hammarström, “The Implications on the PD Characteristics of Unipolar versus Bipolar PWM waveforms,” IEEE Electrical Insulation Conference, Calgary, AB, Canada, pp. 42-45, 2019.

[37] T. Hammarström, “Multi-rise time PWM: A way to reduce PD exposure in motor windings,” IEEE Trans. Dielectr. Electr. Insul., Vol. 27, No. 2, pp. 613-621, 2020

[38] P. Wang, C. J. Zheng, Y. Li, Y. Lei, and A. Cavallini, “The PD and Endurance Features of Enameled Wires at Short Repetitive Impulsive Voltages,” in Proc IEEE Electrical Insulation Conference, San Anotonio, TX, USA, October. 2018, pp. 572-576, DOI: 10.1109/EIC.2018.8481043

[39] P. Wang, A. Cavallini, and G. C. Montanari, “The Influence of Repetitive Square Wave Voltage Parameters on Enameled Wire Endurance,” IEEE Trans. Dielectr. Electr. Insul., Vol. 21, no. 3, pp. 1276-1284, June. 2014

[40] P. Wang, H. Y. Xu, J. Wang, W. Wang, and A. Cavallini, “Effect of Repetitive Impulsive Voltage Duty Cycle on Partial Discharge Features and Insulation Endurance of Enameled Wires for Inverter-fed Low Voltage Machines,” IEEE Trans. Dielectr. Electr. Insul., Vol. 24, No. 4, pp. 2123-2131, September. 2017

[41] J. Wang, P. Wang, W. Wang, K. Zhou, Q. Zhou and Y. Lei, “Novel Repetitive Square Wave Voltage Generator Used for the Insulation Evaluation of Rotating Machines Driven by Power Electronics,” IEEE Trans. Dielectr. Electr. Insul., Vol. 24, No. 4, pp. 2041-2049, 2017.

[42] X. N. Li, G. N. Wu, Y. Yang, Z. J. Wang, X. Ping, Y. X. Li and B. Gao, “Partial Discharge Characteristics of Oil-paper Insulation for On-board Traction Transformers Under Superposed Inter-harmonic AC Voltages,” IEEE Trans. Dielectr. Electr. Insul.,

[43] A. Rachit, L. Hui, Z. H. Guo and P. Cheetham, “DC SST MF Transformer Partial Discharge Characteristics Study with High dV/dT PWM Switching Transients of SiC Devices,” IEEE Applied Power Electronics Conference and Exposition, Houston, TX, USA, 2022, pp. 980-984.

[44] Z. C. Guo, A. Huang, R. E. Hebner, G. C. Montanari and X. Y. Feng, “Characterization of Partial Discharges in High-Frequency Transformer Under PWM Pulses,” IEEE Transactions on power electronics.,Vol. 37, No. 9, pp. 11199-11208, 2022.

[45] J. Jiang, M. Zhao, C. Zhang, M. Chen and H. J. Liu, “Partial Discharge Analysis in High-Frequency Transformer Based on High-Frequency Current Transducer,” Energies., Vol. 11, 2018.

[46] J. Jiang, B. D. Zhang, Z. Li, P. Ranjan, “Partial Discharge Features for Power Electronic Transformers Under High-Frequency Pulse Voltage,” IEEE Transactions on plasma science., Vol. 49, No. 2, pp. 845-853, 2021.

[47] N. Lahoud, M. Q. Nguyen, P. Maussion, D. Malec, and D. Mary, “Lifetime Model of the Inverter-fed Motors Secondary Insulation by using a Design of

Experiments," IEEE Trans. Dielectr. Electr. Insul., Vol. 22, No. 6, pp. 3170-3176, December, 2015.

[48] N, Lahoud, J. Faucher, D. Malec and P. Maussion, "Electrical Aging of the Insulation of Low-Voltage Machines: Model Definition and Test With the Design of Experiments," IEEE Transactions on industrial electronics., Vol. 60, No. 9, pp. 4147-4155.

[49] T. Liu, Q. M. Li, G. J. Dong, M. Asif, X. W. Huang, Z. D. Wan, "Multi-factor model for lifetime prediction of polymers used as insulation material in high frequency electrical equipment," Polym. Test., vol. 73, pp. 193–199, November. 2018.

[50] H. Sun, Y. Wang, Y. Ding, Y. Rui, L. Fan and Y. Yin, "Partial Discharge Detection of Electrical Machine Insulation Under PWM Voltage with High dv/dt for More Electric Aircraft," IEEE Energy Conversion Congress and Exposition, Detroit, MI, USA, 30, November, 2022.

[51] D. R. Meyer, A. Cavallini, L. Lusuardi, D. Barater, G. Pietrini, A. Soldati, "Influence of Impulse Voltage Repetition Frequency on RPDIV in Partial Vacuum," IEEE Trans. Dielectr. Electr. Insul., Vol. 25, No. 3, pp. 873-882, 2018.

[52] E. Sili, J. P. Cambronne, N. Naude, R. Khazaka, "Polyimide lifetime under partial discharge aging: effects of temperature, pressure and humidity," IEEE Trans. Dielectr. Electr. Insul., vol. 20, no. 2, pp. 435-442, May. 2013.

[53] A. Cedric, B. Thibaut, L. Thierry, "Influence of pressure on partial discharge spectra," IEEE Electrical Insulation Conference, Montreal, QC, Canada, June. 2016, pp. 507-510.

[54] E. Christopher, L. Robert, C. Lan, R. Simon and F. Robert, "The Effects of Pressure and Temperature on Partial Discharge Degradation of Silicone Conformal Coatings," IEEE Trans. Dielectr. Electr. Insul., Vol. 24, No. 5, pp. 2986-2994, 2017.

[55] A. A. Abdelmalik, A. Nysveen and L. Lundgaard,"Influence of Fast Rise Voltage and Pressure on Partial Discharges in Liquid Embedded Power Electronics," IEEE Trans. Dielectr. Electr. Insul., Vol. 22, No. 5, pp. 2770-2778, 2015.

[56] B. Moein and G. Mona,"Characterization of Partial Discharge Activities in WBG Power Converters under Low-Pressure Condition,"Energies., Vol. 14, No. 5394, 2021

[57] B. Moein, G. Mona, “A Finite Element Analysis Model for Partial Discharges in Silicone Gel under a High Slew Rate, High Frequency Square Wave Voltage in Low-Pressure Conditions,” Energies., Vol. 13, No. 9, 2020.

[58] H. Liu, R. Liao, X. Zhao and Y. Lin, “The effect of air pressure on the surface electric field intensity characteristics under negative DC corona discharge in a corona cage,” Electrical Power and Energy Systems., Vol. 113, pp. 244-250, 2019

[59] J. Wan, H. Liu and H. Yu, “Voltage distribution in stator windings of the motor driven by PWM inverter,” IEEE International Conference on Power System Technology, Kunming, Yunnan, China, October, 2002.

[60] F. Wen, L. Zhang, G. Wu, and E. He, “Modeling and Simulation of Inter-Turn Voltage Distribution in the Stator Windings of the Pulling Motor,” in Proc IEEE International Conference on Solid Dielectrics, Toulouse, France, July. 2004, pp. 900-903, DOI: 10.1109/ICSD.2004.1350577

[61] A. Krings, G. Paulsson, F. Sahlén, and B. Holmgren, “Experimental investigation of the voltage distribution in form wound windings of large AC machines due to fast transients,” in Proc IEEE International Conference on Electrical Machines, Laussane, Switzerland, September. 2016, pp. 1700-1706, DOI: 10.1109/ICELMACH.2016.7732753

[62] D. E. Moghadam, J. Speck, S. Grosmann and J. Stahl, “Voltage Distribution in the Stator Windings of High Voltage Motors Fed by PWM Drives Part I: Effects of the Pulse Characteristics,” IEEE 2nd International Conference on Dielectrics, Budapest, Hungary, July, 2018.

[63] Y. Zhao, G. Zhang and R. Guo, “The Breakdown Characteristics of Thermostable Insulation Materials under High-Frequency Square Waveform,” IEEE Trans. Dielectr. Electr. Insul., vol. 26, no. 4, pp. 1073–1080, 2019.

[64] A. Garrigós, C. Orts, D. Marroquí, J. M. Blanes, C. Torres and P. Casado, “Bus voltage regulation using sequentially switched ZVZCS converters for spacecraft power systems,” IEEE European Conference on Power Electronics and Applications, Hanover, Germany, September, 2022.

[65] C. Zheng, Q. Wang, H. Wang, Z. Shen and Bak. C. L, “Electrical Stress on the Medium Voltage Medium Frequency Transformer,” Energies., Vol. 14, no. 16, 2021.

[66] C. Zheng, Q. Wang, Z. Shen, Bak. C. L, F. F. Silva and H. Wang, “Influence of pressure on the PD and induced aging behavior of polyimide insulation under

repetitive pulse voltage," IEEE Transactions on dielectric and electrical insulation. (Published online)

[67] C. Zheng, Q. Wang, H. Wang, Z. Shen and Bak. C. L, "Electrical stress suffered by medium voltage medium frequency transformer," IEEE Electrical insulation Conference, Denver, CO, USA, 29, November, 2021, pp. 116-119.

[68] C. Zheng, Q. Wang, H. Wang, Z. Shen, F. F. Silva and Bak. C. L, "Partial discharge inception and deterioration of Nomex paper under repetitive square wave voltage," IEEE International Conference on High Voltage Engineering and Applications, Chongqing, China, December, 2022

[69] C. Zheng, Q. Wang, H. Wang, Z. Shen, F. F. Silva and Bak. C. L, "Comparative PDIV and endurance studies on different insulating materials used for medium frequency transformers," IEEE International Conference on High Voltage Engineering and Applications, Chongqing, China, December, 2022.

[70] P. Huang, C. X. Mao, D. Wang, L. Wang, Y. Duan, J. Qiu, G. Xiu and H. Cai, "Optimal Design and Implementation of High-Voltage High-Power Silicon Steel Core Medium-Frequency Transformer," IEEE Trans. Ind. Electr., Vol. 64, No. 6, pp. 4391-4401, 2017.

[71] J. W. Kolar and G. Ortiz, "Solid-State-Transformers: Key Components of Future Traction and Smart Grid Systems," Proceedings of the International Power Electronics Conference, Hiroshima, Japan, May, 2014.

[72] X. She, Q. Huang and R. Burgos, "Review of Solid-State Transformer Technologies and Their Application in Power Distribution Systems," IEEE Journal of emerging and selected topics in power electronics., Vol. 1, No. 3, pp. 186-198, 2013.

[73] Brigham, E. Fast Fourier transform and its applications, Pearson Education: New Jersey, USA, 1988.

[74] G. Skibinski, R. Kerkman, D. Leggate, J. Pankau and D. Schlegel, "Reflected wave modeling techniques for PWM AC motor drives," IEEE Annual Applied Power Electronics Conference and Exposition, Anaheim, CA, USA, Febrary, 1998, pp. 1021-1029.

[75] D. Reigosa, D. Fernandez, M. Martinez, J. M. Guerrero, A. B. Diez and F. Briz, "Magnet Temperature Estimation in Permanent Magnet Synchronous Machines Using the High Frequency Inductance," IEEE Transactions on industry applications., Vol. 55, No. 3, pp.2750-2757, 2019.

[76] S. Nagai, T. Hayashi and A. Sanada, “Measurements of Anomalous Skin Effect in 1 THz Band,” IEEE MTT-S International Microwave Symposium Digest, Seattle, WA, USA, June, 2013.

[77] A. Alabakhshizadeh and O. Midtgard, “Optimum Core Dimension for Minimizing Proximity Effect Losses of an AC Inductor for a Galvanically Isolated PV Inverter,” IEEE Photovoltaic Specialists Conference, Austin, TX, USA, June, 2012.

[78] Richard, C.D.; Robert, H.B. Modern control systems, 12th ed.; Pearson Education: New Jersey, USA, 2011.

[79] Z. H. Zheng, L. Bai, and T. Jin, “Study on Insulation Design of High Power High Frequency High Voltage Transformer,” in Proc IEEE Conference on Energy Internet and Energy System Integration, Beijing, China, October. 2018, DOI: 10.1109/EI2.2018.8582317

[80] T. Wang, H. Lin and S. S. Liu, “An Active Voltage Balancing Control Based on Adjusting Driving Signal Time Delay for Series-Connected SiC MOSFETs,” IEEE Journal of emerging and selected topics in power electronics., Vol. 8, No. 1, pp. 454-464, 2020.

[81] A. Cavallini, D. Fabiani and G. C. Montanari, “Power Electronics and Electrical Insulation Systems – Part 1: Phenomenology Overview,” IEEE Electrical Insulation Magazine., Vol. 26, no. 3, pp. 7-15, June. 2010.

[82] T. Hammarström, “Combination of Adjustable Inverter Level and Voltage Rise Time for Electrical Stress Reduction in PWM Driven Motor Windings,” IEEE Electrical Insulation Magazine., Vol. 37, No. 1, pp. 17-26, 2021.

[83] T. Hammarström, “Reduction of Electric Stress in High Voltage Motor Insulation by Adjusting Individual PWM Flanks,” IEEE International Conference on Power Systems Technology, Kuala Lumpur, Malaysia, September, 2022.

[84] Y. K. Zhao, G. Q. Zhang, D. Han, K. Li; Z. J. Qiu, and F. Y. Yang, “Experimental Study on the Insulation Properties of Epoxy Casting Resins under High-Frequency Square Waveform,” CSEE Journal of Power and Energy Systems., pp. 1-10, May. 2020

[85] B.V. Sumangala and G.R. Nagabhushana, “Analysis of Surge Voltage Distribution in a Model Transformer for Different Types of Surges with Turn Resolution and its Validation,” TENCON IEEE Region 10 Conference, HongKong, China, 2006.

[86] T. Hammarstrom, “Partial Discharge Characteristics at Ultra-Short Voltage Risetimes,” IEEE Trans. Dielectr. Electr. Insul., Vol. 25, No. 6, pp. 2241-2249, 2018.

[87] P. Wang, A. Cavallini and G. C. Montanri, “The Influence of Square Voltage Rise Time on Partial Discharge Spectra,” IEEE Annual Report Conference on Electrical Insulation and Dielectric Phenomena, Montreal, QC, Canada, December, 2012, pp. 129-132.

[88] P. Wang, P. Li, S. Akram, P. Meng, G. Zhu and G. C. Montanari, “Considering the Parameters of PWM Voltage to Improve the SNR of PD Tests for Inverter fed Motors,” IEEE Transactions on Industrial Electronics., Vol. 69, No. 5, pp. 4545-4554, 2022.

[89] H. Okubo, N. Hayakawa and G. Montanari, “Technical Development on Partial Discharge Measurement and Electrical Insulation Techniques for Low Voltage Motors Driven by Voltage Inverters,” IEEE Trans. Dielectr. Electr. Insul., Vol. 14, No. 6, pp. 1516-1530, 2007.

[90] M. G. Gao; Y. P. Meng, X. Chen, Y. Wang, Y. H. Cheng, K. Wu, and W. Cao, “Study on the feasibility of detection of partial discharge signals under square voltages,” in Proc IEEE Properties and Applications of Dielectric Materials, Harbin, China, July. 2009, pp. 1016-1019, DOI: 10.1109/ICPADM.2009.5252440.

[91] X. Liu, G. N. Wu, L. S. Tong, T. G. Lin, and G. Q. Zhang, “Influence of Impulse Frequency on Partial Discharge under PWM,” in Proc IEEE International Symposium on Electrical Insulation, Toronto, ON, Canada, June. 2006, pp.241-244, DOI: 10.1109/ELINSL.2006.1665302

[92] H. Okubo, Y. H. Lu, M. Morikawa, and N. Hayakawa, “Partial Discharge Inception Characteristics Influenced by Stressed Wire Length of Inverter-Fed Motor,” in Proc IEEE Conference on Electrical Insulation and Dielectric Phenomena, Boulder, CO, USA, October. 2004, pp. 442-445, DOI: 10.1109/CEIDP.2004.1364282.

[93] N. Hayakawa, H. Inano, Y. Nakamura, and H. Okubo, “Time Variation of Partial Discharge Activity Leading to Breakdown of Magnet Wire under Repetitive Surge Voltage Application,” IEEE Trans. Dielectr. Electr. Insul., Vol. 15, No. 6, pp. 1701-1706, December. 2008.

[94] P. Wang, S. Ma, S. Akram, K. Zhou, Y. D. Chen, and M. T. Nazir, “Design of Archimedes Spiral Antenna to Optimize for Partial Discharge Detection of

Inverter Fed Motor Insulation," IEEE Access., Vol. 8, pp. 193202-193213, October. 2020.

[95] D. R. Meyer, A. Cavallini and L. Lusuardi, "Influence of Impulse Voltage Repetition Frequency on RPDIV in Partial Vaccum," IEEE Trans. Dielectr. Electr. Insul., Vol. 25, No. 3, pp. 873-882.

[96] A. Cavallini, E. Lindell, G. C. Montanari and M. Tozzi, "Inception of Partial Discharges under Repetitive Square Voltages: Effect of Voltage Waveform and Repetition Rate on PDIV and RPDIV," IEEE Conference on Electrical Insulation and Dielectric Phenomena, West Lafayette, IN, USA, March, 2011.

[97] L. Lusuardi, A. Cavallini, A. Caprara, F. Bardelli and A. Cattazzo, "The Impact of Test Voltage Waveform in Determining the Repetitive Partial Discharge Inception Voltage of Type I Turn/Turn Insulation Used in Inverter-Fed Induction Motors" IEEE Electrical Insulation Conference, San Antonio, TX, USA, October, 2018, pp. 478-481.

[98] L. Simoni, G. Mazzanti, G. C. Montanari and L. Lefebre, "A Genera Multi-stress life model for insulating materials with or without evidence for thresholds," IEEE Transactions on Electrical Insulation., Vol. 28, No. 3, pp. 349-364, 1993.

[99] D. Aushuman, S. Navid, K. Rahul, E. Wilson and L. Ri, "Improving Thermal Performance of High Frequency Power Transformers using Bobbinless Transformer Design," IEEE Intersociety Conference on Thermal and Thermomechanical Phenomena in Electronic Systems, pp. 291-297, July, 2020.

[100] M. Mogorovic and D. Dujic, "Sensitivity Analysis of Medium-Frequency Transformer Designs for Solid-State Transformers," IEEE Transactions on Power electronics., Vol. 34, No. 9, pp. 8356-8367, 2019.

[101] High Performance Dielectric, Conductivity and Electrochemical Impedance Analyzers, Available: https://www.novocontrol.de/pdf_s/alpha.pdf.

[102] T. Kaji, H. Asai, H. Kojima and N. Hayakawa, "Combined Effect of Temperature and Humidity of Magnet-Wires on Partial Discharge Inception Voltage under Inverter-Surge Voltage," IEEE Conference on Electrical Insulation and Dielectric Phenomena (CEIDP), Cancun, 2018, pp. 554-557.

[103] L. Niemeyer, "A generalized approach to partial discharge modeling," IEEE Transactions on dielectric and electrical insulation., Vol. 2, No. 4, pp. 510-528, 1995.

[104] A. Rumi, A. Cavallini and L. Lusuardi, “Combined Effects of Temperature and Humidity on the PDIV of Twisted Pairs,” IEEE International Conference on Dielectrics, Valencia, Spain, July, 2020, pp. 906-909.

[105] P. Wang, Y. H. Gu, Q. Wu, A. Cavallini, Q. Zhang, J. W. Zhang, P. Li, Y. Li, “Influence of Ambient Humidity on PDIV and Endurance of Inverter-fed Motor Insulation,” IEEE Electrical Insulation Conference, Calgary, AB, Canada, June, 2019, pp. 201-204.

[106] P. Wang, A. Cavallini and G. C. Montanari, “The influence of square wave voltage duty cycle on PD behavior,” IEEE Conference on Electrical Insulation and Dielectric Phenomena, Ann Arbor, MI, USA, October, 2015.

[107] P. Wang, H. Y. Xu, J. Wang and A. Cavallini, “The Influence of Repetitive Square Wave Voltage Duty Cycle on Partial Discharge Statistics and Insulation Endurance,” IEEE International Conference on Condition Monitoring and Diagnosis, Xi An, China, September, 2016.

[108] F.Gutfleisch and L.Niemeyer, “Measurement and insulation of PD in epoxy voids,” IEEE Trans. Dielectr. Electr. Insul., Vol.2, no.5, pp. 729-723, 1995.

[109] D. Fabiani, G. C. Montanari, A. Cavallini, and G. Mazzanti, “Relation between space charge accumulation and partial discharge activity in enameled wires under PWM-like voltage waveforms,” IEEE Trans. Dielectr. Electr. Insul., Vol. 11, no.3, pp. 393-405, October. 2004.

[110] X. Zhong, G. Wu, Y. Yang, X. Wu, Y. Lei, “Effects of nanoparticles on reducing partial discharge induced degradation of polyimide/Al2O3 nanocomposites,” IEEE Transactions on Dielectrics and Electrical Insulation., Vol. 25, No. 2, pp. 594-602.

[111] Y. Luo, G. Wu, J. Liu, G. Zhu, P. Wang, P, Jia and K. Cao,“PD Characteristics and Microscopic Analysis of Polyimide Film Used as Turn Insulation in Inverter-fed Motor,” IEEE Trans. Dielectr. Electr. Insul., Vol. 21, No. 5, pp. 2237-2244, 2014.

[112] P. Yao, H. Zheng, X. Yao, Z. DING, “A Method of Monitoring Partial Discharge in Switchgear Based on Ozone Concentration,” IEEE transactions on plasma science., Vol. 47, No. 1, pp. 654-660, 2019.

[113] H. Okubo, S. Yuasa, K. Ota, N. Hayakawa, M. Hikita, “Discharge Characteristics under Non-uniform Electric Field in He, Ar and Air at Low Pressures,” IEEE Transactions on Dielectrics and Electrical Insulation., Vol. 4, No. 4, pp. 450-455, 1997

[114] G.C. Montanari, S. Schwartz, Q. Yang, D. Nath, R. Ghosh, R. Cuzner, “Towards Partial Discharge Automatic and Unsupervised Monitoring: A Technological Breakthrough for MV Electrical Asset Condition Monitoring and Diagnostics,” IEEE International Conference on Condition Monitoring and Diagnosis, Kitakyushu, Japan, November, 2022, pp. 588-592.

[115] E. Baloji, T. Hammarström, “Classification of Partial Discharges Originating From Multilevel PWM Using Machine Learning,” IEEE Trans. Dielectr. Electr. Insul., Vol. 29, No. 1, pp. 287-294, 2022.

PART. 2

PAPERS

energies

MDPI

Article

Electrical Stress on the Medium Voltage Medium Frequency Transformer

Zheng Changjiang, Wang Qian *, Wang Huai, Shen Zhan and Claus Leth Bak

Department of Energy Technology, Aalborg University, 9220 Aalborg Øst, Denmark; czhe@et.aau.dk (Z.C.); hwa@et.aau.dk (W.H.); zhs@et.aau.dk (S.Z.); clb@et.aau.dk (C.L.B.)
* Correspondence: qiw@et.aau.dk; Tel.: +45-93562161

Abstract: This paper proposes an equivalent circuit model to obtain the transient electrical stress quantitatively in medium voltage medium frequency transformers in modern power electronics. To verify this model, transient simulation is performed on a 1.5 kV/1 kHz transformer, revealing voltage overshoot quantitatively between turns and layers of the transformer's HV winding. Effects of rise time of the input pulse voltage, stray capacitance of the winding insulation, and their interactions on the voltage overshot magnitude are presented. With these results, we propose limiting the voltage overshoot and, thereafter, enhancing medium voltage medium frequency transformer's insulation capability, which throws light on the transformer's insulation design. Additionally, guidance on the future studies on aging and endurance lifetime of the medium voltage medium frequency transformer's insulation could be given.

Keywords: MVMF transformer; insulation; pulse voltage; electrical stress

Citation: Changjiang, Z.; Qian, W.; Huai, W.; Zhan, S.; Bak, C.L. Electrical Stress on the Medium Voltage Medium Frequency Transformer. *Energies* **2021**, *14*, 5136. https://doi.org/10.3390/en14165136

Academic Editor: Sérgio Cruz

Received: 17 June 2021
Accepted: 16 August 2021
Published: 19 August 2021

Publisher's Note: MDPI stays neutral with regard to jurisdictional claims in published maps and institutional affiliations.

1. Introduction

In several modern power electronic systems, a transformer is one of the most critical devices serving as voltage scaling up/down, electrical isolation, and power transmission. One of the typical topologies of the power electronic system with transformers commonly used in power distribution and transportation fields is shown in Figure 1 [1]. Connected with power electronic switches on both sides, these transformers are working under voltage with magnitude from several to tens of kV, while the frequency is in the range from hundreds of Hz to tens of kHz (depending on the electrical capability of modern IGBT and MOSFET). Because of their working conditions characteristics, these transformers are called medium voltage medium frequency (MVMF) transformers. Compared with a conventional transformer working under 50/60 Hz sinusoidal voltages in an HV power delivery system, an MVMF transformer has quite a different overall layout with a smaller size. Combined with power electronic switches, these transformers also have higher controllability than the conventional ones [2]. So, they are widely used in modern power electronic applications, such as railway traction, DC grids, etc. Recently, MVMF transformers have further reduced size to reach lower costs and higher power densities. However, along with the development of MVMF transformers, challenges exist such as increased hysteresis loss and conductor loss due to higher working frequency. These factors can lead the transformer to overheating. Additionally, another important challenge is related to insulation reliability, since the MVMF transformer may be faced with fast insulation degradation due to electrical overstress [3].

The waveform of the voltage applied to the MVMF transformer is the medium-frequency PWM pulse. It has a much shorter rise time compared with the sinusoidal voltage. So, the electrical stress faced by the transformer's insulation system would be different from that of traditional transformers working under power frequency sinusoidal voltages. Previous research on inverter-fed motors shows that when pulse voltage with short rise time is added to the multi-turn winding, oscillation on the rising edge of the

voltage between turns can be induced. As a result, a transient voltage with a much higher peak value than the static voltage drop between turns is reached [4]. What is more, the voltage distribution among turns is uneven. Usually, the turns closest to the voltage source output terminals would suffer from the highest peak voltage values [5]. Since transformers also have multi-turn windings, when working in MVMF power electronic conditions, the similar phenomenon of interturn overvoltage and uneven voltage distribution may also exist. If so, the probability of partial discharge (PD) occurrence in the interturn insulation of the transformer would be higher [6]. Continuous PD can degrade the insulation material quickly and greatly shorten the time-to-failure of the transformer in MVMF application [7]. When PD is combined with temperature rise due to increased hysteresis loss and conductor loss, the insulation aging rate may be even faster [6]. As MVMF transformers are developing to be smaller in size, which means the insulation distance may also be reduced inevitably, insulation issues caused by unusual electrical stress would probably be more serious. In addition, for transformers with multi-layer windings, not only the interturn insulation, but also the interlayer insulation may suffer from electrical overstress brought from the pulse operating voltage. Therefore, research on the insulation problems of the MVMF transformers is also necessary.

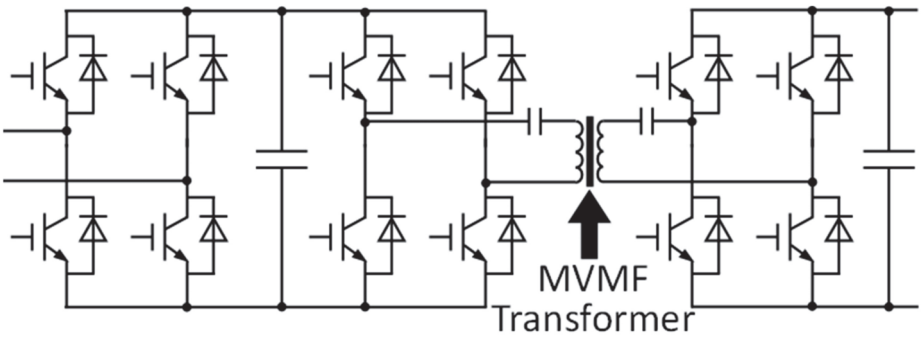

Figure 1. A typical topology with a medium voltage medium frequency transformer.

Some researchers have already investigated the electrical stress on the MVMF transformers and take strategies to deal with it. In [8], the author conducts an FEM electric field simulation and finds that the electrical field concentrates mostly in one side of the turns of HV winding that is facing the LV winding. Zheng in [9], proposes a segmented winding structure to reduce the largest interlayer voltage in an MVMF transformer's winding. Authors in [10] find that adding an angle ring and electrostatic ring within the transformer's structure can reduce the value of peak electric field intensity. For the design of MVMF transformers in [11,12], authors apply extra semi-conductive layers on the surface of the winding insulation. Electric field simulation shows that this method can effectively reduce the electric field intensity in air gaps between winding and core. Although this research can surely be advantageous to the improvement of insulation capabilities of MFMV transformers, they mostly focus on the steady-state electric field/voltage simulation. As mentioned before, the most obvious difference between MVMF and conventional transformers with respect to the insulation problem is the transient overvoltage and uneven voltage distribution that may happen within the MVMF transformer's winding when working under pulse voltage with a short rise time. Steady-state simulation ignores the transient response in the MVMF transformer's winding when exposed to pulse voltage with very short rise time and frequency much higher than the power frequency. Consequently, the maximum electrical field magnitude applied to the winding insulation is underestimated.

Yet, some previous research on the electrical stress of inverter-fed motors provides good suggestions regarding the way of studying the electrical stress of MVMF transformers working under similar electrical condition, since they pay a lot of attention to transient

voltage drop within the winding. In [13], Wan conducts an FEM calculation to obtain stray parameters of a motor prototype's winding and builds an equivalent circuit model of the winding. Based on that, interturn voltage drop simulation under pulse voltage is conducted. Results show that the overshoot of the voltage drop on the first turn is higher than that on other turns, which means voltage distribution within the winding is uneven. In [14], Wen conducts interturn voltage simulation similar to that of Wan's and finds that reducing the capacitance to ground of the turns can decrease the peak interturn voltage value. Krings analyzes inter-coil (consists of several turns) voltage waveform of an HV motor working under PWM voltage [15]. He discovers that the voltage drop between the first two coils is usually the highest and increasing the rise time of pulse voltage makes the voltage between different adjacent coils distribute more evenly. The experiment results on a real prototype are in high accordance with that of simulation. Moghadam conducts experiments on interturn voltage within a single coil of a motor under different electrical parameters [16]. The author finds that besides shorter rise time, the longer pulse width can also bring a stronger interturn voltage drop, leading to a more serious electrical stress on the coil's insulation. Table 1 summarizes the comparison among the reviewed studies and this paper with respect to contributions and inadequacies from the perspective of MVMF transformer.

Table 1. Comparisons between reviewed studies and this paper from the perspective of an MVMF transformer.

Reference Number	Contribution	Inadequacies	Advantage of This Paper
[8–12]	• Reveal the position of the electrical field hot point in the transformer's winding. • Propose a suitable method to reduce the interlayer overvoltage and electric field intensity in the air gap within the winding.	• Transient response from the winding, when exposed to pulse voltage, is not considered. • The maximum electrical stress in the winding insulation is underestimated.	• Sufficiently consider the effect of transient overvoltage in the winding exposed to pulse voltage. The maximum electrical stress in the winding is obtained with enough accuracy.
[13–16]	• Reveal the interturn and inter-coil overvoltage within the winding of inverter-fed motors. • The strongest electrical stress brought from transient overvoltage caused by pulse voltage is adequately considered.	• Not accurate enough to predict the electrical stress of MVMF transformers due to the difference in winding structures between motors and transformers.	• Predict the electrical stress of MVMF transformers with higher accuracy, since this study directly focuses on the MVMF transformer.

Considering that the winding structure of the transformer is not the same as that of the motor, conclusions from the studies on electrical stress of inverter-fed motors cannot be directly used for that of MVMF transformers. Although, in decades before, studies have been conducted focusing on surge distribution in power frequency transformers [17,18], the electrical stress brought from repetitive PWM voltage may not be the same as these single pulses. Besides, the MVMF transformer is different from conventional power transformers with respect to the size and layout of windings and cores, when added with similar pulse voltage, the electrical stress may also show different characteristics. Therefore, investigation on electrical stress suffered by MVMF transformers through transient voltage analysis is necessary.

Aiming at investigating the transient maximum electrical stress of MVMF transformer that is not covered by previous papers and combined with the advanced methods from the studies on inverter-fed motors, this article builds an equivalent circuit model of a transformer' HV winding through software Ansys Q3D and MATLAB. Based on that, a simulation on the electrical stress in the winding is conducted. The results confirm

the existence of interturn and interlayer overvoltage. Mechanism of the occurrence of interturn/layer overvoltage and the factors that can influence it are analyzed. According to the mechanism, measures to improve the insulation capability of an MVMF transformer can be proposed.

2. Transformer Prototype for the Simulation

A transformer prototype proposed in the literature [8,19] is selected as a typical case for the electrical stress study. The reason for choosing this prototype is that this transformer is a typical MVMF transformer, which is inherently different from a power transformer with respect to design and operating voltage. Therefore, this prototype fits with our paper's scope. Besides, its voltage and frequency ratings (1.5 kV and 1 kHz, respectively) are common among the prevailing MVMF transformers. In addition, this transformer is designed to be used in a power electronic transformer system (PET), which will be widely applied in fields such as the distribution system, DC grid, and high-speed railway systems. Therefore, study on this prototype has a certain extent of universality, which can be beneficial for insulation improvement of other MVMF transformers in similar applications. Its basic parameters are depicted in Table 2.

Table 2. Basic parameters of the transformer prototype.

Electrical Parameters	**Value**
Operation frequency	1 kHz
Rated power	35 kW
Turn ratio	120:32
Rated voltage of HV winding	1500 V
Rated voltage of LV winding	400 V
Design Parameters	**Type**
Core material	Ferrite (with permeability 1900)
Core size (width/height/thick)	27 cm/19 cm/10 cm
Core structure	Core type
Window area	105 cm^2
Primary winding conductor	2 mm × 5 mm flat copper wire
Secondary winding conductor	0.4 mm × 110 mm copper foil
Insulation material	Polyimide
Interturn insulation distance	1 mm (primary)/0.3 mm (secondary)
Inter-winding insulation distance	1.5 mm

The transformer's overall 3D outlook and 2D partial cross-section of its winding are shown in Figure 2. Its HV winding is made from flat copper wires with 5 mm in height and 2 mm in width. Its LV winding is made of copper foils. Both of the windings are distributed on each limb of the core evenly, and the HV winding has three layers. Since this paper focuses on the study on electrical stress rather than insulation degradation or breakdown, we simply assume that this transformer prototype is in a very good insulation condition with all the gaps between conductors completely filled with insulation (seen in yellow area in Figure 2). For HV winding, interturn insulation and interlayer insulation distance are 0.6 mm and 1 mm, respectively. While the insulation distance of LV winding is 0.3 mm. The core made by ferrite (with relative permeability 1900) has a core-type structure with dimensions of 27 cm in height, 19 cm in width, and 10 cm in thickness, whereas the window area is 105 cm^2. With today's transformer design and manufacturing technology, usually the electrical field intensity within the LV winding is low [20]. So, the probability of facing serious insulation problems by LV winding is much lower than that of HV winding. Therefore, the study on the electrical stress in this transformer prototype would only focus on the HV winding.

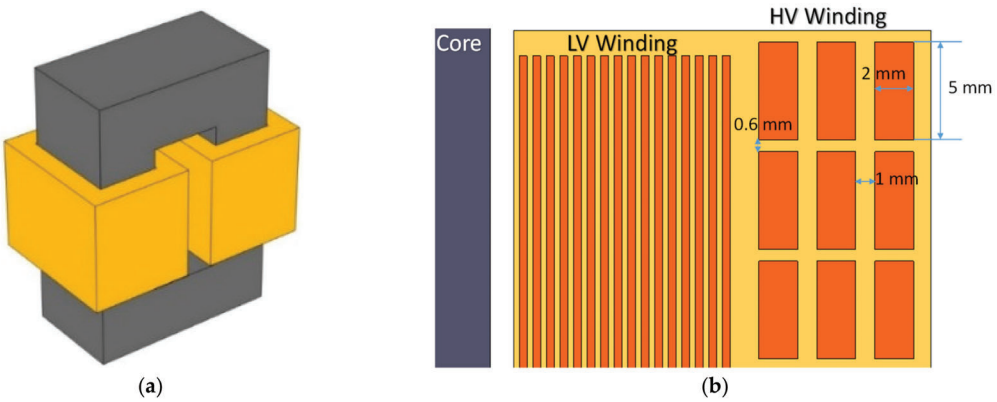

Figure 2. Transformer prototype: (**a**) 3D outlook; (**b**) partial 2D cross-section of the winding.

3. Equivalent Model of HV Winding

To conduct the transient voltage simulation in the HV winding, an equivalent circuit model of the winding should be built [14]. In the building of the circuit model, stray parameters of each turn of the HV winding are considered including resistance, capacitance, and inductance. All of these aforementioned parameters are calculated in FEM-based software, Ansys Q3D. The model used in the FEM calculation is 3D model as depicted in Figure 2. The material of turns is set as copper, while the original insulation material is set as polyimide with relative permittivity of 3.9 (in Section 5, these stray parameters are recalculated with different insulation materials). In the FEM calculation, Dirichlet boundary condition is used as the electromagnetic field boundary condition [14], the potential function is expressed by (1)

$$\varnothing|_r = g(\Gamma_1) = 0 \tag{1}$$

where Γ_1 is the Dirichlet boundary, and $g(\Gamma_1)$ is the ecumenical function of position. The element type is quadrilateral.

3.1. Stray Capacitance

According to the FEM calculation results, capacitances between non-adjacent turns (for example, C_{1-3}) are very small compared with that between adjacent turns (for example, C_{1-2}). In addition, due to the long distance between HV winding and core (longer than 12 mm), turn-to-core capacitances are much smaller than interturn capacitances. Therefore, interturn capacitances between non-adjacent turns and turn-to-core capacitances are ignored. In this three-layer HV winding structure, interlayer capacitances, such as C_{1-40} shown in Figure 3 (numbers in the figure refer to the serial numbers of the turns in the winding), should be taken into consideration because their values are comparable with the interturn capacitances such as C_{1-2}.

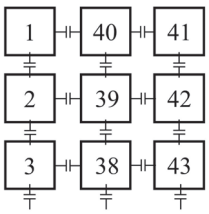

Figure 3. Stray capacitance taken into consideration.

3.2. Inductance and Resistance

In this case study, the voltage waveform for the simulation is square wave pulse voltage with a very short rise time. It is known that this kind of voltage is a combination of a sinusoidal wave voltage with fundamental frequency and a series of odd harmonics [21]. When a higher order of harmonics is added to form the square wave, its waveform is closer to an ideal square wave. That is to say, the rise time is shorter. This formation of the square wave can be expressed through Figure 4, where the peak-to-peak value and frequency of the square wave are in accordance with that listed in Table 2.

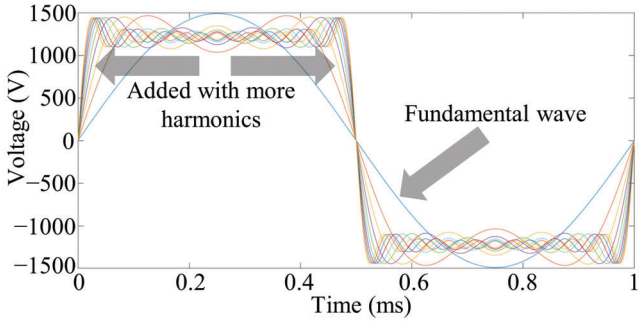

Figure 4. Formation of the square wave.

The equivalent highest frequency f_u of a pulse voltage with a fixed rise time can be calculated approximately by (2) [22]:

$$f_u = \frac{1}{\pi t} \tag{2}$$

where t is the voltage rise time. In PWM-like voltages produced from power electronic switches, it is usually in a range from hundreds of ns to several μs. Inductance can be affected by frequency. Additionally, the resistance will increase due to the skin and proximity effects under higher frequencies. So these two parameters are calculated in the frequency domain with the frequency of the aforementioned high-order harmonics taken into consideration. Because of the effect from the core with high relative permeability, strong mutual inductive coupling exists among the turns even though they are not close to each other. Therefore, a 120 × 120 mutual inductance matrix obtained from the FEM calculation is used in the building of the equivalent circuit model.

4. Analysis on the Mechanism of Overvoltage

With the FEM calculation by Ansys Q3D discussed in the last section, stray parameters of the winding are obtained. These parameters include resistance and self-inductance of each turn along with mutual (interturn/layer) capacitances and mutual inductances between different turns (expressed as Rx, Lx, Cx-y, and Mx-y, respectively, x and y vary from 1 to 120). Based on that, an equivalent circuit model of the transformer's HV winding is constructed in MATLAB's module Simulink, shown in Figure 5. Value ranges of the stray parameters are listed in Table 3, where R, L, and C in the table refer to RX, LX, and Cx-y in Figure 5, respectively. A voltage source that can generate pulse voltage with adjustable magnitude, frequency, and rise time is connected between the first turn and the last turn of the winding's circuit model. Set the pulse voltage's peak-to-peak value and frequency as 1500 V and 1 kHz, respectively, and the rise time as 100 ns, the first simulation is conducted. During this simulation, the interturn voltage drops within the first six turns are recorded (expressed as V1–2, V2–3, V3–4, V4–5, and V5–6, respectively). Typical waveforms of these interturn voltage drops in a half period are shown in Figure 6. It is clear that strong oscillations exist on the rising edge of the pulse voltage. This oscillation lasts for more

than 30 µs and leads to a peak voltage value above 22 V, which is much higher than the static voltage value (around 4.7 V). To understand why this overvoltage would happen and which factors can bring influence on it, analysis is needed.

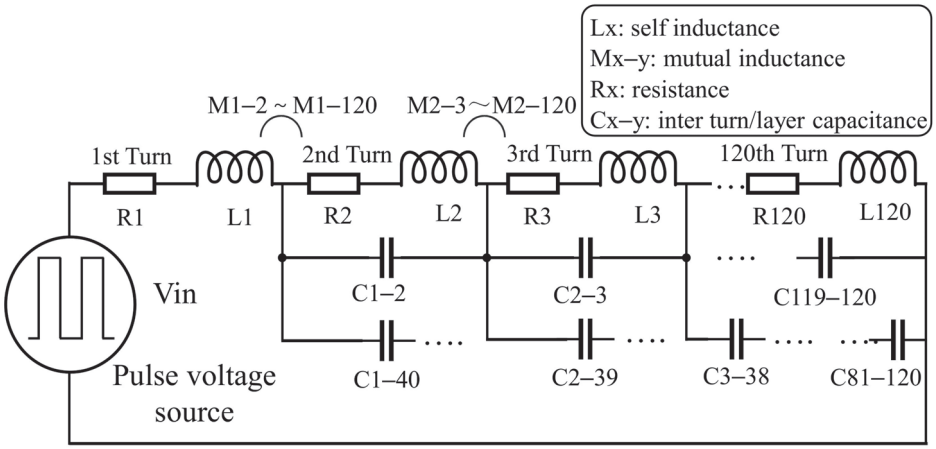

Figure 5. Equivalent circuit model of the transformer's HV winding (values of Lx, Rx, and CX–Y lies in the range of R, L, and C listed in Table 3).

Table 3. Value ranges of the stray parameters of the selected transformer prototype.

Parameters	Range
Resistor (R)	0.03–0.06 Ω
Inductance (L)	50–70 nH
Capacitance (C)	50–80 pF

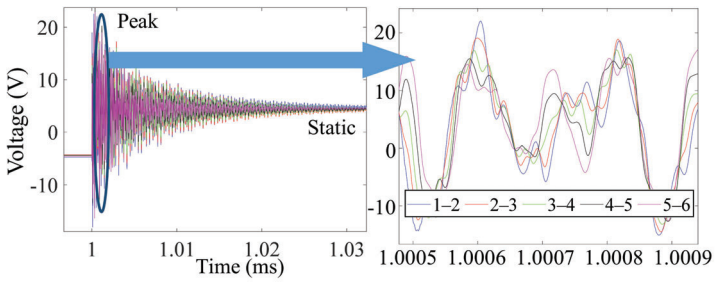

Figure 6. Overall (**left**) and partial zoom in (**right**) of the rising edge interturn voltage drop waveform on the rising edge of pulse voltage.

Since the model in Figure 5 is a very complex model with 120 turns and three layers, analyzing the mechanism of occurrence of overvoltage through this complete model would be very complicated. Yet, in this transformer prototype, interturn insulation distance (0.6 mm) is shorter than interlayer insulation distance (1 mm). So, interturn capacitance is larger than the interlayer capacitance and would play a more important role in affecting the transient interturn voltage. Therefore, to reduce the complexity of the overvoltage mechanism analysis, we simplify this model into a single-layer winding with (n + 1) turns, in which the interlayer capacitances are ignored. This simplified circuit model can be seen in Figure 7. R, L, and C values of each turn are regarded as the same, and the mutual inductance is ignored to reduce the complexity of the following calculation on the

output voltage. Then, we conduct Laplace transformation for the impedance in this circuit. Impedance $Z_{i+1,i+2}$ ($0 < I \leq n$) between adjacent points (point 1 and 2, 2 and 3, ... N + 1 and N + 2) can be expressed by (3).

$$Z_{12}(s) = R + Ls,\ Z_{i+1,\ i+2}\ (s) = \frac{R + Ls}{LCs^2 + RCs + 1} \tag{3}$$

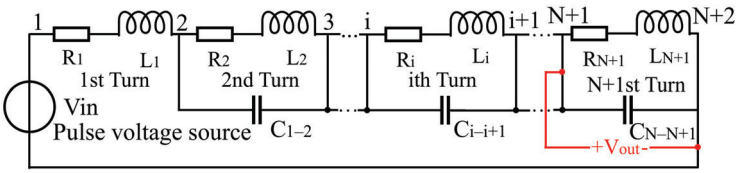

Figure 7. Simplified circuit model.

To find why pulse voltage can generate overvoltage between turns, the relationship between the input pulse voltage V_{in} and interturn output voltage should be expressed. We regard the voltage drop on the (n + 1)th turn as the output voltage V_{out}; then, the transfer function between V_{in} and V_{out} is obtained through (4). Through factorization, (4) can be simplified into (5). In this equation, n + 1 means the total number of turns.

$$\frac{V_{out}(s)}{V_{in}(s)} = \frac{Z_{n+1,n+2}(s)}{Z_{12}(s) + \sum_1^n Z_{i+1,i+2}(s)} = \frac{R + Ls}{L^2Cs^3 + (2RCL)s^2 + (R^2C + (n+1)L)s + (n+1)R} \tag{4}$$

$$\frac{V_{out}(s)}{V_{in}(s)} = \frac{R + Ls}{(R + Ls)(LCs^2 + CRs + n + 1)} = \frac{1}{LC}\left(\frac{1}{s^2 + \frac{R}{L}s + \frac{n+1}{LC}}\right) \tag{5}$$

Then, we can change the circuit model in Figure 7 into an open-loop system shown in Figure 8. Considering that the pulse voltage generated from the practical voltage source is not an ideal step voltage, rise time surely exists. So, the input voltage should be expressed with the combination of a step function and a first-order inertia link $1/(Ts + 1)$ in Function 1 according to the principle of automatic control [23], where T is the time constant, and the rise time equals 2.2 T. Function 2 is a typical two-order system. With these transfer functions in Figure 8, we would be able to analyze the mechanism of the overvoltage and factors that can influence it quantitatively based on the theory of automatic control. Considering the value ranges of R, L, and C obtained from the FEM calculation in Table 3, poles of Function 2 are certainly in the form of A ± jB (both A, B < 0). So, the waveform of interturn voltage drop is a pulse voltage with damping oscillation on its rising edge as seen in Figure 6, which is similar to that from previous research on the inverter-fed motors [4]. From function 2, natural frequency ω_n and damping ratio ξ can be expressed by (6).

$$\omega_n = \sqrt{\frac{n+1}{LC}},\ \xi = R\sqrt{\frac{C}{4L(n+1)}} \tag{6}$$

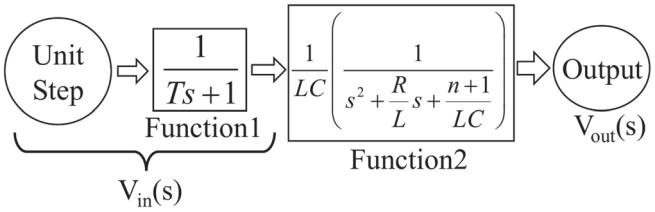

Figure 8. Transfer function of the simplified circuit model.

We can see that increasing the values of R and C can lead to a higher damping ratio, so the oscillation is supposed to be weaker, while increasing the value of L can reduce the damping ratio, giving rise to a stronger oscillation. To prove this deduction, we conducted the simulation with the simplified circuit in Figure 7 to see the changing of the overshoot with the changing of the abovementioned parameters. During the simulation, the value of n in (5) was set to 1 to reduce the simulation time; then, the model in Figure 7 changed into the simplest winding with only two turns. The simulation parameters and the obtained overshoot of the V_{out} are shown in Table 4. Set the transient peak voltage value as V_{peak} and static voltage value as V_{static}; then, overshoot σ is obtained through (7).

$$\sigma = \frac{V_{peak} - V_{static}}{V_{static}} \tag{7}$$

Table 4. Simulation on the simplified circuit model.

Group	L (nH)	R (Ω)	C (pF)	σ (%)
A	50	0.04	50	10.7
B	500	0.04	50	32.84
C	50	0.4	50	8.46
D	50	0.04	500	32.24

Values of the parameters in Group A are in accordance with the value ranges of stray parameters of turns of the transformer model from FEM calculation (listed in Table 3). The other three groups in Table 4 are applied for the comparison of the overshoot under different L, R, and C values. The rise time of the pulse voltage is set to be 20 ns and the peak voltage as 1 V. Comparing the results of group A with groups B and C, we can see that increasing the value of L can lead to a higher overshoot, while a larger R can reduce the overshoot, which is in accordance with the change in damping ratio. However, the comparison between group A and group D shows that larger capacitance gives rise to a larger overshoot even though the damping ratio of Function 2 is higher. This phenomenon is attributed to the decreasing of natural frequency ω_n with an increasing C shown in (6).

The natural frequency ω_n in Function 2 (expressed in (6)) corresponds to the resonant frequency of the circuit. As described in Section 3.2, the pulse voltage has a large content of high-frequency components, of which the highest frequency f_u is calculated approximately in (2). When a circuit is added with pulse voltage, these high frequency components can induce resonance on the output voltage, which is one of the important reasons why the overshoot exists. Considering the values of L and C and rise time t_r in this circumstance, ω_n is much larger (approximately 894 MHz) than f_u (approximately 15.9 MHz). So, if the C is kept constant, reducing the rise time can make the f_u higher and closer to ω_n. Consequently, stronger resonance is induced. Correspondingly, when keeping the rise time unchanged, a higher value of C reduces the ω_n and makes it closer to f_u. Both these two changes can make the overshoot of the output voltage higher. Keeping other parameters the same as that of Group A in Table 4, we repeat the simulation by increasing the capacitance C continuously, and the overshoot with the changing of C can be seen in Figure 9. The curve of the overshoot can be divided into two regions. In region 1, the decreasing of natural frequency ω_n with an increasing C plays the dominant role in the changing of the overshoot, leading to a stronger resonant oscillation. Meanwhile, the damping ratio ξ also keeps increasing, and its effect on suppressing the oscillation becomes stronger. So, when C reaches nearly 80,000 pF, the curve meets a saturation. In region 2, where C is higher than 80,000 pF, the increasing ξ due to increasing C plays the dominant role in changing the overshoot, leading to a weaker oscillation. In the practical situation of a transformer, the interturn capacitance can never be so large as to reach more than 80,000 pF. So, we can draw the conclusion that the interturn voltage overshoot is supposed to increase with the increase in interturn capacitance.

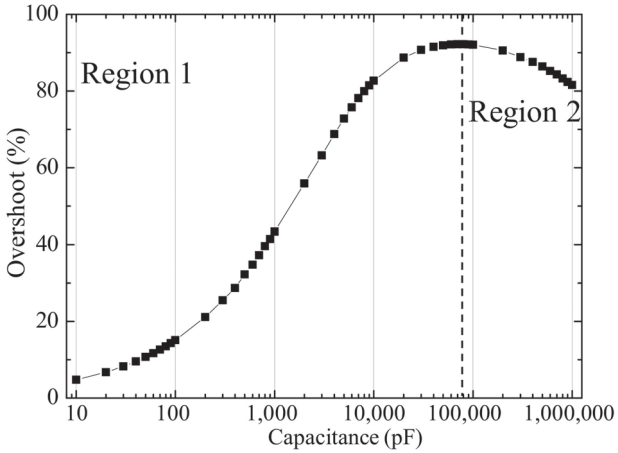

Figure 9. Overshoot with different capacitances.

For different values of C, the overshoot of the output voltage in Figure 7 ($n = 1$) under different rise times are shown in Figure 10 (R and L values are kept as the same as that in Group A of Table 4). We can see, with the decreasing rise time, overshoot increases at first and, then, converges to a stable value. The reason is that for a rise time short enough, the frequency of the high-order harmonics of the pulse voltage can cover the ω_n, which means the strongest resonance is already induced, and further reducing the rise time would not bring much difference. We take the value of the rise time as a critical value with which the overshoot ceases to increase obviously with further reduction in the rise time. We can see that a higher capacitance leads to a larger critical rise time. The reason is that a higher capacitance can reduce the resonant (natural) frequency ω_n expressed in (6). Then, f_u comes closer to ω_n if the rise time does not change, and strong resonance is more easily triggered. Correspondingly, if the rise time reduces (from 100 ns and follows the curve displayed in Figure 10), a relatively longer rise time can already make the frequency of high-order harmonics cover the ω_n to trigger the strongest resonance. This result confirms the explanation for the mechanism of how stray capacitance and rise time influence the overshoot on the voltage drop between different turns.

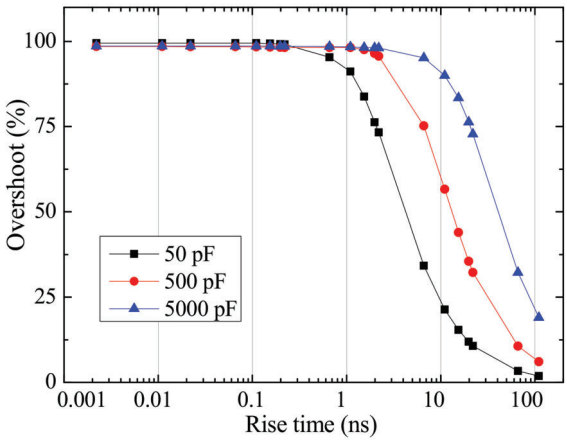

Figure 10. Overshoot under different rise times and capacitances.

The above analysis of the influence of stray capacitance and the pulse voltage rise time on the overvoltage is based on the most simplified one-layer two-turns model. Whether it is suitable for predicting the electrical stress in the complicated three-layer 120-turns model built for the selected practical transformer in Figure 5 needs verification. This will be discussed in the following section.

5. Parameters of the Simulation on the Complete Model

Among the aforementioned parameters in the last section, rise time can be variable in the practical working condition because of the variety of switching capability of semiconductor switches. For the transformer's design, by keeping the overall dimension and the core of the prototype unchanged, the selection of different insulation materials can bring change to the stray capacitance. Besides, previous research focused on static voltage analysis shows that changing the winding structure can be a method to relieve the electrical stress of the transformer [9]. The influence of this method on the transient electrical stress suffered by transformers working under pulse voltage with short rise time is worth study. Therefore, to confirm the correctness of the analysis on the mechanism of the overvoltage in Section 4 and investigate the impact from the aforementioned factors on the electrical stress, further simulations on the complete circuit model of the selected transformer prototype (seen in Figure 5) are necessary. This section would describe the parameters for the simulation in detail.

5.1. Rise Time

Power electronic switches are developing to be faster in switching in order to decrease the switching loss. In recent years, some SiC-based switches can even reach a switching time shorter than 100 ns, which would cause more serious electric stress on the insulation of the devices in medium-voltage and medium-frequency applications. To prove the effect of rise time on the electric stress suffered by the transformer's winding, four rise times from 100 ns to 1 μs are selected.

5.2. Insulation Relative Permittivity

Different insulation materials (include polyimide, polyester, Nomex paper, and DMD paper) are used for the insulation of the transformers according to their different working conditions [24]. Besides the difference in electrical strength of these materials, another variable property that can affect the insulation behavior among these materials is the relative permittivity. It is well known that relative permittivity ε_r is proportional to the value of capacitance. Therefore, for the transformer prototype in this case study, larger ε_r leads to larger interturn and interlayer capacitances. This can in turn increase the interturn overvoltage as analyzed in Section 4. To verify the quantitative effect of stray capacitance on the overvoltage and investigate the effect of different insulation materials on the MVMF transformer's electrical stress, simulations on the complete circuit model with different ε_r of insulation should be conducted. Among the materials usually used for transformer's insulation, ε_r of Nomex can be as low as 1.6, ε_r of DMD is usually lower than 3.0, while that of polyimide can be as high as 3.9 [24]. So, three different ε_r values, 3.9, 2.7, and 1.6, are selected to represent these aforementioned materials for the comparative simulation.

5.3. Winding Structure

C-type and Z-type winding structures can be seen in Figure 11 (numbers in the figure refer to the serial numbers of turns); these two structures are usually applied in the design of the transformer with multi-layer windings. According to the research in [9], comparing with the C-type winding, Z-type winding can reduce the largest interlayer voltage drop by 50%, although this winding type is slightly harder to construct. Suppose that in a two-layer winding, every layer of the winding has 2n turns; then, the interlayer voltage drop under different winding structures can be shown in Figure 12. Under C-type winding, the highest interlayer voltage drop is U, while under Z-type winding, the interlayer voltage drop is

constant as U/2. Yet, this conclusion is obtained from static voltage analysis, the influence of changing the winding structure on the transient electric stress brought from pulse-like voltage needs further investigation.

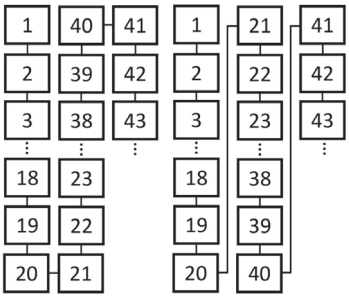

Figure 11. C-type (**left**) and Z-type (**right**) winding layout.

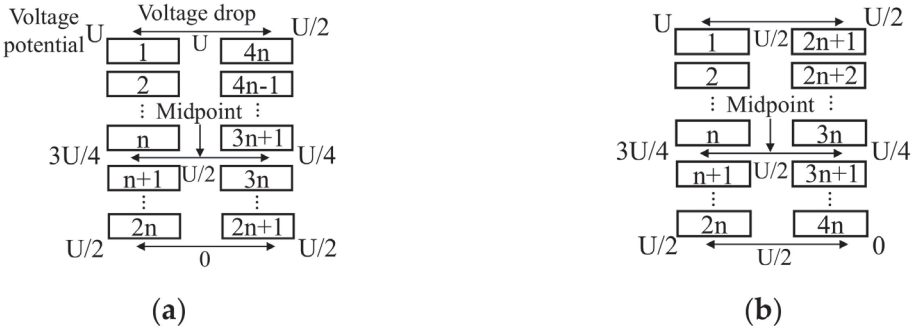

Figure 12. Interlayer voltage drop: (**a**) C-type winding; (**b**) Z-type winding.

According to the description above, the detailed parameters including rise time t_r, relative insulation permittivity ε_r, and winding structure of the electrical stress simulation on the transformer's equivalent circuit model are shown in Table 5.

Table 5. Detailed parameters of the simulation on the complete model.

Group	t_r (ns)	ε_r	Winding Structure
1	100	3.9	C-type
2	200	3.9	C-type
3	500	3.9	C-type
4	1000	3.9	C-type
5	100	2.7	C-type
6	200	2.7	C-type
7	500	2.7	C-type
8	100	1.6	C-type
9	200	1.6	C-type
10	500	1.6	C-type
11	200	3.9	Z-type

6. Results of Simulation on the Complete Model

6.1. Interturn Voltage

During the simulation, within the first layer of the HV winding, voltage waveforms between the 1st and 2nd turns, 2nd and 3rd turns, 3rd and 4th turns, 4th and 5th turns, and 5th and 6th turns are recorded. Accordingly, interturn voltage drops within the first six turns in the second layer (from 21st to 26th turn) and the third layer (from 41st to 46th turn) are also recorded. All these interturn voltage drops are expressed as $V_{n-(n+1)}$. Take Group 1 in Table 5 as an example, peak voltage values between different adjacent turns during the rising flank of the voltage are shown in Figure 13. It can be seen that the voltage drop in different adjacent turns does not decrease monotonously, this phenomenon is different from that of the voltage drop simulation on motor winding, of which the peak voltage drop V_{peak} between the first two turns is usually the largest [14]. The reason is that the structures of the core and winding of the transformer are different from that of the HV form-winding motor presented in [14]. Especially, for the three-layer winding of the transformer prototype in this case study, interlayer capacitance and mutual inductance exist. Therefore, the inductive and capacitive coupling between turns in this transformer is quite different from that of a motor and more complicated. These factors lead to a different voltage distribution. Yet, the peak values of different interturn voltage drops can still be much higher than the static voltage values, which can also be a threat to the transformer's insulation. To describe the overvoltage, the ratio between peak voltage drop value and the static voltage drop value $R_{ov} = V_{peak}/V_{static}$ is applied. The value of R_{ov} under different rise times and relative permittivity are shown in Figures 14 and 15, respectively. From the results, we can see clearly that overvoltage would increase with the decreasing rise time. While with the lower relative permittivity (leads to lower interturn capacitance), the overvoltage would be lower. These results are in accordance with that of the simulation on the simplified model proposed in Section 4. Detailed similarities between simulation results in this section and Section 4 are listed in Table 6. These results are also similar with the experiments reported in [25], which show that voltage drop across each turn increases when the square wave voltage has a shorter rise time, and the voltage value does not decrease monotonously from the first turn to the last turn. So, the correctness of the overvoltage mechanism analysis in Section 4 and the proposed circuit model in Figure 5 are validated.

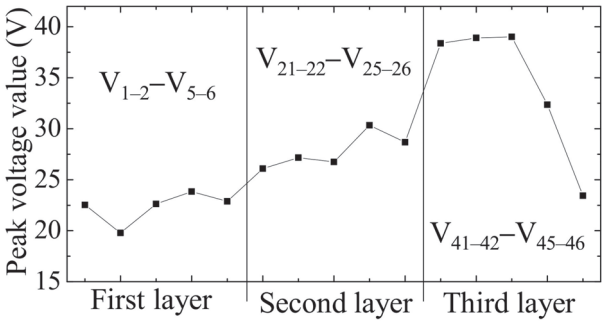

Figure 13. Overvoltage ratio between adjacent turns in different layers.

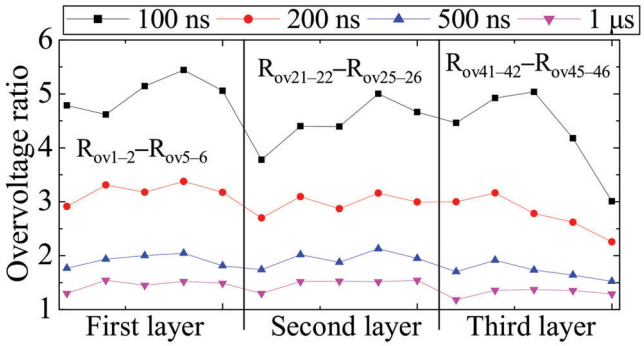

Figure 14. Interturn overvoltage ratio between adjacent turns under different rise times (εr = 3.9, C-type).

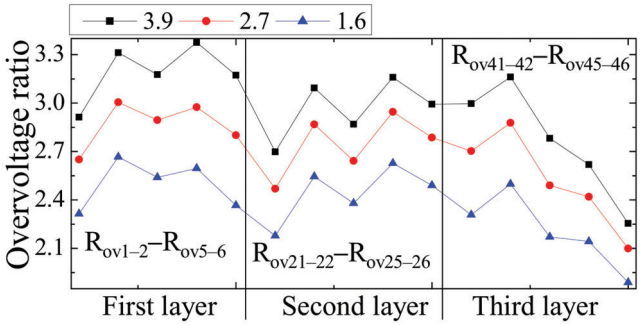

Figure 15. Interturn overvoltage ratio between adjacent turns under different relative permittivity (tr = 200 ns, C-type).

Table 6. Similarities between simulation results in simplified model and complete model.

Simulation Results	Simplified Model	Complete Model
Overshoot on voltage rising edge exists?	Yes	Yes
Peak voltage value with shorter rise time	Higher	Higher
Peak voltage value with larger stray capacitance	Higher	Higher

To investigate the comprehensive effect of relative permittivity and rise time, the interturn overvoltage ratio of the first layer (from 1st to 6th turns) under different rise times and relative permittivity is plotted in Figure 16. The results show that, under shorter rise time, the reduction in ε_r can cause greater decreasing of R_{ov}. Take the interturn voltage between the 1st and 2nd turns as an example, when ε_r changes from 3.9 to 1.6, the R drops by 27.08%, while for the same situation under 500 ns rise time, R_{ov} drops by only 16.07%. Interturn overvoltage ratio under different winding types is shown in Figure 17. Changing the winding structure from C-type to Z-type cannot only reduce the maximum static interlayer voltage drop as seen in Figure 12 but can also reduce the transient interturn overvoltage.

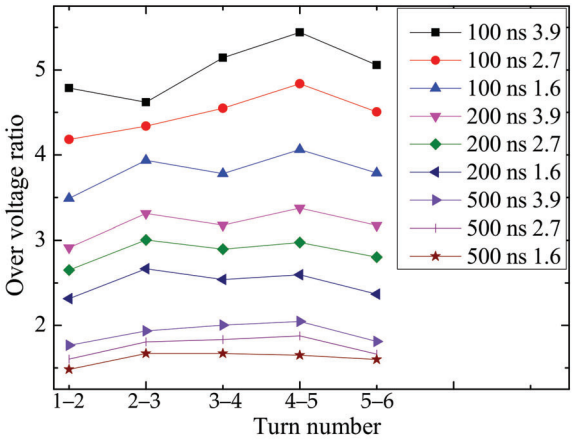

Figure 16. Interturn overvoltage ratio under different rise times and relative permittivity.

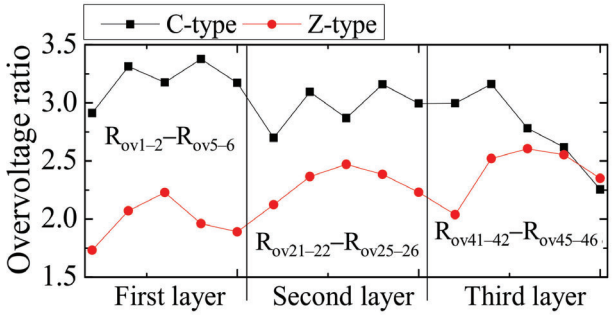

Figure 17. Interturn overvoltage ratio under different winding structures (tr = 200 ns, εr = 3.9).

6.2. Interlayer Voltage

As mentioned in the introduction, for transformers with multilayer windings, interlayer insulation may also suffer from the electrical stress brought from the fast wave front of power electronic switches, so the simulation on interlayer voltage is also needed. For the measurement of interlayer voltage drop, six test points are applied and seen in Figure 18. V1–V3 are used for detection of the voltage drop between layer 1 and layer 2, V3–V6 are used for that between layer 2 and layer 3. Typical waveforms of the interlayer voltage drops (Group 1 in Table 5) are seen in Figure 19. Unlike the adjacent interturn voltage, of which the static values are almost the same (seen in Figure 6 with time range >1.03 ms), the static voltage drop in different interlayer voltage test points is of a great difference; this is normal for transformer with a multi-layer C-type winding [9]. So, although overvoltage ratio of V2 in Figure 19 maybe higher than that of V1, the transient peak voltage of V1 is still obviously higher than that of V2. Under this circumstance, the overvoltage ratio R_{ov} is not suitable for the comparison of overvoltage in difference test points under different parameters. So, we use the peak voltage value instead, since it displays transient maximum potential difference between adjacent layers, which reflects the interlayer electrical stress. The peak interlayer voltage values under different rise times and relative permittivity are shown in Figures 20 and 21, respectively. The numbers 1–3 and 4–6 refer to the voltage test points V1–V3 (between 1st layer and 2nd layer) and V4–V6 (between 2nd layer and 3rd layer), respectively. Similar to the results from interturn voltage simulation, the interlayer peak voltage is higher under a shorter rise time. When the rise time is 100 ns, the highest peak value in test point V6 can reach more than 450 V, exceeding its static voltage drop by more

than 190 V. In a practical situation, the insulation condition of the transformer is usually not as good as what we assumed in Section 2; small air ducts may be left unintentionally in the insulation between adjacent turns and layers. If that happens, the ionization strength of the air duct may be exceeded. Then, partial discharge (mainly in the form of corona discharge) may be triggered with high probability. Decreasing the relative permittivity can also slightly reduce the peak interlayer voltage.

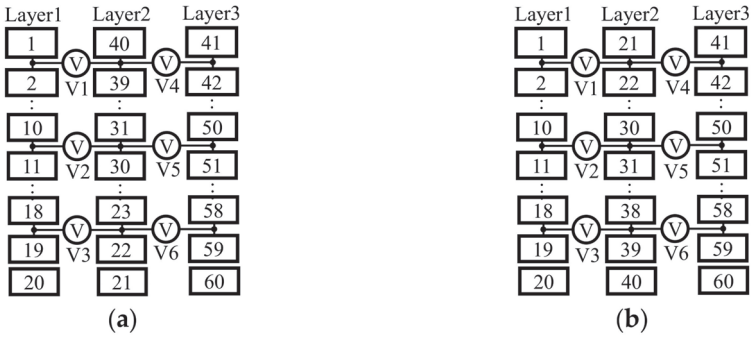

Figure 18. Testing points of the interlayer voltage drop in different winding structures: (**a**) C-type; (**b**) Z-type.

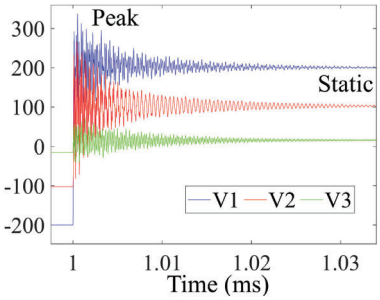

Figure 19. Typical waveform of layer1-to-layer2 voltage drop (C-type).

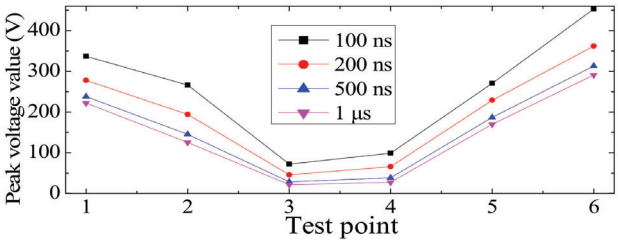

Figure 20. Peak interlayer voltage under different rise times (εr = 3.9, C-type).

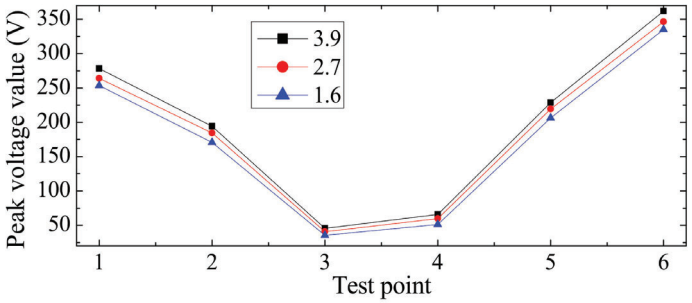

Figure 21. Peak interlayer voltage under different relative permittivity (tr = 200 ns, C-type).

The results of comparative interlayer voltage simulation under different winding structures are shown in Figure 22. In most of the test points, the peak voltage drops in Z-type winding are very different from C-type winding. The reason can be found in Figure 18. For C-type winding, taking the region between Layer 1 and Layer 2 as an example, we can see that in the top area where lies V1, the interlayer voltage drop equals the voltage difference between the 1st turn and the 40th turn. In the downward area, such as the positions of V2 or V3, the turns between the two sides are relatively much closer with respect to electrical connect (V2 between 10th and 31st turns, V3 between 18th and 23rd turns). This is the main reason why the voltage drop value in V1 is much higher than that of V2 and V3. A similar situation can be found in the region between Layer 2 and Layer 3. While in Z-type winding, for different areas in the region between adjacent layers, the distances with respect to electrical connection between turns on the two sides are the same (V1 between 1st and 21st turns, V2 between 10th and 30th turns, V3 between 18th and 38th turns). So, the interlayer voltage values in Z-type winding changes only slightly among different test points. Because of this even distribution of interlayer voltage, the largest peak interlayer voltage value of Z-type winding is only half of C-type winding.

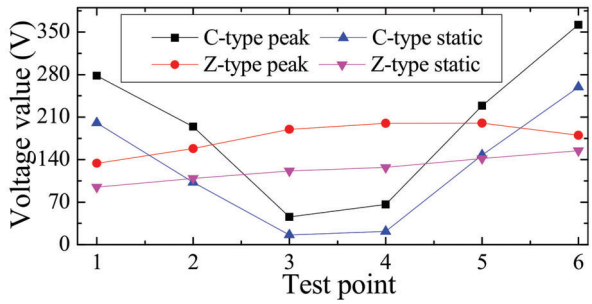

Figure 22. Peak and static interlayer voltage under different winding structures (tr = 200 ns, εr = 3.9).

To display the difference between transient interlayer voltage simulation and static interlayer voltage analysis presented in the previous study [9], we added values of static voltage drop under different winding structures in Figure 22. Although the overall trending of static voltage value vs. time is similar to that of peak voltage value, an obvious difference can be found in test points V2 and V5, which are midpoints between adjacent layers similar to the midpoints displayed in Figure 12. In these two points, static voltage drops under different winding structures are almost the same. However, the results of peak voltage values show that with the existence of voltage overshoot caused by pulse voltage, peak voltage values in V2 and V5 under Z-type winding are lower than that of C-type winding.

It is clear that for transformers working in MVMF applications, using Z-type winding can also effectively relieve its electrical stress. So, in the design of the MVMF transformer, it is suggested to apply this kind of winding structure.

7. Conclusions

Working under PWM voltage with very short rise time, an MVMF transformer may be faced with the problem of overvoltage in the winding, which can be a threat to the transformer's insulation reliability. Therefore, it is necessary to investigate the detailed situation of the electrical stress in the winding of MVMF transformer. This would be beneficial to the study of the MVMF transformer's insulation aging and failure mechanism and finding suitable strategies to reduce the electrical stress. Focusing on the study of electrical stress, the work done by this paper and the conclusions can be summarized as follows:

1. Based on the FEM calculation, an equivalent circuit model of a 1.5 kV, 1 kHz transformer's HV winding is built. Simulations and mechanism analysis verify the correctness of this model and its ability to obtain the transient electrical stress in the winding of MVMF transformer quantitatively.
2. Transient interturn/layer voltage simulation on the model shows the characteristics of transient voltage overshoot in the winding fed by pulse voltage that cannot be observed by steady-state voltage/electric field analysis. The results also indicate that pulse voltage with shorter rise time can induce higher interturn and interlayer overvoltage. Based on that, guidelines about choosing appropriate voltage waveform for aging and endurance lifetime studies on the MVMF transformer insulation can be given. This would help researchers build a life-time model of the insulation with more accuracy.
3. Electrical stress of the MVMF transformer's winding with different design parameters (in this paper, mainly different insulation materials and winding structures) can be obtained through this model. Simulation results show that using insulation material with lower relative permittivity and changing the winding structure from C-type to Z-type can reduce the interturn and interlayer overvoltage. Based on that, we propose limiting the voltage overshoot and, thereafter, enhancing the MVMF transformer's insulation capability in its design phase, which throws light on the MVMF transformer's insulation design.

Author Contributions: Conceptualization, Z.C. and W.Q.; methodology, Z.C.; software, C.L.B.; validation, W.Q., W.H. and S.Z.; formal analysis, Z.C.; investigation, Z.C.; resources, C.L.B.; data curation, W.Q.; writing—original draft preparation, Z.C.; writing—review and editing, W.Q., C.L.B., W.H. and S.Z.; visualization, Z.C.; supervision, W.Q., C.L.B., W.H. and S.Z.; project administration, C.L.B.; funding acquisition, C.L.B. and W.H. All authors have read and agreed to the published version of the manuscript.

Funding: This research received no external funding.

Informed Consent Statement: This study did not involve humans.

Data Availability Statement: Data supporting reported results in this paper can be obtained through contacting the 1st and corresponding authors.

Conflicts of Interest: We declare that this research has no conflict of interest.

References

1. Heinemann, L. An actively cooled high power high frequency transformer with high insulation capability. In Proceedings of the 2002 7th Annual IEEE Applied Power Electronics Conference and Exposition, Dallas, TX, USA, 10–14 March 2002; pp. 352–357. [CrossRef]
2. Mogorovic, M. Modeling and Design Optimization of Medium Frequency Transformers for Medium-Voltage High-Power Converters. Ph.D. Thesis, Swiss Federal Institute of Technology in Lausanne, Lausanne, Switzerland, 2019. [CrossRef]

3. Liu, T.; Li, Q.M.; Huang, X.W.; Lu, Y.F.; Asif, M.; Wang, Z.D. Partial discharge behavior and ground insulation life expectancy under different voltage frequencies. *IEEE Trans. Dielectr. Electr. Insul.* **2018**, *25*, 603–613. [CrossRef]
4. Wan, J.; Lin, Z.; Yu, H. Research of PWM Pulse Voltage Distribution in Motor Winding. In Proceedings of the 2001 5th International Conference on Electrical Machines and Systems, Shenyang, China, 18–20 August 2001; pp. 43–46. [CrossRef]
5. Melfi, M.; Sung, A.M.J.; Bell, S.; Skibinski, G.L. Effect of surge voltage risetime on the insulation of low-voltage machines fed by PWM converters. *IEEE Trans. Ind. Appl.* **1998**, *34*, 766–775. [CrossRef]
6. Kaufhold, M.; Borner, G.; Eberhardt, M.; Speck, J. Failure mechanism of the interturn insulation of low voltage electric machines fed by pulse controlled inverters. *IEEE Elect. Insul. Mag.* **1996**, *12*, 9–16. [CrossRef]
7. Fabiani, D.; Montanari, G.C.; Contin, A. Aging Acceleration of Insulating Materials for Electrical Machine Windings Supplied by PWM in the Presence and in the Absence of Partial Discharges. In Proceedings of the 2001 7th IEEE International Conference on Solid Dielectrics, Eindhoven, The Netherlands, 25–29 June 2001; pp. 283–286. [CrossRef]
8. Huang, P.; Mao, C.; Wang, D. Electric Field Simulations and Analysis for High Voltage High Power Medium Frequency Transformer. *Energies* **2017**, *10*, 371. [CrossRef]
9. Zheng, Z.H.; Lu, B.; Tao, J.; Li, L.G.; Chu, P.; Wen, Q.Y. Study on Insulation Design of High Power High Frequency High Voltage Transformer. In Proceedings of the 2018 2nd IEEE Conference on Energy Internet and Energy System Integration, Beijing, China, 20–22 October 2018. [CrossRef]
10. Lu, F.C.; Li, D.R.; Guo, Y.X.; Fu, C.; Wang, H. Optimal design of compact main insulation structure of PETT. In Proceedings of the 2015 18th International Conference on Electrical Machines and Systems, Pattaya, Thailand, 25–28 October 2015; pp. 303–306. [CrossRef]
11. Chen, Q.; Raju, R.; Dong, D.; Agamy, M. High Frequency Transformer Insulation in Medium Voltage SiC enabled Air-cooled Solid-State Transformers. In Proceedings of the 2018 IEEE Energy Conversion Congress and Exposition, Portland, OR, USA, 23–27 September 2018; pp. 1–10. [CrossRef]
12. Guillod, T.; Krismer, F.; Kolar, J.W. Electrical shielding of MV/MF transformers subjected to high dv/dt PWM voltages. In Proceedings of the 2017 Applied Power Electronics Conference and Exposition, Tampa, FL, USA, 26–30 March 2017; pp. 2502–2510. [CrossRef]
13. Wan, J.R.; Liu, H.C.; Yu, H.J. Voltage distribution in stator windings of the motor driven by PWM inverter. In Proceedings of the IEEE International Conference on Power System Technology, Kunming, China, 13–17 October 2002; pp. 727–731. [CrossRef]
14. Wen, F.X.; Zhang, L.L.; Wu, G.N.; He, E.G. Modeling and Simulation of Inter-Turn Voltage Distribution in the Stator Windings of the Pulling Motor. In Proceedings of the 2004 IEEE International Conference on Solid Dielectrics, Toulouse, France, 5–9 July 2004; pp. 900–903. [CrossRef]
15. Krings, A.; Paulsson, G.; Sahlen, F.; Holmgren, B. Experimental investigation of the voltage distribution in form wound windings of large AC machines due to fast transients. In Proceedings of the 2016 International Conference on Electrical Machines, Lausanne, Switzerland, 4–7 September 2016; pp. 1700–1706. [CrossRef]
16. Moghadam, D.E.; Speck, J.; Grossmann, S.; Stahl, J. Voltage Distribution in the Stator Windings of High Voltage Motors Fed by PWM Drives Part I: Effects of the Pulse Characteristics. In Proceedings of the 2018 2nd IEEE International Conference on Dielectrics, Budapest, Hungary, 1–5 July 2018. [CrossRef]
17. Fergested, P.I.; Henriksen, T. Transient Oscillations in Multiwinding Transformers. *IEEE Trans. Power Appar. Syst.* **1974**, *93*, 500–508. [CrossRef]
18. Stein, G.M. A study of the Initial Surge Distribution in Concentric Transformer Windings. *IEEE Trans. Power Appar. Syst.* **1974**, *83*, 877–893. [CrossRef]
19. Huang, P.; Mao, C.X.; Wang, D.; Wang, L.B.; Duan, Y.P.; Qiu, J.; Xu, G. Optimal Design and Implementation of High-Voltage High-Power Silicon Steel Core Medium-Frequency Transformer. *IEEE Trans. Ind. Electr.* **2017**, *64*, 4391–4401. [CrossRef]
20. Guillod, G.; Jonans, E.H.; Gabriel, O.; Ankan, D.; Christian, M.F.; Johann, W.K. Characterization of the Voltage and Electric Field Stresses in Multi-Cell Solid-State Transformers. In Proceedings of the 2014 IEEE Energy Conversion Congress and Exposition, Pittsburgh, PA, USA, 14–18 September 2014. [CrossRef]
21. Brigham, E. *Fast Fourier Transform and Its Applications*; Pearson Education: Cranbury, NJ, USA, 1988.
22. Skibinski, G.; Kerkman, R.; Leggate, D.; Pankau, J.; Schlegel, D. Reflected wave modeling techniques for PWM AC motor drives. In Proceedings of the 1998 13th Annual Applied Power Electronics Conference and Exposition, Anaheim, CA, USA, 15–19 February 1998; pp. 1021–1029. [CrossRef]
23. Richard, C.D.; Robert, H.B. *Modern Control Systems*, 12th ed.; Pearson Education: Cranbury, NJ, USA, 2011.
24. Zhao, Y.K.; Zhang, G.Q.; Guo, R.R.; Yang, F.Y. The breakdown characteristics of thermostable insulation materials under high-frequency square waveform. *IEEE Trans. Dielectr. Electr. Insul.* **2019**, *26*, 1073–1080. [CrossRef]
25. Sumangala, B.V.; Nagabhushana, G.R. Analysis of Surge Voltage Distribution in a Model Transformer for Different Types of Surges with Turn Resolution and its Validation. In Proceedings of the TENCON 2006—2006 IEEE Region 10 Conference, Hong Kong, China, 14–17 November 2006. [CrossRef]

J2:

Influence of pressure on the PD and induced aging behavior of polyimide insulation under repetitive pulse voltage

Changjiang. Zheng, Qian Wang, Zhan Shen, Claus Leth Bak, Filipe Faria da Silva and Huai Wang

***Abstract*—Reduction of air pressure can influence insulation material's behavior with respect to resisting partial discharge (PD) generation and its induced aging process. This may bring threat to the insulation reliability of medium frequency transformers working under low pressure condition, considering they are exposed to high probability of PD inception caused by PWM voltage. Aiming at investigating the performance of insulation of medium frequency transformer being operated in an environment with a decreasing pressure, this paper introduces a test system that can conduct partial discharge and endurance lifetime tests under repetitive pulse voltage and controlled pressure. Using this test system and focusing on polyimide film, which is one of the main insulation materials used by medium frequency transformers, partial discharge and endurance lifetime tests are conducted under different pressures. The results show that partial discharge inception voltage decreases with decreasing pressure. However, the changing of partial discharge magnitude, time lag and its induced insulation lifetime do not change monotonously. Surface of the failed insulation samples show that the erosion area caused by partial discharge is larger under lower pressure. The mechanisms behind the changing of partial discharge time lag, discharge magnitude, endurance lifetime, along with the discharge eroded area with pressure are discussed in detail.**

***Index Terms*— Medium frequency transformer, partial discharge (PD), Low pressure, polyimide, Insulation aging**

I. INTRODUCTION

In many modern power electronic systems, transformers are necessary for voltage scaling up/down and electrical isolation. These transformers are usually called medium frequency transformer for they usually work with PWM voltage with frequency higher than 50/60 Hz power frequency [1]. With this higher working frequency, the core of the transformer can reach smaller size, which gives rise to lower manufacturing costs. Also, combined with power electronic switches, medium frequency transformers have higher controllability. Because of these advantages, medium frequency transformers are widely used in modern power electronic applications, such as railway traction, DC grids, etc.

Working under PWM voltage with short rise time, overvoltage can be induced in the winding of the electrical devices such as motors and transformers and the probability of partial discharge (PD) inception would be higher. Continuous PD can degrade the insulation material quickly and lead to premature breakdown [2].

Studies on the insulation failure mechanism under continuous PDs show that environment factors can affect the PD behavior and its aging speed on the insulation [3]. Among these factors, pressure is very important. According to the Paschen Curve in Fig. 1, if the distance of the air gap remains the same, before reaching the critical point (minimum breakdown strength), breakdown strength of gaseous dielectrics will be reduced with the reduction of pressure [4]. Paschen curve is obtained under uniform electric field. Yet, whether the field is uniform or not, the influence of reducing air density on the air's dielectric strength is still the same. Therefore, similar phenomenon can be expected also under non-uniform filed. For solid insulation with air ducts as defects, the change of breakdown strength of air can directly affect its insulation reliability to resist PD inception. In addition, the reducing of gas density can also affect the mean free path of charge (or electron), which can in turn affect the discharge intensity.

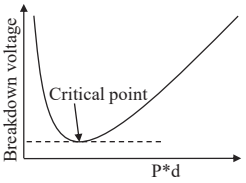

Fig. 1. Paschen Curve

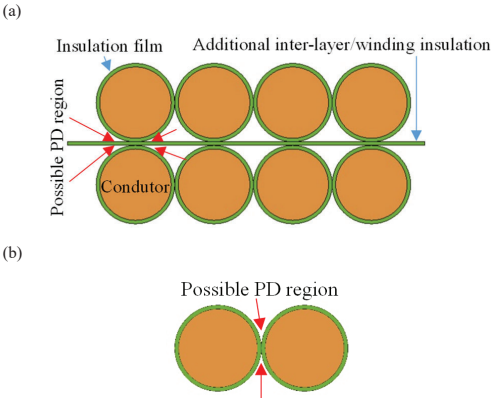

Fig. 2. Possible PD region in the winding of the transformer: (a) With

additional inter layer/winding insulation. (b) Without additional inter layer insulation.

For medium frequency transformers, the effect of pressure is a practical problem. Some medium frequency transformers are working in high-altitude area and recently aircrafts are relying more on power electronic systems in which transformers are usually applied [5]. Besides, unlike the conventional transformer that usually use oil-paper insulation, medium frequency transformers usually use dry-type insulation. Thus, air ducts may exist between adjacent winding layers or adjacent windings where lies a high voltage drop and are more likely to be the source of PD. One of the examples can be seen in Fig. 2(a), the conductors of the upper side and down side may belong to adjacent layers of a winding or belong to different windings. Strong electric field due to high voltage drop and dielectric refraction would concentrate on the places where the red arrows point at, leading to a PD that can erode the surface of the insulation film. For the sake of a compact design, some of the medium frequency transformer may not apply an additional inter-layer insulation. If the gap between the conductors of adjacent winding layers is not enough like in Fig. 2(b), PD is more likely to be triggered and cause greater threat to the insulation film that directly covers the conductor. If the pressure goes lower in these abovementioned air ducts, the probability of PD inception may be even greater.

Previous studies focusing on pressure's effects on PD behavior and its induced aging process provide some information and reference for the future insulation studies in the field of medium frequency transformer. In [3], the author finds lower pressure give rise to lower PDIV and shorter lifetime with presence of PD. Under high pressure, before the breakdown, PD energy shows larger variety along with the aging than that under low pressure. In [6], PDIV tests are conducted on the voids in epoxy. The author finds that with the size of void fixed, for the P*d around the critical point of Paschen curve (alike depicted in Fig. 1), the test result is usually higher than the calculated one. This may be due to the reason that under these low pressures, when the voltage magnitude reaches the calculated PDIV, the PD intensity is too weak (well below the noise) to be detected by the traditional current sensor [7]. Higher voltage magnitude is needed to generate PDs strong enough to be detected, which leads to an unprecise result. Authors in [7] also analyze the PD light waveform and find that when the pressure goes below 260 Pa, the rise time of the PD waveform increases obviously. They propose the speculation that PD type changes from streamer discharge into Townsend discharge when pressure goes extremely low. In [8], the authors conduct PD experiments on gas dielectrics including air, He and Ar. Under non-uniform electric field provided by different electrode types, the shapes of PDIV-pressure curves under different gas dielectrics all agree well with the Paschen Curve. Larger PD glow can be observed under lower pressure, which indicate that PD volume expands with the decreasing of pressure. Literature [9] measures the space charge density during the corona discharge under different pressures. Results show that, more space charge would be produced under lower pressure. Since stronger discharge causes stronger ionization and creates more space charge, the author believes that low pressure can give rise to stronger PD intensity. Literature [10] observes the number of the PDs under extremely low pressure condition. With pressure drops from 100 Pa to 3 Pa, the number of PDs during the same time interval decreases. Literature [11] proposes comparative simulations of PD features under one atmosphere pressure (1 atm) and a half atmosphere pressure (0.5 atm). With 0.5 atm, although the individual PD intensity is weaker than that under 1 atm, the occurrence rate of PD is doubled. This makes the total amount of charge per cycle under 0.5 atm obviously larger than that under 1 atm. Literature [12] conducts PD aging tests on the PCB board under different pressures. It finds that growth rate of silicon coating surface crack due to PD erosion is obviously faster under lower pressures.

Since changing of PD features with pressure can affect the accuracy of PD monitoring and the long term reliability of different kinds of insulation, these above-mentioned studies remind the field of medium frequency transformers of the necessity to pay attention to the influence of the pressure. However, studies in [3, 6-12] are conducted using traditional power frequency sinusoidal voltage or DC voltage, of which the frequency and voltage rise time is very different from that of PWM voltage. With different voltage parameters, the influence of pressure on the PD feature (including the magnitude and phase distribution) may also be different [13]. Comparative studies between PWM voltage and sinusoidal voltage are conducted in [14]. Under sinusoidal voltage, with pressure decreasing, the main energy distribution of PD signal would shift to lower frequency range. While under PWM voltage, PD energy distribution in frequency domain shows no obvious change with decreasing pressure. Therefore, conclusions from the studies using AC sinusoidal voltage or DC voltage cannot be used directly for studies on the insulation working under PWM-like pulse voltage.

There are a few research regarding effects of pressure on PD behaviors induced by pulse voltage. Literature [15] proposes PD inception tests under different pressures using pulse voltage and find that with lower pressure, repetitive PDs can be generated with lower voltage magnitude. In [16], a FEM model is proposed to simulate the PD characteristics under pulse voltage and different pressures. According to the simulation results, with the decreasing of the pressure, longer time has to be waited for the PD inception, while PD duration time and PD true charge are both higher under lower pressures. The study object is the cavity in the silicone gel used for the IGBT/MOSFET module's package. Although its geometric and dielectric properties are quite different from the insulation of transformers, the study indicates a stronger PD erosion when pressure is lower, which should not be ignored for the insulation design of other electrical devices. In [17], PD studies on the trench of PCB board under different pressures are conducted under unipolar pulse voltage. Both PD magnitude and number of PDs per minute become larger when pressure decreases. This trending keeps the same whether the pulse voltage is positive or negative. These literatures remind the possibility of greater PD

threat under lower pressure for other electrical devices like medium frequency transformer working under PWM-like voltage and necessity of more studies. For the first step, systematic investigation on pressure's effect on the insulation material that is usually applied in medium frequency transformers is needed.

This paper builds a test system with abilities to generate repetitive pulse voltage, conduct PD detection and create low pressure condition. Based on this system, under different pressures, PD and endurance lifetime tests on the polyimide film, which is usually used for the insulation of medium frequency transformer [18], are conducted. Change trending of the PD inception, PD features and endurance lifetime with pressure drops from 1 Bar to 0.3 Bar are shown and the mechanism for the results are discussed in detail. These above results reveal that polyimide film suffers from greater risk of PD inception and deterioration when pressure decreases within the above mentioned range, which indicates the necessity of similar studies on the whole medium frequency transformer prototype or transformer related insulation structures.

II. EXPERIMENT SETUP

To investigate the influence of pressure on the medium frequency transformer's insulation reliability, PD and endurance lifetime tests on the insulation sample under different pressures should be conducted. To realize these experiments, a test system is needed. This system should be able to generate repetitive pulse voltage and create low pressure circumstances (since this study focuses on the PD and its aging process on insulation working under high-altitude area or aircrafts, the pressure higher than sea level pressure is not considered) and detect PD with high accuracy. This section introduces the test system and experiment parameters in detail.

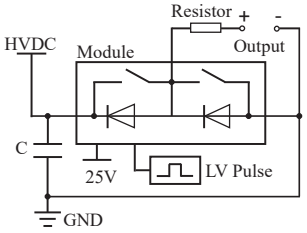

Fig. 3. Pulse voltage generator based on a half bridge power electronic power module

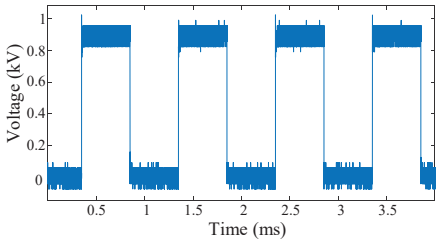

Fig. 4. Repetitive pulse volage waveform with 1 kV peak value and 1 kHz frequency

A. PULSE VOLTAGE GENERATOR

To conduct PD and aging studies, a voltage generator is needed to generate a pulse voltage that can simulate the medium frequency and short rise time of the PWM voltage. In this paper, a pulse voltage generator is built based on a half-bridge power electronic module. Seen in Fig. 3, a HVDC source is applied as high voltage input, while a capacitor is used for DC voltage stabilization. The resistor is used for regulating the pulse voltage rise time and restricting the output current to prevent the module from overheating. The half bridge module is powered by a 25 V DC source and triggered by a 5 V pulse generator. This generator can produce repetitive unipolar pulse voltage. A typical output waveform of this pulse voltage generator can be seen in Fig. 4.

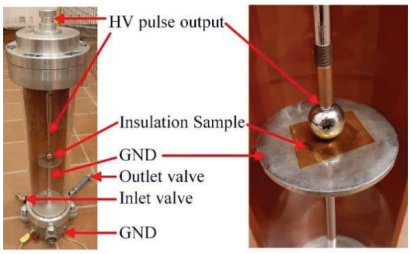

Fig. 5. Pressure tank and the electrodes inside

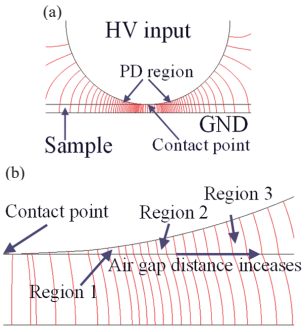

Fig. 6. Electric field distribution of the sphere-plate electrode: (a) Overall electric field distribution; (b) Zoom in of the air duct close to the contact point

B. PRESSURE CONTROLLING

A pressure tank seen in Fig. 5 is used to control the pressure for the experiments. By pumping out gas through the outlet valve, it can change the pressure inside from 1 Bar (corresponding to 100 kPa) to 0.3 Bar (corresponding to 30 kPa). A sphere-plate electrode is placed inside for fixing the insulation film. The sphere electrode with 20 mm diameter is added with HV output while the plate electrode with 75 mm diameter is connected to ground. When voltage is added on the insulation sample, the electric field distribution can be briefly expressed by Fig. 6. The density of lines represents the electric field intensity. It can be seen that the electric field distribution is not uniform and the air duct close to the contact point suffers from strongest electric field, where PD may be induced. This PD can break through the air duct and touch the insulation surface. As it can be seen in Fig. 6(b), dielectric refraction

would happen in the interface between the air and the insulation film, which changes the direction of the lines and enhance the electric field intensity in the air duct a little bit. As described in the Introduction and Fig. 2, for medium frequency transformers, PDs are likely to happen in the air duct between turns belonging to adjacent winding layers or different windings. These PDs can break through the air duct and cause erosion on the surface of insulation film. Therefore, this sphere-plate electrode is suitable for analyzing the PD behavior and its induced aging process on the insulation film used by the medium frequency transformer with the assumption that the electrical overstress already exists.

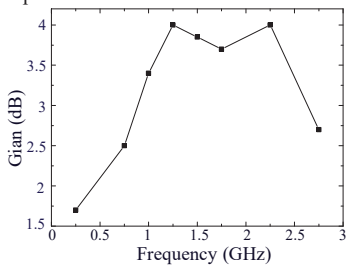

Fig. 7. Gain of the UHF antenna

C. PD DETECTION

According to studies on PD detection, under pulse voltage with short rise time (from tens of ns to several μs), strong interference would be caused by the on-off of the power electronic switches. This would make traditional detection method such as current sensor or high frequency current transducer (HFCT) unreliable to figure out the PD signal. Yet difference exists in the energy distribution in frequency domain among PD and interference signals. For the interference, most of its energy lies below 400 MHz. While for PD, its energy can spread up to more than 1.5 GHz [19]. Therefore, an Ultra-High-Frequency (UHF) antenna is the best choice for PD detection under PWM voltages. The gain of the UHF antenna used in this study is shown in Fig. 7. In frequency range from 500 MHz to 1.5 GHz, its gain is more than 2 dB. To further reduce the interference, a 400 MHz – 3 GHz band-pass filter is connected to the antenna's output interface. The waveform detected by this antenna with filter is shown in Fig. 8. The magnitude of the interference has been attenuated to around 1 mV while the PD signal can be detected effectively. Since the antenna detects the electromagnetic wave signal radiated by PD, to avoid too much attenuation when it travels through the air, the antenna is placed with distance of around 8 cm from the pressure tank (seen in Fig. 9).

With these above-mentioned devices together with control and data processing unit, the test system is constructed, as shown in Fig. 10. The computer is used for controlling the HV pulse voltage generator's output voltage magnitude and frequency, and for overcurrent protection (combined with current sensor)

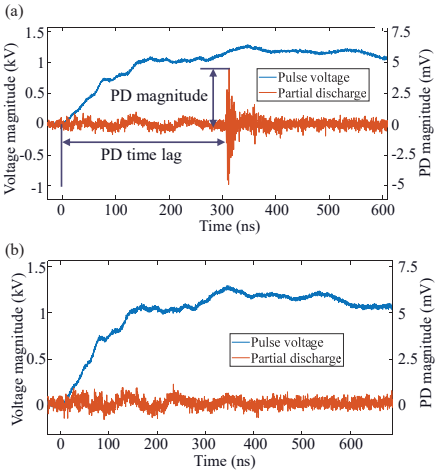

Fig. 8. Waveform detected by antenna with filter: (a) PD happens; (b) No PD happens.

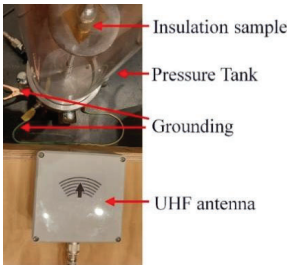

Fig. 9. UHF antenna

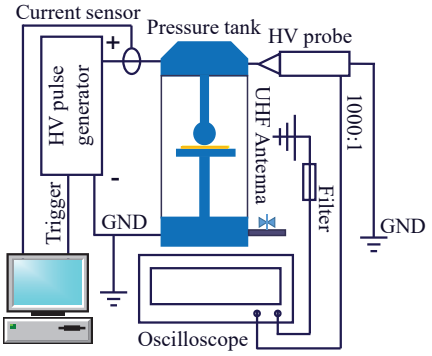

Fig. 10. Test system

D. INSULATION SPECIMEN

The insulation specimen used for the tests is the Kapton polyimide film. This insulation material is often used in the medium voltage electric devices such as motors and transformers. The thickness of the film is 0.05 mm and all the specimens for the tests are cut into square shape with 3 cm side length. Before the experiments, all specimens are cleaned by

alcohol and dried in the oven for 24 hours.

E. EXPERIMENT PARAMETERS

Although overcurrent protection is available for the test system, to avoid a too high impulse current due to expected breakdown in endurance test or unexpected breakdown in other tests, the resistance of resistor in Fig. 3 is set as 1kΩ. Since the resistor is connected in serial with the insulation sample, the time constant τ of output pulse voltage would mainly be decided by the resistance and the insulation sample's capacitance, expressed as τ=RC. Because of this, the rise time of the pulse voltage is 250 ns and would be kept unchanged. Before the PD and endurance tests, PDIV test under sea level pressure is conducted in advance and the average value of the PDIV is 1.3 kV. To analyze the statistical PD features and PD's aging on insulation material, repetitive PDs should be generated during each voltage cycle, which means the voltage magnitude added on the insulation sample should be higher than PDIV. For a single transformer, although the environment condition may change, it usually works under a certain voltage rating. Considering these two factors, peak voltage value for the following PD feature and endurance tests is kept as 1.96 kV, 1.5 times the average PDIV value under sea level pressure. Different pressure values from 1 Bar to 0.3 Bar are chosen for the comparative studies. The detailed parameters for the PDIV/PD experiments are listed in Table 1. For the endurance lifetime tests, the voltage frequency is increased into 2 kHz to accelerate the aging speed while other parameters are the same as that in Table I.

Table I

PARAMETERS FOR PDIV AND PD FEATURE TESTS

Group	Rise time	Frequency	Pressure	Voltage peak value (For PD tests)
1	250 ns	1 kHz	1 Bar	1.96 kV
2			0.9 Bar	
3			0.8 Bar	
4			0.7 Bar	
5			0.6 Bar	
6			0.5 Bar	
7			0.4 Bar	
8			0.3 Bar	

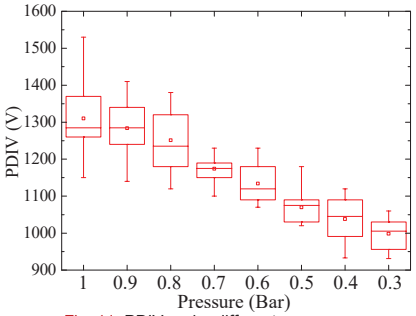

Fig. 11. PDIV under different pressures

III. EXPERIMENT RESULTS

A. PDIV EXPERIMENTS

For the PDIV tests, the oscilloscope is set as single step trigger mode, voltage magnitude is raised slowly with 10 V/s until the PD is triggered like Fig. 8(a), then the PDIV value is defined as the peak value of pulse voltage when the first PD is triggered. 5 specimens are used in each group of Table I. Then statistical PDIV values under different pressures are shown in Fig. 11. It is clear that PDIV decreases monotonously with pressure decreasing. Although for the sphere-plate electrodes, the electric field distribution in the air duct is non-uniform, the results show trending similar with Paschen's Curve that is obtained under uniform electric field.

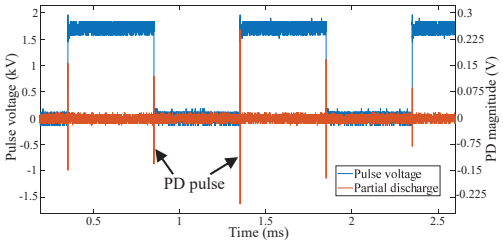

Fig. 12 PD generated by repetitive pulse voltage

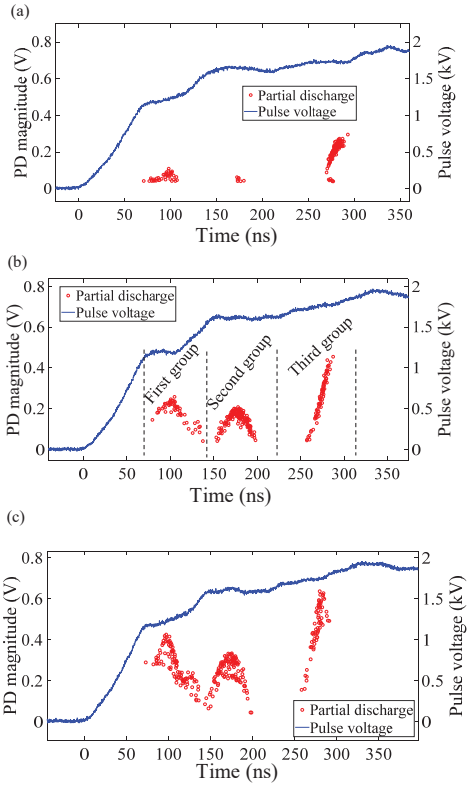

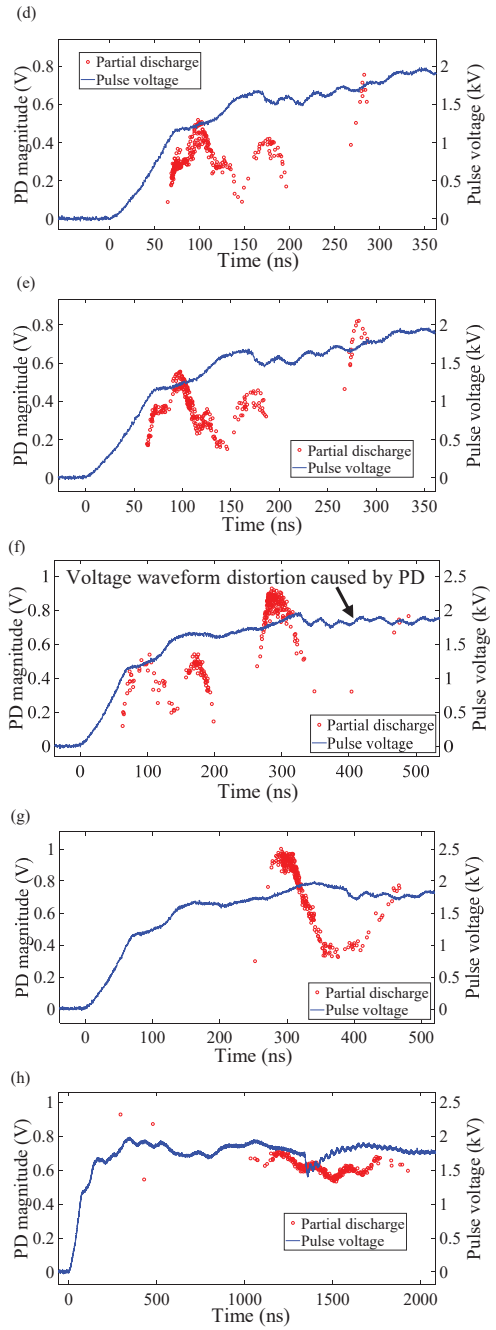

Fig. 13. Time resolved PD pattern under different pressures: (a) 1 Bar; (b) 0.9 Bar; (c) 0.8 Bar; (d) 0.7 Bar; (e) 0.6 Bar; (f) 0.5 Bar; (g) 0.4 Bar; (h) 0.3 Bar.

B. PD FEATURES

Seen as Fig. 12, PDs are generated on the rising/falling edge of the pulse voltage, or at least close to the pulse edges. No obvious PD can be found on the rest of the plateau regions of the pulse voltage. Under symmetric pulse voltage with 50% duty cycle, the statistic PD features around both the rising edge and falling edge are very similar [20]. Therefore, in the analyzing of PD feature under different pressures, we focus on the PDs generated around the rising edge. In order to get statistical PD features, 300 cycles of data are collected through the oscilloscope. Time resolved partial discharge patterns are plotted in Fig. 13. It can be seen that in most of the situations (from 1 Bar to 0.5 Bar), PDs show a similar distribution with three clusters. We divide the PDs into three groups according to which cluster they belong to as shown in Fig. 13(b). In the first group, PD happens at around 100 ns after the zero point of pulse voltage. In the second group, PD happens at around 170 ns after the zero point while the third group of PD at around 270 ns. We define the instantaneous voltage value when PD happens as PD firing voltage, then it is sure that the second group of PD has higher PD firing voltage than the first group. However, although PD magnitude shows a great variety (randomness) even under the same voltage and pressure condition, statistical PD magnitude of the second group is lower than that of the first group in most of the situation (from 1 Bar to 0.6 Bar). Apparent discharge q is one of the important factors to determine the PD intensity [21]. For analyzing the PD that bridges air duct between the sphere electrode and the insulation surface in our experiments, we can regard the air duct as a capacitor and estimate the q through Equation (1).

$$q = C \bullet V_c = C \bullet h \bullet f \bullet E_i \tag{1}$$

Where V_c is the applied voltage value when PD happens, C is the capacitance of air duct, h is the height of the air duct. While f is field enhancement factor. In the region that PD is possible to be triggered, voltage is added between two dielectrics, air and polyimide. Since permittivity of polyimide is much higher than that of air, an enhancement of electric field is present in the air duct [4]. Notice that in Fig. 6, the air duct height is not constant from the contact point to outer area. Also, the bottom side of the air duct is not contacted with the metal plate electrode but with the insulation film. These factors make the values of C and f difficult to be determined. So (1) can only be used for a rough estimation. The total electric field strength E_i can be expressed as E_a-E_q, where E_a is the applied electric field and E_q is the electric field produced by surface charge, which usually has polarity opposite to E_a.

Seen in Fig. 6, starting from the contact point, if the distance goes longer, the air duct length d is also longer. This means under the same added voltage, the electric field intensity is lower according to E=U/d. Therefore, higher added voltage amplitude is needed for longer air duct to meet breakdown. Then the PD situation can be analyzed approximately by simply dividing the air duct into three regions shown in Fig. 6(b). This separation is based on breakdown voltage of air duct (corresponds to partial discharge inception field E_{pdiv} multiplied by d). For region 1, the breakdown voltage is lower than 1.58

kV. For region 2, the breakdown voltage lies from 1.58 kV to 1.7 kV. For region 3, the breakdown voltage is higher than 1.7 kV. These breakdown voltage value ranges cover the ranges of PD firing voltages in the three PD groups (seen from Fig. 14) respectively. Notice that, after the electric field intensity of air duct exceeds the E_{pdiv}, for triggering the PD, there is a time delay Δt to be waited for the presence of initial electron (this process is not affected by pressure) and the forming of electron avalanche. This factor may make the E_i when PD happens different from E_{pdiv}. And the decreasing of pressure can make the time for forming the electron avalanche longer (this would be discussed in detail in section IV). Yet, in relatively high pressure range (higher than 0.4 Bar), the total Δt would not be very long, the practical breakdown voltage of these three air duct regions lies within the above-mentioned breakdown voltage value ranges correspondingly. During the pulse voltage rising edge, the electric field of region 1 would exceed the partial discharge inception field E_{pdiv} at first. This mainly contributes to the first group of PD. When the voltage instantaneous value continuous to increase to more than 1.58 kV (150 ns from the zero point), the E-field in region 2 can reach the E_{pdiv} and triggers PD mainly in the second group. Due to stray parameters of the power electronic modules and the resistor in Fig. 3, the rising edge of the pulse voltage is not a smooth curve. Zoom-in of the pulse voltage rising edge is shown in Fig. 14. For the PD happens in region 1, during Δt, the voltage keeps rapid rising and give rise to a higher E_i when PD is triggered. While for the second group of PD happens in region 2, during Δt, the voltage shows no obvious increasing and even drops a little bit, which give rise to a relatively lower E_i. This is the reason why second group of PD usually has lower magnitude compared to that of first group. When the voltage further rises to exceed the E_{pdiv} of region 3, the PDs of this region that mainly form the PDs in the third group can be triggered. Seen from Fig. 14, in this time range, voltage also keeps rising, and due to a longer air gap distance, longer time delay Δt is needed for forming the electron avalanche. These factors make E_i higher when the third group of PD happens and give rise to stronger PD intensity. It should be noticed that, although the situation of PDs in the three regions of Fig. 6(b) mainly contributes to the PD pattern shown in Fig. 13 from 0.9 Bar to 0.5 Bar, it does not mean that the PDs in these three regions fully correspond to the PD groups in Fig. 14. A typical exception can be found in Fig. 13(a). With 1 Bar pressure, the PDIV is highest, while we conduct all the PD feature tests under the same 1.96 kV peak voltage value. This means under 1 Bar, the overvoltage compared to the PDIV is relatively lowest. This may lead to a result that less PD can happen in the first group (in the time region of first group in Fig. 14, pulse voltage instantaneous value is not very large) even in region 1 while more PDs on the third group. In this situation, the PD in the third group would not only be the PD happens in region 3, but also in region 2 and region 1.

Taking one of the regions of the air duct in Fig. 6(b) as an example, the change of the electric field strength is similar with that proposed in [2] and can be expressed by Fig. 15. At first, the E_i increases along with the rising edge of the applied electric field E_a and exceeds E_{pdiv}. After the generation of initial electron, the PD happens. Then a large amount of surface charge deposit on the insulation surface, which formed E_q with an opposite direction to E_i. Thus, E_i is reduced to $E_{res1}= E_a-E_q$ that is smaller than E_{pdiv}. Afterwards, the applied E_a reaches the plateau region and stops increasing. Although due to the insulation material's surface conductivity, some of the surface charge would be dissipated, it would not be enough for the E_i to exceed the E_{pdiv} again before meeting the falling edge. When the E_a meets the falling edge, E_q is still very strong. The absolute value of $E_i= E_a-E_q$ reaches a high value and exceeds the E_{pdiv} in an opposite polarity. Then, another PD happens and E_i decreases into E_{res2}. When the next cycle of pulse voltage comes, the above-mentioned process repeats. This is why PDs are mainly incepted around the rising/falling edge.

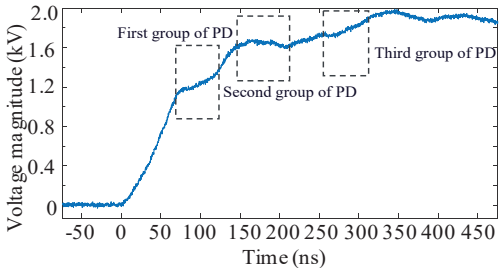

Fig. 14. Zoom in of rising edge of the pulse voltage

To show the changing of statistical PD magnitude and time lag more directly, box-charts of PD magnitude and PD time lag are plotted in Fig. 16 and Fig. 17 respectively. Note: the definitions of PD magnitude and time lag are shown in Fig. 8 (a). We can see that PD magnitude increases with pressure decreases from 1 Bar to 0.4 Bar. Yet, when pressure drops from 0.4 Bar to 0.3 Bar, PD magnitude decreases. When air pressure is larger than 0.7 Bar, PD time lag decreases with pressure decreasing. When pressure is lower than 0.7 Bar, PD time lag increases with pressure decreasing. When pressure change from 0.4 Bar to 0.3 Bar, there is a tremendous increase in time lag.

C. LIFETIME

In the lifetime tests, specimens are added with pulse voltage until the final breakdown. 5 specimens are used in each group of Table I to get a set of statistical lifetime data. Fig. 18 shows the results. Although the lifetime of polyimide film is of a bit variety, in the range from 1 Bar to 0.4 Bar, we can see an overall trending that endurance lifetime decreases with pressure decreasing. This is in accordance with the changing of PD magnitude. When the pressure drops to 0.3 Bar, the statistical lifetime is longer than that under 0.5 and 0.4 Bar, and its average value is even longer than that under 0.7 Bar. Fig. 19 shows the eroded areas of the specimen aged under 1 Bar, 0.4 Bar and 0.3 Bar. For the sake of observing under the same lens, other parts of these aged insulation films are cut off. Under continuous PDs generated by the pulse voltage, polyimide molecules matrix would be degraded gradually. Some of the chemical bonds like C-N-C bond in imide ring and C-H bond

in aromatic ring would be destroyed in advance, and then followed by other stronger bonds [22]. The above mentioned aging process forms an unsmooth low density region of byproducts on the surface of insulation film as seen in Fig. 19. Cavities may exist in these eroded areas. In addition, some byproducts with higher conductivity such as amic acid and nitric acid would be generated, which make surface conductivity of the PD eroded area higher [22]. This increased surface conductivity can help dissipate the surface charge faster. Then, PD number during the first stage of aging process decreases since the surface charge is one of the main sources of initial electron [23]. However, with further PD aging, the roughness of the eroded area with cavities can distort the electric field distribution, making PD stronger and easier to be incepted. The specimen aged under 1 Bar has only a small circle eroded around the contact point. While for the specimens aged under low pressure condition (0.4 and 0.3 Bar), the eroded area is larger and can be divided into inner circle and outer circle. The inner circles of these specimens are rougher than that aged under 1 Bar, which indicate a more serious erosion. It can also be noticed that the outer circle aged under 0.3 Bar is larger than that under 0.4 Bar. This implies the PD expands to larger area though the PD magnitude under 0.3 Bar is relatively lower.

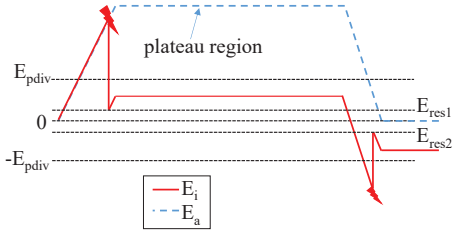

Fig. 15. Changing of the electric filed during the pulse voltage application

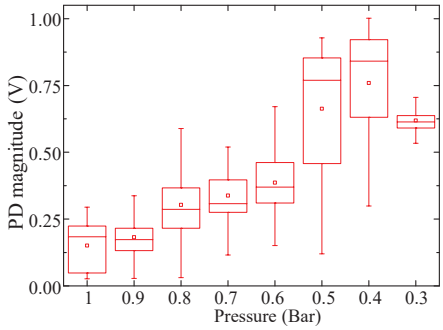

Fig. 16. PD magnitude under different pressures

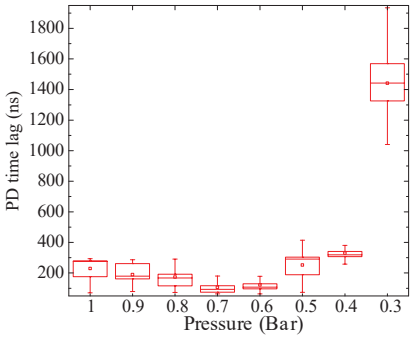

Fig. 17. PD time lag under different pressures

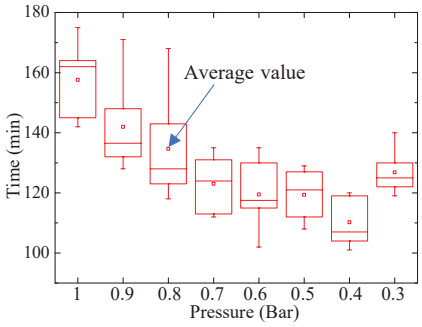

Fig. 18. Endurance lifetime under different pressures

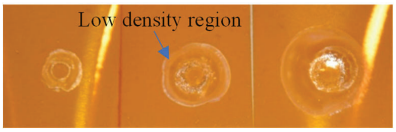

Fig. 19. Eroded area aged under 1 Bar (left), 0.4 Bar (middle) and 0.3 Bar (right)

IV. DISCUSSIONS

In this section, the mechanism of changes of PD features and endurance lifetime with decreasing of pressure would be explained in detail.

A. PD TIME LAG AND MAGNITUDE

For triggering PD, two conditions should be fulfilled, one is that the electrical field strength of the air duct E_i exceeds E_{pdiv}, another is the presence of the initial electron to lead the electron avalanche. So, the total time lag for the PD can be divided into 2 parts expressed by Fig. 20. A time lag t_l should be waited for E_i to reach E_{pdiv} and another statistical time delay Δt is needed for the generation of initial electron and the forming of electron avalanche. If the pressure goes lower, E_{pdiv} decreases, then the E_i can reach E_{pdiv} earlier (t_l decreases). This factor can cause PD happens with a shorter total time lag when pressure decreases in high pressure range (in this case, above 0.7 Bar). Yet, when air pressure decreases, the gas density N is lower, then the number of molecules that can be ionized is reduced. Distance between these molecules is longer and the electron mean free

path increases. This means longer Δt is needed for forming the electron avalanche. Therefore, Δt is increased. Under low pressure range, (in this case, below 0.7 bar), the prolong of electron avalanche plays a dominant role in determining the PD total time lag. When the pressure further drops to 0.4 Bar, the time for forming the avalanche becomes so long that the first and second groups of PDs cannot be triggered under the same electrical stress. So, the time resolved PD pattern under 0.4 Bar in Fig. 13(g) is completely different from that under higher pressures. It is known from the Paschen Curve (seen in Fig. 1) that the breakdown voltage of air duct is affected by air duct length d times pressure p [4]. If d is very short and p is already very low, with further decrease of p, the breakdown voltage of air duct would be raised from the critical point. Therefore, when pressure drops from 0.4 Bar to 0.3 Bar, a part of region 1 (closest to the contact point) in Fig. 6(b) meets an increase in breakdown voltage (corresponds to E_{pdiv} multiplied by d), i.e. the product of p and d in this part of region 1 falls to the left side of the critical point in Pachen's curve. So, PD is less likely to be triggered in this place. However, for the rest regions of the air duct, the product of p and d still lies on the right side of the critical point, which makes PDIV lower when pressure decreases. Meanwhile, compared with that in region 1, the distance of PD in other regions is longer, which can be expressed in Fig. 21. Both the increasing of PD distance and the decreasing number of air molecules prolong the time for forming the electron avalanche, which cause a tremendous increase in PD time lag when pressure drops from 0.4 Bar to 0.3 Bar.

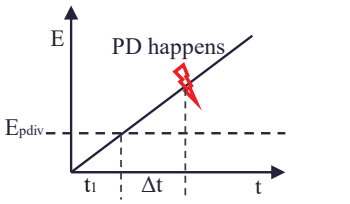

Fig. 20. PD time lag

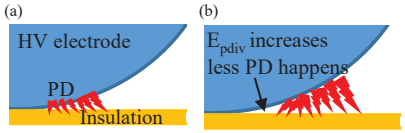

Fig. 21. Main source of PD: (a) Under higher pressures, (b) Under 0.3 Bar

The decreasing of pressure has two effects in the PD intensity. Firstly, if the electric field intensity E keeps unchanged, lower air density N will make E/N higher. E/N is usually used to represent the electron energy [9]. With higher electron energy, stronger PD can be expected with the similar time lag. Secondly, as described in the previous paragraph, under low pressure range, further reducing pressure can make the PD time lag longer. Although there is a segment in the rising edge where voltage drops a little bit (in Fig. 14 where second group of PD happens) and leads to a lower E_i (especially for the PD in region 2 in Fig. 6(b), discussed in section III (b)), in other parts of the rising edge we can still assume that longer PD time lag leads to higher PD firing voltage and higher E_i. In high pressure range (higher than 0.7 Bar), the decreasing of PD time lag and the increasing of electron energy have opposite effects on determining the PD magnitude while the latter plays a dominant role. In low pressure range, the increasing of time lag and increasing of electron energy both enhance the PD intensity. Under 0.3 Bar, PDs mainly happen behind the pulse voltage rising edge and most of them concentrate in time range from 1300 ns to 1600 ns as shown in Fig. 17 and Fig. 22. In this time range, the instantaneous voltage value (from 1.68 kV to 1.82 kV) is obviously lower than the peak value (1.96 kV). Therefore, compared with PDs under 0.4 Bar and the third group of PDs under 0.5 Bar (these PDs mainly happen around the peak point of the pulse voltage, with PD firing voltage usually higher than 1.9 kV), the E_i of the PDs under 0.3 Bar is relatively lower, which leads to lower statistical PD magnitude.

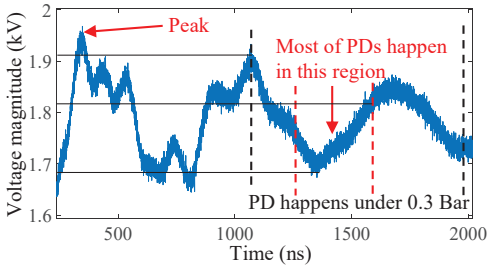

Fig. 22. PD region under 0.3 Bar

B. ENDURANCE

Insulation aging due to PD is a complicated process. PD induced partial temperature rise and chemical reaction will break the molecule chain of the organic insulation material progressively. Among the chemical reaction, intense oxidation is an important factor to degrade the insulation material [22]. With the presence of strong discharge, O_2 molecules can change into O_3 [24], which has stronger oxidability and is more harmful to the organic insulation material. Although higher PD intensity can surely enhance the abovementioned aging factor, when pressure goes lower, O_2 and other compositions in the air that can participate in the insulation aging process become scarcer. Therefore, under low pressure condition, the chemical reaction may be suppressed although the PD activity is still intense, which give rise to a longer lifetime under 0.3 Bar (even longer than that under 0.7 Bar in average).

In this experiment, PD happens in the air duct between sphere electrode and insulation film. If we take both electric field intensity E and pressure p into consideration, for a certain kind of gas dielectric (including air), there is a constant $(E/p)_C$ (represented by a constant C_0 in Fig. 23) to define its breakdown threshold [4]. If the applied (E/p) exceeds C_0 of the air, PD can be triggered in the air duct with the presence of initial electron. Fig. 23 shows the right half of the cross section of the electrodes and insulation sample briefly. For a certain pressure p_1, the value of E/p_1 is a function of the distance L from the contact point, i.e. $E/p_1=f(L)$ as the black curve shows in Fig. 23 [8]. The black curve intersects with the y-axis at point A. With distance shorter than L_1, E/p_1 is higher than C_0. Thus, PD happen in the circle with the contact point as center and L_1 as the radius. If we keep the applied voltage magnitude unchanged and decrease the pressure into p_2, then $E/p_2=f(L)$ is changed into the red curve in

Fig. 23. The curve intersects with y-axis at point B. In this case, PD happen in the circle with the contact point as center and L_2 as the radius. This is the main reason why PD eroded area expands with pressure deceasing.

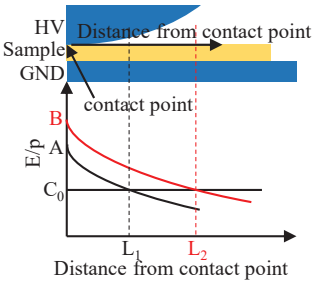

Fig. 23. Expansion of PD area with pressure decreasing

Based on the above studies, we can see that under lower pressures, polyimide film's capability against PD inception and PD aging is obviously weakened. Since this insulation material is usually applied in medium frequency transformers, these experiment results indicate a possible reduction of insulation behavior of medium frequency transformer with pressure decreasing. More into depth studies of actual medium frequency transformer's insulation design are necessary.

V. CONCLUSIONS

To investigate the influence of pressure on PD and its induced aging behavior on the polyimide film, a test system with the abilities of generating pulse voltage, detecting PD, controlling the pressure along with breakdown protection is built. Based on this system, PD (including PDIV and PD features) and endurance tests on the polyimide insulation film under different pressures are conducted. The results show that:

1. PDIV decreases with pressure decreasing under pulse voltage, which fits the right part of Pashen's Curve obtained under sinusoidal voltage.
2. In high pressure range, PD time lag decreases with pressure decreasing because of the reducing partial discharge inception electric field. Yet, with less air molecules, longer time is needed for forming the electron avalanche. When pressure further decreases, PD time lag would be longer due to this factor.
3. With the decreasing of pressure, longer PD time lag (within the voltage rising edge) that leads to higher PD firing voltage and the increasing of electron energy would increase the PD magnitude. Yet, when pressure further decreases, PD would happen behind the voltage rising edge, which give rise to lower PD firing electric field intensity and reduces the PD magnitude.
4. Stronger PD intensity under lower pressure can surely intensify the aging process including the partial temperature rise and chemical reactions and leads to shorter insulation endurance. Yet when pressure continuous decreases, oxygen and other gas molecules in the air that participate in the chemical reaction are greatly reduced, which suppresses the aging process and leads to longer insulation endurance.
5. PD erosion area is larger on the insulation film aged under lower pressure. This is due to that larger area of the air duct exceeds the breakdown threshold when the pressure decreases.

These results show that polyimide insulation film suffer from greater risk of PD inception and deterioration when pressure goes lower and bring focus to the need of more into depth studies of actual medium frequency transformer's insulation design.

REFERENCES

[1] M Mogorovic, "Modeling and Design Optimization of Medium Frequency Transformers for Medium-Voltage High-Power Converters," Phd dissertation, Power Electronics Laboratory., Swiss federal Institute of Technology in Lausanne, Lausanne, 2019.
[2] D. Fabiani, G. C. Montanari, A. Cavallini, and G. Mazzanti, "Relation between space charge accumulation and partial discharge activity in enameled wires under PWM-like voltage waveforms," IEEE Trans. Dielectr. Electr. Insul., Vol. 11, no.3, pp. 393-405, October. 2004.
[3] E. Sili, J. P. Cambronne, N. Naude, R. Khazaka, "Polyimide lifetime under partial discharge aging: effects of temperature, pressure and humidity," IEEE Trans. Dielectr. Electr. Insul., vol. 20, no. 2, pp. 435-442, May. 2013.
[4] High voltage engineering, Butterworth-Heinemann, 2nd ed., Oxford, UK, 2000
[5] S. Jean, B. Reda, M. Xavier, M. Philippe, M. Arnaud, G. Stephane, B. Taoufik, "Planar Magnetic Components in More Electric Aircraft: Review of Technology and Key Parameters for DC–DC Power Electronic Converter," IEEE Transactions on Transportation Electrification., Vol. 3, no. 4, pp. 831-842.
[6] D. James, I. Sauers, A. Elis, M. Pace and D. Deschenes, "Effect of gas pressure on partial discharge in voids in epoxy," Annual Report Conference on Electrical Insulation and Dielectric Phenomena, Albuquerque, NM, USA, October, 2003.
[7] M. Kamarol, S. Ohtsuka, M. Hikita, H. Saitou, M. Sakaki, "Determination of Gas Pressure in Vacuum Interrupter Based on Partial Discharge," IEEE Trans. Dielectr. Electr. Insul., Vol. 14, No. 3, pp. 593-599, 2007.
[8] H. Okubo, S. Yuasa, K. Ota, N. Hayakawa, M. Hikita, "Discharge Characteristics under Non-uniform Electric Field in He, Ar and Air at Low Pressures," IEEE Transactions on Dielectrics and Electrical Insulation., Vol. 4, No. 4, pp. 450-455, 1997
[9] H. Liu, R. Liao, X. Zhao and Y. Lin, "The effect of air pressure on the surface electric field intensity characteristics under negative DC corona discharge in a corona cage," Electrical Power and Energy Systems., Vol. 113, pp. 244-250, 2019
[10] Y. Nakano, M. Kozako, T. Tanaka, M. Kobayashi, "Estimation of Internal Pressure of Vacuum Interrupter by Measuring Partial Discharge Current," IEEE International Symposium on Discharges and Electrical Insulation in Vacuum, Greifswald, Germany, September. 2018, pp. 611-614.
[11] B. Moein and G. Mona,"Characterization of Partial Discharge Activities in WBG Power Converters under Low-Pressure Condition,"Energies., Vol. 14, No. 5394, 2021.
[12] E. Christopher, L. Robert, C. Lan, R. Simon and F. Robert, "The Effects of Pressure and Temperature on Partial Discharge Degradation of Silicone Conformal Coatings," IEEE Trans. Dielectr. Electr. Insul., Vol. 24, No. 5, pp. 2986-2994, 2017.
[13] N. S. Ali, S. Saeed, S. Greg, K. Behzad, "Investigation of Corona Partial Discharge Characteristics under Variable Frequency and Air Pressure," IEEE Electrical Insulation Conference, San Antonio, TX, USA, June. 2018, pp. 31-34
[14] A. Cedric, B. Thibaut, L. Thierry, "Influence of pressure on partial discharge spectra," IEEE Electrical Insulation Conference, Montreal, QC, Canada, June. 2016, pp. 507-510.
[15] D. R. Meyer, A. Cavallini, L. Lusuardi, D. Barater, G. Pietrini, A. Soldati, "Influence of Impulse Voltage Repetition Frequency on RPDIV in Partial Vacuum," IEEE Trans. Dielectr. Electr. Insul., Vol. 25, No. 3, pp. 873-882, 2018.
[16] B. Moein, G. Mona, "A Finite Element Analysis Model for Partial Discharges in Silicone Gel under a High Slew Rate, High Frequency Square Wave Voltage in Low-Pressure Conditions," Energies., Vol. 13, No. 9, 2020.
[17] A. A. Abdelmalik, A. Nysveen and L. Lundgaard,"Influence of Fast Rise Voltage and Pressure on Partial Discharges in Liquid Embedded Power

Electronics," IEEE Trans. Dielectr. Electr. Insul., Vol. 22, No. 5, pp. 2770-2778, 2015.

[18] Y. Zhao, G. Zhang and R. Guo, "The Breakdown Characteristics of Thermostable Insulation Materials under High-Frequency Square Waveform," IEEE Trans. Dielectr. Electr. Insul., vol. 26, no. 4, pp. 1073–1080, 2019.

[19] W. Y. Zhou, P. Wang, Z. J. Zhao, Q. Wu, and A. Cavallini, "Design of an Archimedes spiral antenna for PD tests under repetitive impulsive voltages with fast rise times," IEEE Trans. Dielectr. Electr. Insul., Vol. 26, no. 2, pp. 423–430, March. 2019

[20] P. Wang, H. Xu, J. Wang and W. Wang, "Effect of Repetitive Impulsive Voltage Duty Cycle on Partial Discharge Features and Insulation Endurance of Enameled Wires for Inverter-fed Low Voltage Machines," IEEE Trans. Dielectr. Electr. Insul., Vol. 24, No. 4, pp. 2123-2131, 2017.

[21] L. Niemeyer,"A generalized approach to partial discharge modeling," IEEE Trans. Dielectr. Electr. Insul., Vol.2, No. 4, pp. 510-528, 1995.

[22] X. Zhong, G. Wu, Y. Yang, X. Wu, Y. Lei, "Effects of nanoparticles on reducing partial discharge induced degradation of polyimide/Al2O3 nanocomposites," IEEE Transactions on Dielectrics and Electrical Insulation., Vol. 25, No. 2, pp. 594-602.

[23] Y. Luo, G. Wu, J. Liu, G. Zhu, P. Wang, P, Jia and K. Cao,"PD Characteristics and Microscopic Analysis of Polyimide Film Used as Turn Insulation in Inverter-fed Motor," IEEE Trans. Dielectr. Electr. Insul., Vol. 21, No. 5, pp. 2237-2244, 2014.

[24] P. Yao, H. Zheng, X. Yao, Z. DING, "A Method of Monitoring Partial Discharge in Switchgear Based on Ozone Concentration," IEEE transactions on plasma science., Vol. 47, No. 1, pp. 654-660, 2019.

[25] T. Liu, Q. M. Li, G. J. Dong, M. Asif, X. W. Huang, Z. D. Wan, "Multi-factor model for lifetime prediction of polymers used as insulation material in high frequency electrical equipment," Polym. Test., vol. 73, pp. 193–199, November. 2018.

Electrical stress suffered by medium voltage medium frequency transformer

Changjiang. Zheng
Department of Energy Technology, Aalborg University
Aalborg Denmark
czhe@et.aau.dk

Qian Wang
Department of Energy Technology, Aalborg University
Aalborg Denmark
qiw@et.aau.dk

Huai Wang
Department of Energy Technology, Aalborg University
Aalborg Denmark
hwa@et.aau.dk

Zhan Shen
Department of Energy Technology, Aalborg University
Aalborg Denmark
zhs@et.aau.dk

Claus Leth Bak
Department of Energy Technology, Aalborg University
Aalborg Denmark
clb@et.aau.dk

2021 IEEE Electrical Insulation Conference (EIC) | 978-1-6654-1564-4/21/$31.00 ©2021 IEEE | DOI: 10.1109/EIC49891.2021.9612278

***Abstract*—Medium voltage medium frequency transformers may face electrical stress different from that of conventional transformers. Working under PWM-like voltages, inter-turn and inter-layer overvoltage could be induced within the transformer's winding. This overvoltage can increase the probability of partial discharge that can degrade the insulation quickly and lead to premature breakdown. Therefore, an investigation on the electrical stress of medium-frequency transformer is necessary. This paper chooses a transformer prototype as a case and creates its equivalent circuit. Based on this circuit, transient inter-turn and inter-layer voltage simulation is conducted under different voltage rise times, relative insulation permittivity and winding structures. The simulation results confirm the existence of inter-turn and inter-layer overvoltage and reveal the influence of the above-mentioned parameters on the overvoltage.**

***Keywords*—Medium voltage medium frequency transformer, insulation, electrical stress, inter-turn voltage**

I. INTRODUCTION

In some of the modern power electronic systems, transformers are one of the important components that serve as the function of voltage scaling up/down and electrical isolation [1]. Working under PWM voltage generated by power electronic switches, with voltage magnitude range from several to tens of kV and frequency from hundreds of Hz to tens of kHz, these transformers are usually called medium voltage medium frequency (MVMF) transformers. Since the working voltage of these transformers usually has the characteristic of short rise time, the insulation of the winding suffers from electrical stress different from that of conventional transformers. Previous studies on inverter-fed motors have shown that when the winding of the motor is added with pulse voltage, inter-turn voltage overshot can be triggered on the rising edge of the voltage, which can lead to a peak value, which is much higher than the static voltage drop [2]. In addition, usually, the first few turns closest to the pulse voltage output terminal would suffer from the highest peak voltage [3]. This electrical stress can significantly increase the risk of partial discharge. Continuous partial discharge can greatly accelerate the aging speed of the insulation, which in turn leads to premature breakdown [4]. For transformers also have multi-turn windings, when working under similar operating voltage, this kind of electrical stress may also exist. Moreover, in a transformer with a winding of multi-layers, not only the turn to turn insulation but also the layer to layer insulation may suffer the overvoltage from the pulse voltage with short rise time. To guarantee the long-term reliability of the transformers working in MVMF application, investigation on its inter-turn and inter-layer electrical stress is necessary. This paper chooses a transformer prototype designed by previous literature as a case and builds its equivalent circuit model. Then transient inter-turn and inter-layer simulations are conducted under different voltage rise times, permittivity, and winding structures. Short rise time and higher relative permittivity give rise to higher overvoltage, while Z-type winding can reduce the overvoltage.

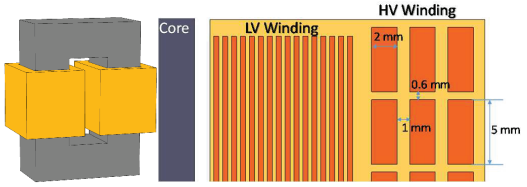

Fig. 1 3D (left) overall outlook and 2D (right) zoom out of winding of the transformer prototype

II. BUILDING OF THE MODEL

A. Selecting the transformer prototype

A transformer prototype designed by previous researches is selected as the object of study [1, 5]. This transformer is used in a 10 kV cascaded power electronic transformer (PET) system, which is a typical field that MVMF transformers are applied. So studies on this prototype can reflect the electrical stress suffered by MVMF transformers accurately. Its overall 3D outlook and 2D zoom out of the winding layout are shown in Fig. 1, while its basic parameters are listed in TABLE. I. Its LV winding is made from copper foils while its HV winding from flat copper wires. For the HV winding, the height of the conductor is 5 mm, and the width is 2 mm. The insulation distance of LV winding

is 0.3 mm, whereas inter-turn and inter-layer insulation distances of HV winding are 0.6 mm and 1 mm, respectively. The core is made of ferrite with a permeability of 1900. Since the rated voltage of the LV winding is only 400 V, it would not face any serious insulation problems normally. Thus the study on the electrical stress of this prototype would only focus on the HV winding.

TABLE I. BASIC PARAMETERS OF THE TRANSFORMER PROTOTYPE

Parameter	Values
Operating frequency	1 kHz
Rated power	35 kW
Turn ratio	120:32
Rated voltage (HV winding)	1500 V
Rated voltage (LV winding)	400 V
Maximum operating temperature	100 ℃
Core dimension	27/19/10 cm (height/width/thickness)

B. Equivalent circuit model

To conduct transient voltage simulation, stray parameters including resistance, inductance of each turn along with capacitance and mutual inductance between turns should be obtained [3]. All these parameters are calculated in Ansys Q3D – an FEM-based software. Inter-turn capacitances $C_{x\text{-}y}$ are calculated based on Electrostatics. According to the results, capacitances between non-adjacent turns (for example, $C_{1\text{-}3}$) are very small compared with that between adjacent turns (for example, $C_{1\text{-}2}$), while the inter-layer capacitance such as $C_{1\text{-}40}$ is large enough to be included in the simulation due to the short distance (1 mm). Therefore, in the circuit model, inter-turn capacitance between adjacent turns and inter-layer capacitance are taken into consideration, shown in Fig. 2. The numbers in the Fig.2 refers to serial numbers of the turns.

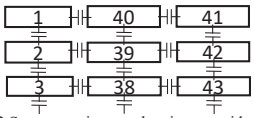

Fig. 2 Stray capacitance taken into consideration

Inductance and resistance are calculated based on Electromagnetic Field in frequency domain. In this study, the voltage waveform for the simulation is square wave pulse voltage with very short rise time. According to Fourier analysis, square wave voltage is a combination of a series of sinusoidal wave voltages with different frequencies. The equivalent highest frequency f_u of a pulse voltage can be calculated approximately by (1) [3]:

$$f_u = \frac{1}{\pi t} \tag{1}$$

Where t is the voltage rise time. In PWM-like voltages produced from power electronic switches, it is usually in a range from hundreds of *ns* to several μs. Inductance can be affected by frequency. Also, the resistance increases due to the skin and proximity effect under higher frequencies. So, the values of these two parameters are obtained under f_u. After the calculation of the stray parameters in the last section, an equivalent circuit model for the transformer's HV winding is constructed in Matlab, shown in Fig. 3.

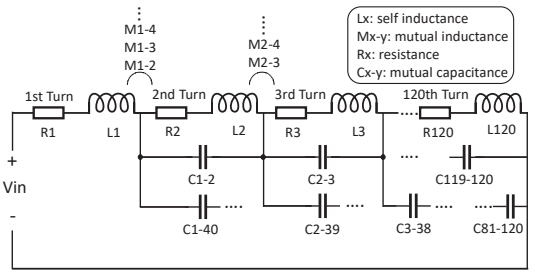

Fig. 3 Equivalent circuit model of the transformer's HV winding.

III. SIMULATION SETUP

In the simulation, parameters including the voltage rise time, the relative permittivity of insulation material, and winding structure are taken into consideration.

A. Rise time

It is known that power electronic switches are reaching shorter rise/fall times to reduce the switching loss. Yet this may bring more serious electrical stress on the winding of MV/LV electric apparatus. Considering that rise time of modern power electronic switches is usually less than 1 μs and some of them can even be around 100 ns, 4 different rise times from 100 ns to 1μs are selected for the simulation.

B. The relative permittivity of insulation material

Transformers use different materials for the insulation, including polyimide, polyester, DMD and Nomex papers [6]. Among these insulation materials, relative permittivity ε_r is variable, and it can affect the stray capacitance through (2), which may, in turn, affect the inter-turn/layer overvoltage.

$$C = \frac{\varepsilon_r S}{4\pi k d} \tag{2}$$

Where S is the area, d is the distance. Symbol k is calculated through $1/4\pi\varepsilon_0$, where ε_0 is the permittivity of vacuum. ε_r of the above-mentioned materials is in the range from 1.6 to 3.9. Three values of ε_r within this range is selected for the simulation.

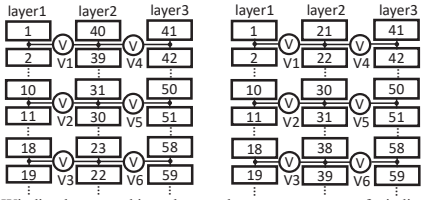

Fig. 4 Winding layout and inter-layer voltage measurement of windings with C-type (right) and Z-type (left)

C. Winding structure

For transformer with windings of multi-layers, two structures, including C-type and Z-type are usually selected in the design of the winding. Although Z-type winding is a bit harder to construct, it can reduce the inter-layer voltage drop effectively comparing with the C-type winding [7]. This

conclusion is obtained under the static voltage analysis. Changing the winding structure can also change the stray parameters of the winding, and its influence on the transient inter-turn and inter-layer electrical stress under pulse voltage with short rise time is worth study. The layout of these two winding structures can be seen in Fig. 4.

Considering the factors described above, the detailed parameters (including rise time t, relative permittivity ε_r, and winding structure) for the simulation are listed in TABLE. II. The pulse voltage's peak to peak value is set as 1.5 kV and its frequency as 1 kHz.

TABLE II. PARAMETERS FOR THE SIMULATION

Group	t (ns)	ε_r	Winding structure
1	100	3.9	C-Type
2		2.7	
3		1.6	
4	200	3.9	
5		2.7	
6		1.6	
7	500	3.9	
8		2.7	
9		1.6	
10	1000	3.9	
11	200	3.9	Z-type

IV. SIMULATION RESULTS

During the simulation, inter-turn voltage between within the first 6 turns of the transformer's HV winding are recorded, expressed as $V_{1\text{-}2}$, $V_{2\text{-}3}$, $V_{3\text{-}4}$, $V_{4\text{-}5}$ and $V_{5\text{-}6}$, respectively. For the inter-turn layer voltage simulation, 6 test points (from V1 to V6 in Fig. 4) are selected for the measurement of inter-layer voltage. The typical waveform (Group 1 of TABLE II) of the inter-turn and inter-layer voltage drop during a half cycle of the pulse voltage are shown in Fig. 5 and Fig. 6 respectively.

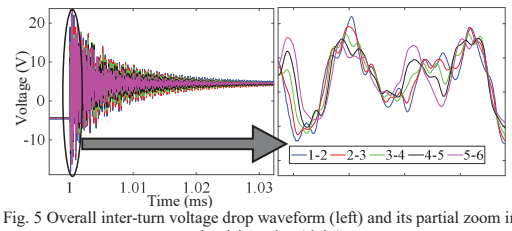

Fig. 5 Overall inter-turn voltage drop waveform (left) and its partial zoom in on the rising edge (right).

It can be seen that strong oscillations on the rising edge exist both on inter-turn and inter-layer voltage drop, noticing that under C-type winding, the static inter-layer voltage drop in different test points varies a lot, which is in accordance with the analysis from [7]. Peak values of the inter-turn voltage are plotted in Fig. 7. It can be seen that unlike the voltage distribution in the inverter-fed motors [3-4], of which peak voltage value between the first two turns is the largest and the value drops monotonously, changing of inter-turn peak voltage value of the MVMF transformer does not show a clear trend. The reason is that structures of core and winding of transformer is different from that of the HV form-winding motor presented in [3]. Especially for the three-layer winding of the transformer prototype in this case study, inter-layer capacitance and mutual inductance exist. Therefore, the inductive and capacitive coupling between turns in this transformer is quite different from that of motor and more complicated. These factors lead to a different voltage distribution. Yet, the peak values of different inter-turn/layer voltage drops can still be much higher than the static voltage values (around 4.6 V), which can also be a threat to the transformer's insulation.

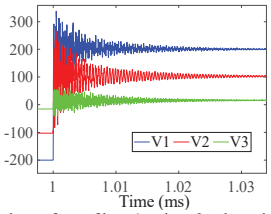

Fig. 6 Typical waveform of layer1-to-layer2 voltage drop (C-type).

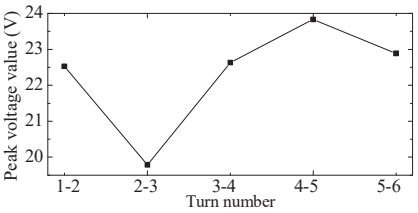

Fig. 7 Inter turn peak voltage value (In Group 1 of TABLE II)

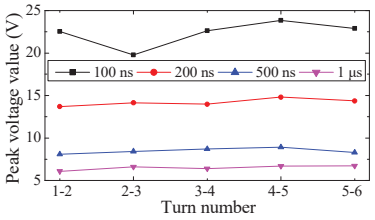

Fig. 8 Inter turn peak voltage value under different rise times

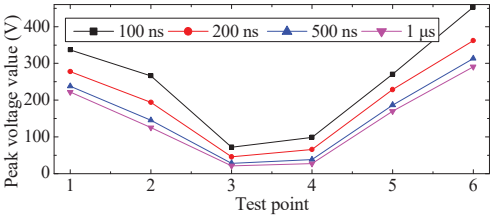

Fig. 9 Inter-layer peak voltage value under different rise times

A. *Different rise times*

Inter turn and inter-layer peak voltage values under different rise times (results from Group 1, 4, 7 and 10 in TABLE. II) are shown in Fig. 8 and Fig. 9. It can be seen that a short rise time can lead to higher overvoltage. Especially for the inter-layer voltage drop in test point 6 (test point 1-6 corresponds to V1-V6 in Fig. 4). Under 100 ns pulse voltage, the peak value can reach 453 V, which exceeds its static voltage drop (259 V) by more than 190 V. If air ducts exists between these adjacent layers, corona discharge may happen with high probability.

B. *Different insulation relative permittivity*

Results of inter-turn and inter-layer peak voltage values in Group 1-9 are plotted in Fig. 10 and Fig. 11, respectively. Decreasing relative permittivity can reduce the peak voltage value. When rise time is shorter, this reducing effect is more obvious. For example, under 100 ns rise time, when ε_r changes from 3.9 to 1.6, the peak value of inter-turn voltage $V_{1\text{-}2}$ drops by 27.1%. While under 500 ns rise time, with the same changing in ε_r, the peak voltage value drops only by 15.3%.

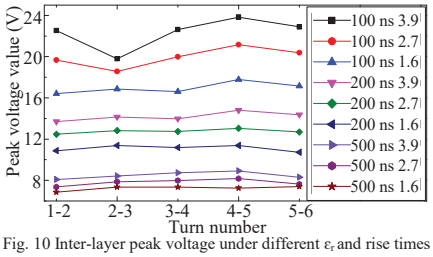

Fig. 10 Inter-layer peak voltage under different ε_r and rise times

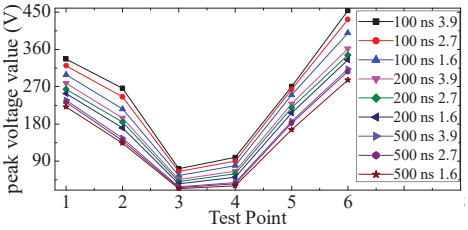

Fig. 11 Inter-layer peak voltage under different ε_r and rise times

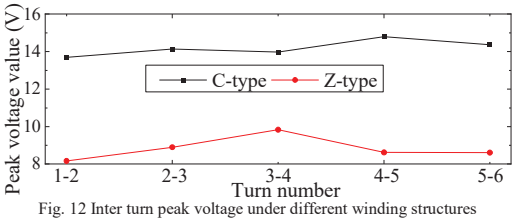

Fig. 12 Inter turn peak voltage under different winding structures

C. *Different winding structures*

Inter turn/layer peak voltage simulation results from Group 4 and 11 are shown in Fig. 12 and Fig. 13, respectively. Changing the winding structure from C-type to Z-type can not only decrease the static inter-layer voltage but also make the inter-turn and inter-layer peak voltage lower. The static inter layer voltage values are also included, which are the same as depicted in Fig. 6, to Fig. 13 to show the difference between results in this transient overvoltage simulation and the previous static voltage analysis [7] with respect to inter layer electrical stress under different winding structures. For test points 2 and 5, which are the midpoints of the region between adjacent layers, the static voltage under C-type and Z-type windings are almost the same, which is similar to the results presented in the literature [7]. Yet for the transient voltage simulation, with the exist of voltage overshot seen in Fig. 6, we can see the peak voltage in points 2 and 5 under Z-type winding is obviously lower than that of C-type. Noticing that the static inter-layer voltage drop increases from test points V1 to V6. This result is different from the result in [7] that inter-layer voltage drop under Z-type winding should be constant. It is because the turns in the outer layer (layer2 and layer3) are longer than that of the inner layer (layer1), so the resistance of the turns of the outer layer is relatively larger, which can lead to a higher static voltage value.

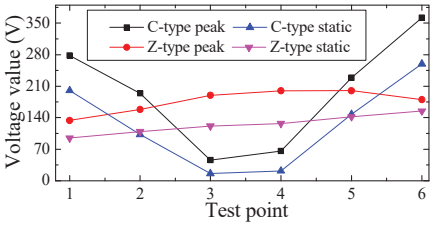

Fig. 13 Peak and static values of inter-layer voltage under different winding structures

CONCLUSIONS

To investigate the electrical stress suffered by medium voltage and medium frequency transformers, transient inter-turn/layer voltage simulations are conducted on the equivalent circuit model of a practical transformer prototype. The results show: 1) Overvoltage exists between adjacent turns and layers. A shorter rise time can lead to higher overvoltage. 2) Decreasing the relative permittivity of the insulation can lower the overvoltage. When the rise time is shorter, this decreasing effect is more obvious. 3) Z-type winding can reduce the inter-turn and inter-layer electrical stress effectively when the transformer is working under pulse voltage. Therefore, medium voltage medium frequency transformer can use Z-type winding and insulation material with lower relative permittivity to better resist the electrical stress brought from PWM voltage.

REFERENCES

[1] P. Huang, C. Mao, D. Wang, L. Wang, Y. Duan, J. Qiu, G. Xu and H. Cai, "Optimal Design and Implementation of High-Voltage High-Power Silicon Steel Core Medium-Frequency Transformer," IEEE Trans. Ind. Electr, Vol. 64, no. 6, pp. 4391-4401, 2017.

[2] W. Jianru, L. Hongchi and Y. Huanjun, "Voltage distribution in stator windings of motor driven by PWM inverter," in Proc. Power System Technology Conf., Vol. 2, pp. 727-731, October, 2002.

[3] F. Wen, L. Zhang, G. Wu, E. He, "Modeling and Simulation of Inter-Turn Voltage Distribution in the Stator Windings of the Pulling Motor", IEEE International Conference on Solid Dielectrics (IDSD), pp. 900-903, July, 2004.

[4] M. Kaufhold, G. Borner, M. Eberhardt and J. Speck, "Failure mechanism of the interturn insulation of low voltage electric machines fed by pulse controlled inverters," IEEE Elect. Insul. Mag., vol. 12, pp. 9–16, Sept. 1996

[5] P. Huang, C. X. Mao and D. Wang, "Electric Field Simulations and Analysis for High Voltage High Power Medium Frequency Transformer," MDPI Energies., Vol. 10, no.3, 2017.

[6] Y. Zhao, G. Zhang and R. Guo, "The Breakdown Characteristics of Thermostable Insulation Materials under High-Frequency Square Waveform," IEEE Trans. Dielectr. Electr. Insul., vol. 26, no. 4, pp. 1073–1080, 2019.

[7] Z. H. Zheng, Lu. Bai and T. Jin, "Study on Insulation Design of High Power High Frequency High Voltage Transformer," IEEE Conference on Energy Internet and Energy System Integration, October, 2018.

C2:

Partial discharge inception and deterioration of Nomex paper under repetitive square wave voltage

Changjiang. Zheng
AAU Energy
Aalborg University
Aalborg, Denmark
czhe@energy.aau.dk

Qian Wang
AAU Energy
Aalborg University
Aalborg, Denmark
qiwaau@163.com

Huai Wang
AAU Energy
Aalborg University
Aalborg, Denmark
hwa@energy.aau.dk

Zhan Shen
AAU Energy
Aalborg University
Aalborg, Denmark
zhs@scu.edu.cn

Filipe Faria da Silva
AAU Energy
Aalborg University
Aalborg, Denmark
ffs@energy.aau.dk

Claus Leth Bak
AAU Energy
Aalborg University
Aalborg, Denmark
clb@energy.aau.dk

2022 IEEE International Conference on High Voltage Engineering and Applications (ICHVE) | 978-1-6654-0750-2/22/$31.00 ©2022 IEEE | DOI: 10.1109/ICHVE53725.2022.9961729

***Abstract*—Working under PWM voltage with fast voltage rise time and high frequency, medium frequency transformers may suffer from overvoltage and temperature rise in the winding. As a result, partial discharge may be triggered with high probability, threating the insulation reliability. Therefore, it is necessary to evaluate the insulation capability of medium frequency transformers with respect to partial discharge and deterioration. This paper introduces a test system based on power electronic modules that can generate repetitive pulse voltage. Then, by using this system, partial discharge inception voltage test under different temperatures and endurance lifetime test are conducted on Nomex paper, which is an insulation material usually used in medium frequency transformers. The results show the change trending of the partial discharge inception voltage of Nomex paper with temperature and indicate an accelerated aging of this material with the presence of continuous discharge.**

Keywords—Medium frequency transformer, partial discharge, insulation, Nomex paper

I. INTRODUCTION

In some modern power electronic systems, transformers serve as electrical isolation and power transmission, by scaling up/down the voltage level. These transformers working along with the power electronic switches are called medium frequency transformers. The working voltage waveform of these transformers is PWM voltage with frequency in the range from hundreds of Hz to tens of kHz (much higher than 50/60 Hz) and very short rise time (from ten of ns to several μs) [1]. When voltage with very fast rising edge is added to the winding, inter-turn overvoltage may occur. This problem has been discovered firstly in the field of inverter-fed motors [2]. With the presence of the overvoltage, partial discharge (PD) may be triggered in the inter-turn insulation with higher probability. PD is considered as a main factor degrading the insulation in the long term. In addition, with higher frequency of the PWM voltage, more heat would be generated due to increased copper and core losses, leading the winding into higher temperature [1]. With the combined electrical-thermal aging, the insulation may face the premature failure [3].

In our previous study, it is found that similar to the inverter-fed motor, inter-turn overvoltage also exists in the winding of transformer if injected with PWM-like voltage [4]. Moreover, its winding may have multi-layers. Usually, the voltage drop between adjacent layers is very high compared with the inter-turn voltage. With the afore-mentioned overvoltage, the risk of PD inception in the inter-layer insulation would be greater. Since the medium frequency transformers are developing to be smaller in size, which means shorter insulation distance along with poor heat dissipation, this potential problem cannot be ignored.

Therefore, it is necessary to evaluate the insulation capability of medium frequency transformer with respect to partial discharge inception and deterioration under voltage pulses. This paper introduces a test system we built based on power electronic modules. It can generate repetitive pulse voltage and detect PD signals of higher frequency compared with that under 50/60 Hz AC scenarios. Then, by using this system, partial discharge inception voltage (PDIV) test are conducted under different temperatures on Nomex paper, which is an insulation material usually used in the medium frequency transformer. The results show that the PDIV of the Nomex paper decreases with temperature increase. Afterwards, endurance lifetime test with the presence of PD are conducted and the results show that Nomex paper is quite vulnerable to the degradation from PD generated by pulse voltage. The above results indicate that working under PWM voltage, transformers in the power electronic systems would face higher risk of premature breakdown compared with that of conventional transformer.

II. EXPERIMENT SETUP

A. Pulse voltage generator

Based on a half-bridge power electronic switch module, a HV pulse voltage generator is built and its schematic is shown in Figure 1. With 25V low voltage supply and a controllable low voltage pulse generator, this module can be triggered and square wave pulse voltage can be generated between the Output terminals. The high voltage DC source is applied as the HV input for the module while the capacitor is used for stabilizing the DC voltage. A resistor is connected in serious of the output terminals to regulate the pulse voltage rise time and restrict the output current. This generator can output unipolar pulse voltage with magnitude up to 20 kV and frequency up to 50 kHz, which covers the working frequency and voltage ratings of most of the medium frequency transformers [1]. A typical waveform generated by this circuit is shown in Figure 2.

978-1-6654-0750-2/22/$31.00 ©2022 IEEE

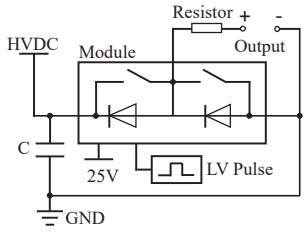

Figure 1. HV pulse generator

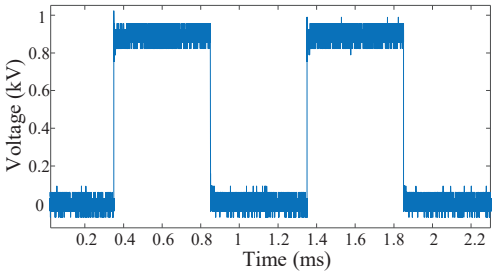

Figure 2. Repetitive pulse voltage waveform with 1 kV peak amplitude and 1 kHz frequency

B. PD detection

PDIV is defined as the peak value of the pulse voltage when the PD is first triggered. To acquire accurate PDIV value, PD signals should be detected in high accuracy. In traditional HV field (working under power frequency sinusoidal voltage), PD detection is conducted using current sensor or HFCT. Since sinusoidal voltage at power frequency would not bring much electromagnetic interference, these devices can catch PD signal effectively. In comparison, pulse voltage would bring strong interference due to its fast rise/fall time, which makes these devices very difficult to distinguish PD. Previous researchers have detected that the energy of the interference mainly concentrates below 500 MHz while the energy of PD triggered by pulse voltage can spread up to more than 1.2 GHz [5]. So, an Ultra High Frequency (UHF) antenna can be a suitable device for detecting this kind of PD signal. In this paper, an UHF antenna is chosen as the PD detection device, its peak gain in frequency domain is shown in Figure 3. From 1 GHz to 2 GHz, the gain of antenna can reach more than 3 dB, much higher than the gain below 0.5 GHz. Thus, this antenna can detect PD signal under pulse voltage with high signal-to-noise ratio.

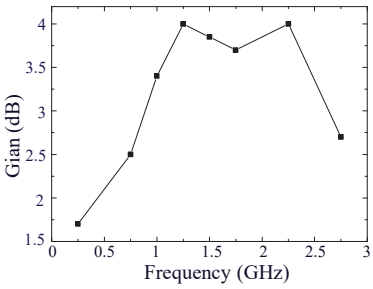

Figure 3. Gain of the UHF antenna

C. Insulation specimen

The insulation specimen used in this study is Nomex 410 paper (seen in Figure 4), which is typical in the insulation of medium frequency transformers. Its thickness is 0.05 mm , the dielectric strength is 34 kV/mm, its intrinsic short time breakdown voltage is 1700 V and each specimen is cut into square shape with 2.5 cm side length. Before starting the tests, all the specimens were cleaned through alcohol and dried in the oven with 50 °C for 24 hours. During the experiments, the insulation paper would be fastened between the sphere and plate electrodes seen in Figure 5. Repetitive pulse voltage from the HV pulse generator would be injected to the insulation specimen through the sphere electrode while the plate electrode would be connected with the ground.

Figure 4. Nomex paper

Combining the above-mentioned HV pulse generator and PD detection system, the integrated test system is shown in Figure 6. The applied voltage waveform measured by the HV probe and PD signal by the antenna is displayed on the oscilloscope synchronously. The current sensor is used for breakdown protection. If the insulation specimen fails electrically during the tests, the current magnitude would exceed the threshold current value set in the control program. Then the computer would send a response signal to the HV pulse generator to block the module's triggering; thus, the output of the generator can be stopped to prevent the module from damage due to overcurrent. Above all, with the ability to generate repetitive pulse voltage and effective PD detection method and breakdown protection, this test system can be used for PDIV and endurance lifetime tests on the insulation of medium frequency transformer. The oven in this system is used for drying the insulation specimen before the experiments and controlling the temperature during the experiments.

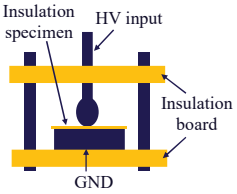

Figure 5. Sphere-plate electrodes

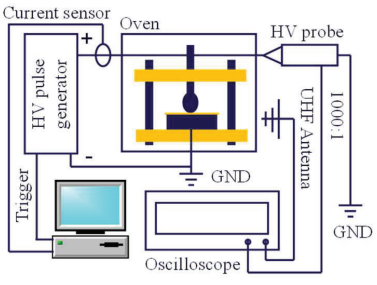

Figure 6. Test system

D. Parameters of the PDIV experiments

It is known that power electronic switches are developing to be faster in switching speed to reduce the switching losses. Recently, some of the SiC-based modules can reach the voltage rise time of tens of ns. Therefore, to simulate the fast voltage rise time on the medium frequency transformer, the rise time of the voltage generator is set as 40 ns. While the frequency is kept as 1 kHz since this is a common working frequency among the prevailing medium frequency transformers. Studies on the thermal stress of the medium frequency transformer show that, due to increased copper and core losses brought from the higher working frequency, medium frequency transformer's temperature rise would be greater comparing with conventional transformer [1]. In some cases, it may reach more than 100℃ [7]. To simulate the thermal condition that is faced by the medium frequency transformer and analyze the effect of temperature rise on the Nomex paper's capability to withstand PD inception, four different temperature values from room temperature (20℃) to 110℃ are chosen for the experiments. The detailed parameters of the PDIV tests are shown in TABLE I.

TABLE I. Parameters for the PDIV tests on Nomex paper

Group	Applied voltage rise time	Frequency	Temperature
1	40 ns	1 kHz	20 ℃
2			50 ℃
3			80 ℃
4			110 ℃

E. Parameters of the endurance experiments

In the endurance experiments, both the rising of temperature and peak voltage value are taken into consideration. The selection of temperature is the same as that of TABLE I. In the PDIV experiments, PDIV value obtained in each group of TABLE I may be different. We set the lowest PDIV value recorded among these groups as $PDIV_m$. Three peak voltage values including $1.5\times PDIV_m$, $1.4\times PDIV_m$ and $1.3\times PDIV_m$ are chosen. Then detailed parameters of endurance test are shown in TABLE II.

TABLE II. Parameters for the endurance tests

Group	Peak voltage value	Frequency	Temperature
1	$1.5\times PDIV_m$	1 kHz	20 ℃
2			50 ℃
3			80 ℃
4			110 ℃
5	$1.4\times PDIV_m$		
6	$1.3\times PDIV_m$		

III. Experiment Resutlts

A. PDIV experiments

In our experiments, PDIV is defined as the instantaneous peak value of the applied pulse voltage when the first PD happens. This definition can be seen more clearly in Figure 7, and PD inception can be confirmed when the waveform in this figure is displayed in the oscilloscope (set as single-step trigger mode) after adding the voltage. During the experiments, the voltage value is raised at a step of 10 V/s until the PD is triggered. 5 samples are tested for each group in TABLE I, and average PDIV values of these 5 samples are recorded. Then the PDIV under different temperatures are displayed in Figure 8. Although PDIV values show variety to a certain extent, we can still see the overall trending that PDIV decreases with rising temperature. At higher temperature, the density of air is lowered, then the breakdown strength of the air duct between the sphere electrode (HV input) and the insulation specimen would be decreased [3]. Therefore, PD would be triggered with relatively lower applied voltage.

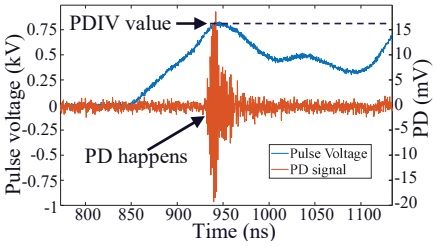

Figure 7. PD detected by the UHF antenna

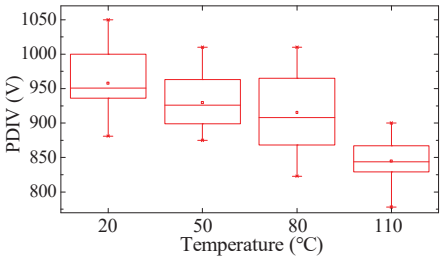

Figure 8. PDIV under different temperatures

B. Endurance experiments

Alike the PDIV experiments, 5 specimens are also used for each group in the endurance tests. For group 1-5, continuous PD are generated in every pulse voltage cycle (one PD at voltage rising edge and another one at falling edge). When a PD happens on the rising edge, space charge (with electrical strength E_q, direction opposite to the applied electrical strength E) deposits on the insulation surface. Then the total electrical strength E_i drops into $E-E_q$. When the voltage falling edge comes, the applied electrical strength drops to zero quickly. Then the total electrical strength becomes $-E_q$, which exceeds the PD inception electrical strength and triggers another PD. While for group 6, PD is generated with a very low probability (less than 1 PD per 5000 voltage cycles). The results of statistical lifetime from Group 1-4 are shown by box-chart in Figure 9. It can be seen that the lifetime of the Nomex paper decreases with the rising temperature. According to the previous literature focusing on the electrical-thermal aging of insulation, coupling effect exists between the electrical stress and thermal stress. When electrical overstress exists, the threshold temperature beyond which thermal aging is induced would be lower [7]. Therefore, under continuous PDs, the rising of temperature can accelerate the combined electrical-thermal aging even when the temperature is well below the material's thermal rating (220 ℃).

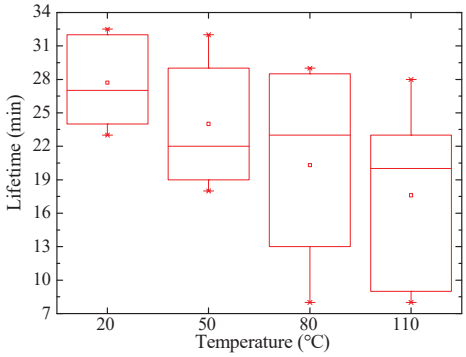

Figure 9. Endurance lifetime of Nomex paper under different temperatures

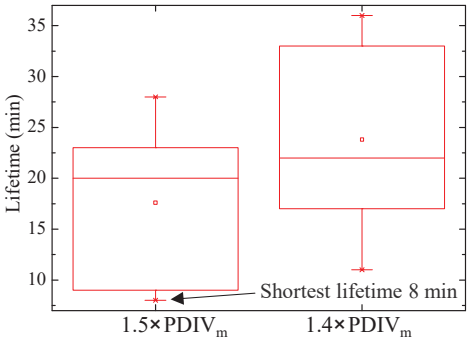

Figure 10. Endurance lifetime under different peak voltage values

Results from group 4-5 are shown in Figure 10. While for group 6 none of the specimens shows breakdown even when they are aged for more than 6 hours. With the presence of continuous PD, lower peak voltage value would surely make the PD magnitudes smaller, yet the endurance lifetime can only be prolonged by a few minutes. Only when the PD activity is effectively suppressed can the insulation material avoid breakdown in a short time.

It is clear that Nomex paper is extremely vulnerable to the deterioration from PD generated by pulse voltage. In the most serious situation, within 500000 voltage cycles, the insulation breaks down (8 min shown in Figure 10) even though the applied voltage magnitude is 440 V lower than the material's breakdown strength. Unlike conventional transformers that usually use oil-paper insulation, medium frequency transformers usually use dry type insulation. Air ducts may exist between adjacent winding layers or adjacent windings where lies a high voltage drop. With the overvoltage reported in [4], the above-mentioned voltage drop can be even higher. Along with greater temperature rise due to higher working frequency (compared with 50/60 Hz power frequency with which conventional transformer works), the PD inception probability in the air ducts can be very high. On the other hand, higher voltage frequency can increase the PD number per second, thus further accelerate the insulation aging speed. All these above factors make medium frequency transformer face greater risk of insulation premature failure compared with the conventional transformer. To guarantee the long-term insulation reliability for medium frequency transformer, designers should give higher margins for setting the insulation distance or apply other materials that can better withstand the PD inception and deterioration.

IV. Conclusions

To investigate the partial discharge inception and deterioration on the insulation of medium frequency transformer, a test system is built. This system consists of a pulse voltage generator that can generate repetitive unipolar pulse voltage to simulate the fast rise time and medium frequency of PWM voltage with which the medium frequency transformers are working. Along with the UHF antenna for PD detection and effective breakdown protection method, this system can be used for PDIV and endurance tests on the insulation of medium frequency transformers.

By using this test system, partial discharge inception voltage and endurance tests under repetitive pulse voltage and different temperatures are conducted on Nomex paper, which is one of the main insulation materials used for medium frequency transformers. The results show that: 1) PDIV of Nomex paper is lower at higher temperature. 2) Nomex paper would breakdown very quickly with the presence of continuous PDs generated by pulse voltage. 3) With temperature rising, the lifetime of the insulation would be further shortened even if the temperature is well below the material's thermal rating. These results indicate that the insulation of medium frequency transformer would face the risk of accelerated aging by PD since overvoltage and overtemperature, which can make the PD inception probability higher, have been proved exist by previous studies. Higher margin for insulation distance or better insulation material should be considered in the medium frequency transformer's design to cope with this risk.

References

[1] M Mogorovic, "Modeling and Design Optimization of Medium Frequency Transformers for Medium-Voltage High-Power Converters," Phd dissertation, Power Electronics Laboratory., Swiss federal Institute of Technology in Lausanne, Lausanne, 2019.

[2] F. Wen, L. Zhang, G. Wu, E. He, "Modeling and Simulation of Inter-Turn Voltage Distribution in the Stator Windings of the Pulling Motor," IEEE International Conference on Solid Dielectrics (IDSD), pp. 900-903, July, 2004.

[3] M. Kaufhold, G. Borner, M. Eberhardt, and J. Speck, "Failure mechanism of the interturn insulation of low voltage electric machines fed by pulse controlled inverters," IEEE Elect. Insul. Mag., vol. 12, pp. 9-16, September. 1996.

[4] C. Zheng, Q. Wang, H. Wang, Z. Shen and L. B. Claus, "Electrical Stress on the Medium Voltage Medium Frequency Transformer," Energies., Vol. 14, no. 16, 2021C. Zheng, Q. Wang, H. Wang, Z. Shen and L. B. Claus, "Electrical Stress on the Medium Voltage Medium Frequency Transformer," Energies., Vol. 14, no. 16, 2021.

[5] P. Wang, S. Ma, S. Akram, K. Zhou, Y. D. Chen, and M. T. Nazir, "Design of Archimedes Spiral Antenna to Optimize for Partial Discharge Detection of Inverter Fed Motor Insulation," IEEE Access., Vol. 8, pp. 193202-193213, October. 2020.

[6] D. Aushuman, S. Navid, K. Rahul, E. Wilson and L. Ri, "Improving Thermal Performance of High Frequency Power Transformers using Bobbinless Transformer Design," IEEE Intersociety Conference on Thermal and Thermomechanical Phenomena in Electronic Systems, pp. 291-297, July, 2020.

[7] L. Simoni, G. Mazzanti, G. C. Montanari and L. Lefebre, "A Genera Multi-stress life model for insulating materials with or without evidence for thresholds," IEEE Transactions on Electrical Insulation., Vol. 28, No. 3, pp. 349-364, 1993.

C3:

Comparative PDIV and endurance studies on different insulating materials used for medium frequency transformers

Changjiang. Zheng
AAU Energy
Aalborg University
Aalborg, Denmark
czhe@energy.aau.dk

Qian Wang
AAU Energy
Aalborg University
Aalborg, Denmark
qiwaau@163.com

Huai Wang
AAU Energy
Aalborg University
Aalborg, Denmark
hwa@energy.aau.dk

Zhan Shen
AAU Energy
Aalborg University
Aalborg, Denmark
zhs@scu.edu.cn

Filipe Faria da Silva
AAU Energy
Aalborg University
Aalborg, Denmark
ffs@energy.aau.dk

Claus Leth Bak
AAU Energy
Aalborg University
Aalborg, Denmark
clb@energy.aau.dk

2022 IEEE International Conference on High Voltage Engineering and Applications (ICHVE) | 978-1-6654-0750-2/22/$31.00 ©2022 IEEE | DOI: 10.1109/ICHVE53725.2022.9961619

***Abstract*—Medium frequency transformers in the power electronic system suffer from unusual electrical stress. With short rise time and higher frequency of the PWM voltage, inter-turn/layer overvoltage and overheating can be induced in the transformer's winding. Partial discharge may be triggered with higher probability and may lead to premature failure of the insulation. Therefore, it is necessary to improve the insulation capability of medium frequency transformers with respect to resisting partial discharge generation and deterioration under PWM-like voltage and high temperature. To achieve this goal, selection of better insulation material is critical. This paper presents comparative partial discharge inception voltage and endurance lifetime studies on three different materials including polyimide, polyester and Nomex paper, which are usually used for the insulation of medium frequency transformers. Results show that polyimide and polyester behave better than Nomex paper in resisting partial discharge inception. While polyimide shows longest endurance against continuous partial discharge.**

Keywords—Medium frequency transformer, partial discharge, Insulation material

I. INTRODUCTION

Transformers working in medium frequencies (from hundreds of Hz to tens of kHz) are defined as medium frequency transformers. The voltage waveform with which these transformers are working is usually PWM pulse voltage generated by power-electronic switches. Comparing with power frequency (50/60 Hz) sinusoidal voltage, PWM voltage has much shorter rise time (from several μs to tens of ns) and much higher frequency (from hundreds of Hz to tens of kHz) [1].

According to our previous study, short rise time of the PWM-like voltage can cause inter-turn and inter-layer overvoltage within the winding [2]. For a transformer with multi-layer windings, voltage drop between adjacent layers is usually very high. With the presence of the overvoltage brought from the fast voltage rising front, inter-layer insulation may be overstressed. In addition, higher frequency can obviously increase the copper loss and core loss, leading the whole transformer to higher temperature [3]. These above factors can make the probability of partial discharge (PD) inception higher in the transformer's winding. Continuous discharge along with the high temperature can degrade the insulation faster and lead to premature breakdown [4].

Therefore, it is necessary to improve the medium frequency transformer's insulation quality with respect to resisting PD generation and deterioration under rising temperature. To achieve this goal, selection of better materials for the transformer's insulation is an important step. This paper chooses three different materials including polyimide, polyester and Nomex paper as study objects. These materials are often used for the medium frequency transformer's insulation [5]. Based on a test system that can generate repetitive pulse voltage and detect high frequency PD signals with high accuracy, comparative partial discharge inception voltage (PDIV) tests under different temperatures are conducted. The results show that polyimide and polyester have higher PDIV values compared with that of Nomex paper. With the temperature rise, Nomex paper shows most obvious decrease in PDIV. Afterwards, comparative endurance lifetime tests are conducted among these materials. Under continuous PDs, Nomex paper breaks down much faster than the other two materials while polyimide has the longest lifetime against the PD degradation.

II. EXPERIMENT SETUP

A. Test system

A test system shown in Figure 1 is used for the PDIV tests. HV pulse generator based on power-electronic switches and DC source can generate repetitive pulse voltage with magnitude up to 20 kV and frequency up to 50 kHz. Typical output voltage waveform of this generator is shown in Figure 2. A computer is used to control the on-off and parameter (including voltage peak value and frequency) of this generator. The insulation specimen is held by a sphere-plate electrode system seen in Figure 3 inside the oven. Current sensor can monitor the current value and send the data to the computer during tests. If overcurrent (for example, when the insulation specimen breaks down) happens, computer would stop the generator.

When conducting PD tests under pulse voltage, strong interference would be induced by the on-off of the power electronic switches, which makes the traditional PD detecting apparatus such as current sensor or HFCT unable to detect PD

978-1-6654-0750-2/22/$31.00 ©2022 IEEE

signals. In fact, difference exists in the energy distribution of PD signals and interference in frequency domain [6]. The energy of PD signal can spread up to more than 1.2 GHz while the energy of interference mainly distributes in frequency range below 500 MHz. Therefore, an UHF antenna with gain higher than 3 dB in the frequency range from 1 GHz to 2 GHz is utilized in this system for PD detection. It can effectively detect the PD signal and avoid the influence from the interference (seen in Figure 4). During the tests, the applied voltage waveform and PD signal would be displayed on the oscilloscope (with 20 Gs/s sampling rate and 4 GHz band width).

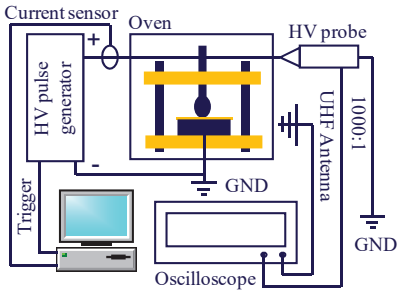

Figure 1. Test system

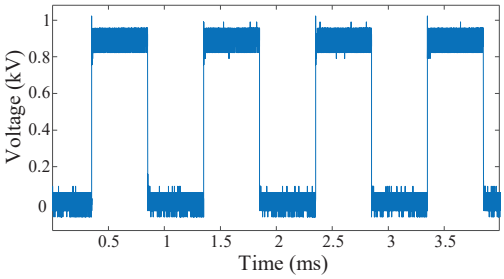

Figure 2. Repetitive pulse volage waveform with 1 kV peak value and 1 kHz frequency

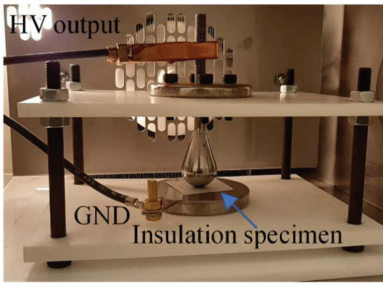

Figure 3. Sphere-plate electrode in the oven

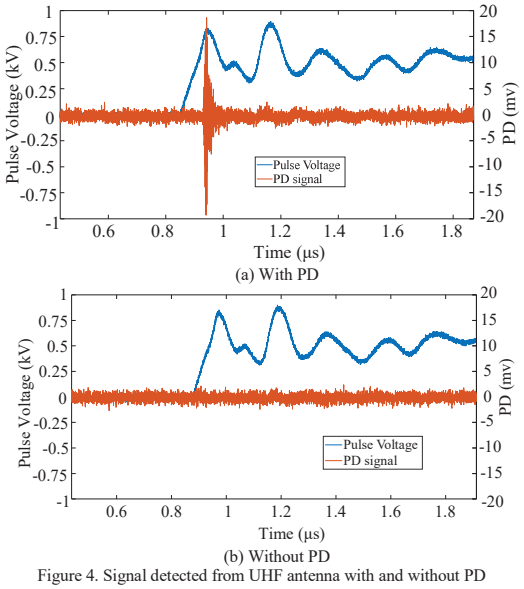

Figure 4. Signal detected from UHF antenna with and without PD

B. *Insulation specimen*

Three different materials shown in Figure 5 are chosen as the study objects including polyimide 6050, polyester 6020 and Nomex 410 paper. All the materials are with the same thickness of 0.05 mm and are cut into the same shape (square shape with side length of 2.5 cm). Before staring the experiments, insulation specimens are all cleaned by alcohol and dried in the oven with 50 ℃ for 24 hours.

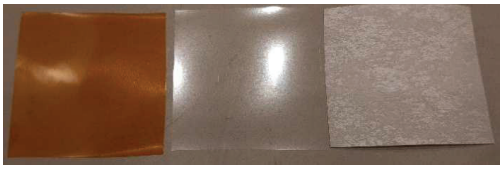

Figure 5. Polyimide (left), Polyester (middle) and Nomex paper (right) for the experiments

C. *Parameters for the experiments*

In the comparative PDIV tests, rise time (t_r) of the pulse voltage is kept as 40 ns for it fits with the range of the PWM voltage rise time that the modern SiC switches can achieve. Voltage frequency (f) is kept as 1 kHz for it is one of the typical working frequencies of the medium frequency transformer. Considering that due to the increased copper and core losses brought from higher frequency, temperature of the whole transformer can reach more than 100℃ [3], 4 different temperature values from room temperature (20℃) to 110℃ are chosen. The detailed parameters of the comparative PDIV tests are shown in TABLE I.

TABLE I. Parameters for the Comparative PDIV tests

Group	Material	Rise Time	Frequency	Temperature
1	Polyimide	40 ns	1 kHz	20 ℃
2				50 ℃
3				80 ℃
4				110 ℃

5	Polyester			20 ℃
6				50 ℃
7				80 ℃
8				110 ℃
9	Nomex paper			20 ℃
10				50 ℃
11				80 ℃
12				110 ℃

In the comparative lifetime tests, rise time and frequency of the voltage is kept as same as that of PDIV tests. While the peak voltage value is raised to 1.5 times PDIV (depends on the results from the PDIV tests under highest temperature) to guarantee that PD can be triggered on every kind of the selected insulation materials in every voltage cycle. The temperature is kept as 110 ℃. The detailed parameters for the comparative lifetime tests are shown in TABLE II.

TABLE II. Parameters for the Comparative endurance lifetime tests

Group	Material	Peak Voltage	Frequency	Temperature
1	Polyimide	1.5×PDIV	1 kHz	110 ℃
2	Polyester			
3	Nomex			

III. EXPERIMENT RESUTLS

A. Comparative PDIV experiments

During the Comparative PDIV experiments, voltage is raised with 10V/s until the first PD is detected by the UHF antenna. 5 samples are used for each group in TABLE I. The average PDIV values of these materials with rising temperatures are shown in Figure 6. It is clear that Polyimide and Polyester can better resist the PD generation comparing with that of Nomex paper. When temperature rises from 20 ℃ to 110 ℃, PDIV of Nomex paper shows most obvious decreasing (decreases by 12.2%). In lower temperature range (from 20℃ to 80℃), polyimide has lower PDIV than that of polyester. Yet when the temperature is raised to 110℃, PDIV of polyimide is higher. When temperature rises, the air molecule density reduces, making the breakdown strength of the air gap lower [4]. That's why in most of the situation, PDIV decreases with temperature rising. Yet, higher temperature can also increase the insulation materials' surface conductivity [7]. Then the surface charge would be dissipated faster, making the probability of initial electron generation lower. Therefore, higher voltage magnitude would be necessary to light the PD. That's why in some situation (for polyimide from 20℃ to 50 ℃, for polyester from 80 ℃ to 110℃), PDIV increases with temperature rising.

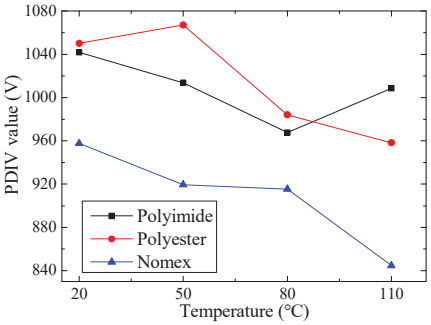

Figure 6. PDIV values under different temperatures

B. Comparative endurance experiments

During the experiments, the insulation specimen is aged under repetitive pulse voltage until the final breakdown. Same as the PDIV tests, 5 specimens are used for each group in TABLE II. Lifetime of different materials is shown in Figure 7. Under continuous PDs generated by the pulse voltage, Nomex paper breaks down much faster than the other two materials. While polyimide behaves best in resisting the PD degradation. The appearance of breakdown area and unaged material observed by the microscope with 200 times zoom in are shown in Figure 8. For polyimide, it can be seen that near the breakdown point, a new layer filled with clusters of particles is formed due to the PD aging. For polyester, a new but relatively smooth layer can also be observed. While for the Nomex paper, the region that surrounds the breakdown point is still the same as the unaged material. It is certain that PD aging process on the Nomex paper is somewhat different from that on the polyimide and polyester films. This may contribute to the great difference of lifetime between Nomex paper and the other two materials and should be further investigated in our future studies.

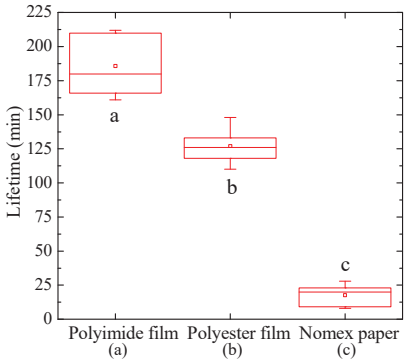

Figure 7. Lifetime of different materials

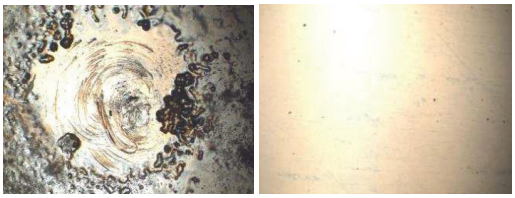

(a) Polyimide

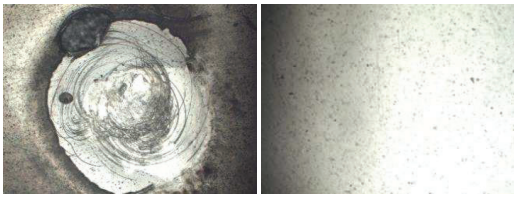

(b) Polyester

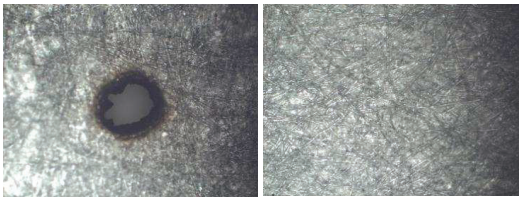

(c) Nomex paper

Figure 8. Breakdown area (left) and unaged area (right) of different materials

According to the above results, Nomex paper is most vulnerable to PD inception and degradation under medium frequency pulse voltage. If this material is used as the medium frequency transformer's insulation, higher margin of insulation distance (thickness) should be adapted. Considering the relative high temperature faced by the medium frequency transformer and its developing trending to be smaller in size (limited insulation thickness), polyimide is the best choice among these materials because of its best behavior in resisting PD inception at high temperature and longest endurance.

IV. CONCLUSIONS

Using pulse voltage, PDIV tests under different temperatures and endurance lifetime tests are conducted on three different materials including polyimide, polyester and Nomex paper that are often used for the insulation of medium frequency transformer. The results show that:

1. Nomex paper has lowest PDIV among these three materials.

2. With temperature rising, the decrease of PDIV of Nomex paper is most obvious.

3. In lower temperature range, Polyimide has lower PDIV than that of polyester. When temperature rise to 110℃, PDIV of polyimide is higher.

4. Under the degradation from continuous PDs, lifetime of Nomex paper is much shorter than the other two materials. While the lifetime of polyimide is the longest.

These results indicate that for the construction of insulation of medium frequency transformer, polyimide is the best choice.

REFERENCES

[1] M Mogorovic, "Modeling and Design Optimization of Medium Frequency Transformers for Medium-Voltage High-Power Converters," Phd dissertation, Power Electronics Laboratory., Swiss federal Institute of Technology in Lausanne, Lausanne, 2019.

[2] C. Zheng, Q. Wang, H. Wang, Z. Shen and L. B. Claus, "Electrical Stress on the Medium Voltage Medium Frequency Transformer," Energies., Vol. 14, no. 16, 2021C. Zheng, Q. Wang, H. Wang, Z. Shen and L. B. Claus, "Electrical Stress on the Medium Voltage Medium Frequency Transformer," Energies., Vol. 14, no. 16, 2021.

[3] D. Aushuman, S. Navid, K. Rahul, E. Wilson and L. Ri, "Improving Thermal Performance of High Frequency Power Transformers using Bobbinless Transformer Design," IEEE Intersociety Conference on Thermal and Thermomechanical Phenomena in Electronic Systems, pp. 291-297, July, 2020.

[4] M. Kaufhold, G. Borner, M. Eberhardt, and J. Speck, "Failure mechanism of the interturn insulation of low voltage electric machines fed by pulse controlled inverters," IEEE Elect. Insul. Mag., vol. 12, pp. 9-16, September. 1996

[5] Y. Zhao, G. Zhang and R. Guo, "The Breakdown Characteristics of Thermostable Insulation Materials under High-Frequency Square Waveform," IEEE Trans. Dielectr. Electr. Insul., vol. 26, no. 4, pp. 1073–1080, 2019.

[6] P. Wang, S. Ma, S. Akram, K. Zhou, Y. D. Chen, and M. T. Nazir, "Design of Archimedes Spiral Antenna to Optimize for Partial Discharge Detection of Inverter Fed Motor Insulation," IEEE Access., Vol. 8, pp. 193202-193213, October. 2020.

[7] T. Liu, Q. M. Li, X. W. Huang, Y. F. Lu, M. Asif, and Z. D. Wang, "Partial discharge behavior and ground insulation life expectancy under different voltage frequencies," IEEE Trans. Dielectr. Electr. Insul., vol. 25, no. 2, pp. 603-613, April. 2018

ISSN (online): 2446-1636
ISBN (online): 978-87-7573-700-0

AALBORG UNIVERSITY PRESS